Volume 7, Issue 1, 2025

Print ISSN: 2663-1024
Online ISSN: 2663-1016

EURASIA JOURNAL OF SCIENCE AND TECHNOLOGY

Eurasia Journal of Science and Technology

Volume 7, Issue 1, 2025

Published by Upubscience Publisher

Eurasia Journal of Science and Technology
Print ISSN: 2663-1024 Online ISSN: 2663-1016
Email: info@upubscience.com
Website: http://www.upubscience.com/

Table of Content

Eurasia Journal of Science and Technology
ISSN: 2663-1016
DOI: https://doi.org/10.61784/ejst3059

OPTIMIZATION OF MECHANIZED RAPID CONSTRUCTION STEP DISTANCE FOR HARD ROCK BODY OF MA BAISHAN TUNNEL

YuSheng Huang[1], GuiLin Wei[1], Kai Wen[2], ChuanJun Ji[2], YouLiang Xiong[2], XinZhi Li[1*]
[1]Department of Civil Engineering, Shijiazhuang Tiedao University, Shijiazhuang 050043, Hebei, China
[2]China Railway 18th Bureau Group Third Engineering Co., Baoding 072750, Hebei, China.
Corresponding Author: XinZhi Li, Email: hshaocun@163.com

Abstract: This study aims to determine the rational construction safety step distance for hard rock tunnels, with the goal of effectively organizing the implementation of various construction processes to meet the requirements of rapid construction in hard rock tunnels. The FLAC3D finite difference software was utilized to establish a three-dimensional model based on the tunnel's cross-sectional form, excavation method, and support parameters, followed by numerical simulation analysis. The deformation patterns of the tunnel surrounding rock and the stress characteristics of the support structure under different construction step distances for II and III grade surrounding rocks were analyzed, and the stability of the tunnel surrounding rock and support structure was investigated. The results indicate that: 1) Under different rock grade conditions, as the tunnel construction step distance increases, the deformation of the tunnel surrounding rock and the stress on the initial support structure both show varying degrees of increase; 2) Considering the actual operation tool configuration and operational space requirements at the construction site of the Ma Bai Shan Tunnel, the bottom plate step distance for II and III grade surrounding rocks is adjusted to 300m, and the secondary lining step distance is adjusted to 400m, achieving the goal of rapid construction in hard rock tunnels while ensuring safety.
Keywords: Tunnel engineering; Mechanized construction; Hard rock formation; Step distance optimization

1 INTRODUCTION

With the rapid development of the global economy, more and more long tunnels have begun to emerge. However, as the scale of tunnel construction continues to expand, tunnel collapse accidents are becoming increasingly common [1-3], leading to severe casualties and property damage. Scholars, both domestically and internationally, have conducted investigative analyses of the causes and mechanisms underlying tunnel collapse accidents [4-5]. Research has revealed that the excavation of the invert arch has a significant impact on the deformation of the surrounding rock in tunnels [6]. Thus, it can be inferred that the inadequate safety distances during tunnel construction are a significant factor in causing tunnel collapse accidents. However, existing technical standards lack specific guidelines on the safe step distances for tunnel construction. Although Chinese railway construction documents [2008] No. 160 and [2010] No. 120 specify the invert arch and secondary lining step distances for tunnel projects, the prescribed values are determined based on engineering experience, relying solely on a simple classification according to rock mass levels and fail to comprehensively consider factors such as groundwater conditions, support conditions, and construction plans [7]. To ensure construction safety, construction units often opt for smaller safety step distances. However, with the increasing mechanization of tunnel construction, more and more large machinery is being used to replace manual labor throughout the entire tunnel construction process to ensure the rapid construction of tunnels [8-9]. Consequently, the excessively conservative step distance requirements pose significant obstacles to the placement of large machinery on-site, severely impacting the progress of current tunnel construction. In response to such issues, numerous scholars at home and abroad have updated the invert arch and secondary lining step distances for tunnels based on typical engineering cases, employing various approaches.

Tong Kai [10], based on the V-grade surrounding rock section of the Zhengwan High-speed Railway Xinhua Tunnel, conducted corresponding research on the secondary lining and face safety step distances under different burial depths in the construction tunnel, using the elastic foundation beam theory. Using both mechanical models and numerical simulations, the maximum construction step distance was determined to be 60 meters. Hao Junming [11], relying on the Heping Tunnel and Chongli Tunnel projects in the Tai-Chong section of the Tai-Xi Railway, established village lining and invert arch models under different construction step distances using FLAC numerical simulation software. The study explored the step distances for the inclined arch and secondary lining construction under different rock mass construction levels when meeting the requirements of mechanized rapid construction. Wang Haizhou [12] derived a formula for calculating the safe step spacing, taking into account seven influencing parameters. This formula was successfully applied to an actual project. Shi Jiyao et al. [13] relied on the Guchengling Tunnel of BaoLan Hub to establish a numerical model that accurately reflects the actual engineering practice. Their study aimed to analyze the deformation characteristics of large section tunnels with soft rock and investigate the impact of the elevated arch step distance and step length on the deformation of the initial support; Zhou Xueliang [14] collected a large amount of data on the collapse of the Dongshan tunnel. He combined this data with monitoring data on the deformation trend of the

surrounding rock to conduct a comprehensive prediction. He studied the relationship between the deformation of the section, the excavation time, and the spacing of the palm face of the second lining. This study aimed to determine the optimal timing for applying the second lining; R.B. ROKAHR [15] selected five tunnels with similar mechanical parameters of the surrounding rock for analysis and comparison, selected the appropriate support parameters, and calculated the construction step under different surrounding rock conditions in the case, and finally determined the optimum safety step value for this tunnel.

In summary, for the relatively understudied optimization of step distances in Grade II and III hard rock tunnels, this study relies on the Grade II and III hard rock sections of the Ma Bai Shan Tunnel in the Qinling Mountains to conduct research on step distance optimization. The objective is to propose a long-distance safety step distance that meets the requirements of full-face excavation using large machine excavation and the corresponding support conditions, thereby achieving rapid construction in hard rock tunnels.

2 PROJECT OVERVIEW

The Qinling Ma Bai Shan Tunnel is located in the jurisdictions of Lantian County, Shaanxi Province, and Shangluo City. It is a dual-bore, single-track tunnel with a total length of 22,918 meters. Grade II and Grade III surrounding rocks account for 75.5% of the total length of the tunnel. It is a high-speed railway tunnel traversing large segments of hard rock formations. In the project area, the overall distribution of the Qinling mountain range trends northeast, with elevations ranging from 800 to 2000 meters and a relative height difference of 500 to 1000 meters. The northern slope of the Qinling Mountains is steep, characterized by short gullies, steep longitudinal slopes in the gully beds, and a general pattern of "U"-shaped valleys in the upper reaches and "V"-shaped valleys in the lower reaches with steep slopes. The southern slope has longer gullies and often exhibits a tree-branch-like water system.

The left line of the tunnel extends from DK46+393 to DYIIK69+311, with a total length of 22,918 meters and a maximum depth of burial of 620 meters. The tunnel's right line extends from DYIIK46+393 to DYIIK69+312, covering a total length of 22,919 meters and reaching a maximum burial depth of 620 meters. In the tunnel alignment area, with the exception of a small amount of Quaternary artificial fill and alluvial layers within the gullies, the bedrock is exposed in other sections. In exposed layers, the predominant geological formations consist of quartzite from the Middle-Lower Cambrian Kuanping Group's Sichakou Formation, sericite-chlorite-quartz schist from the Zhulin Formation, and granite from the Yanshan period. The tunnel passes through the fractured zone of the F8 fault and, in addition, traverses several areas with densely packed joint systems. The overall geological conditions of the tunnel are characterized by predominantly weak to moderately water-rich rock formations, with the presence of adverse geological conditions such as hazardous rockfall, significant deformation in soft rock, and high ground stress.

3 NUMERICAL SIMULATION AND SIMULATED WORKING CONDITIONS

3.1 Computational Modeling

Combined with the current construction situation of the tunnel, the FLAC3D finite difference software is utilized to create a numerical simulation 3D model. According to previous experience with tunnel excavation simulation modeling, in order to minimize the impact of boundary effects, the model boundary is set at 3~5 times the diameter of the hole, considering the setup of the tunnel safety step, the model is taken as 450m in the longitudinal direction. Therefore, the dimensions of the 3D simulation model for the level II surrounding rock are selected as: 450m×100m×130m (length×width×height). Similarly, the dimensions of the 3D simulation model for the level III surrounding rock are also selected as: 450m×100m×130m (length×width×height). The displacement boundary adopts fixed boundary conditions, with horizontal constraints on the left and right sides of the tunnel, vertical constraints on the lower part, constraints perpendicular to its surface on the front and back, and a free boundary on the ground surface. The overall Moore Cullen model is used before excavation, and the initial support and secondary lining during excavation are simulated using elastomeric units after rigidity equivalence. The initial support and secondary lining are both calculated using solid units for consistent calculation. The three-dimensional simulation model of Class II rock tunnel is shown in Figure 1. The three-dimensional simulation model of Class III rock tunnel is shown in Figure 2.

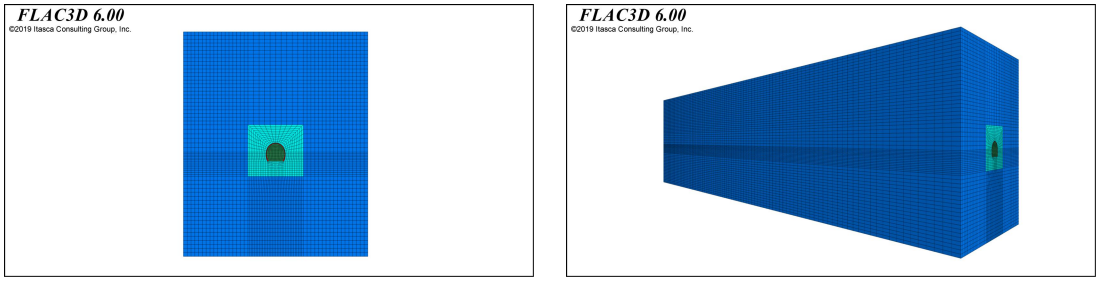

(a) Front View (b) Oblique View

Figure 1 Three-Dimensional Simulation Model of Class II Perimeter Rock Tunnel

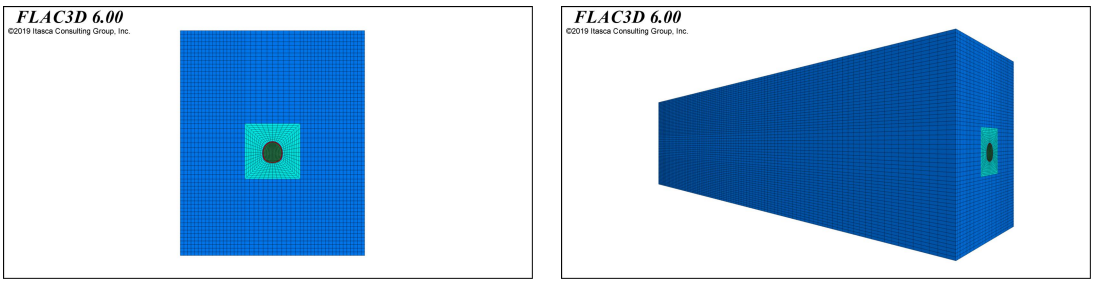

(a) Front View (b) Oblique View

Figure 2 Three-Dimensional Simulation Model of Class III Perimeter Rock Tunnel

3.2 Parameter Selection

The physical and mechanical parameters of the tunnel surrounding rock and lining structure are selected according to the "Design Code for Railway Tunnels" (TB 10003-2016) and "Design Code for Concrete Structures" (GB50010-2010). The simulated physical and mechanical parameters of the tunnel excavation with Class II surrounding rock are shown in Table 1, while those of Tunnel Excavation with Class III Surrounding Rock are shown in Table2. The physical and mechanical parameters of the initial support concrete are shown in Table 3.

Table 1 Physical and Mechanical Parameters of Class II Surrounding Rock Model

materials	Modulus of deformation E(GPa)	Heaviness γ (KN/m^3)	Poisson's ratio (μ)	Angle of internal friction θ (°)	Adhesion cohesion c (MPa)	thicknesses (m)
surrounding rock	27	27	0.25	54	1.8	
Initial support	23	23	0.2			0.05
secondary lining	31.5	25	0.2			0.3

Table 2 Physical and Mechanical Parameters of Class III Surrounding Rock Model

materials	Modulus of deformation E (GPa)	Heaviness γ (KN/m^3)	Poisson's ratio (μ)	Angle of internal friction θ (°)	Adhesion cohesion c (MPa)	thicknesses (m)
surrounding rock	14	25	0.3	44	1.0	
Initial support	23	23	0.2			0.10
secondary lining	31.5	25	0.2			Arch wall 0.35/Elevation arch 0.40

Table 3 Physical and Mechanical Parameters of Initial Concrete

Concrete grade	Heaviness γ (KN/m^3)	Modulus of deformation E(GPa)	Poisson's ratio (μ)	compressive strength (MPa)	tensile strength (MPa)
C25	23	23	0.2	19.0	2.0

4 OPTIMIZATION OF MECHANIZED RAPID CONSTRUCTION STEPS

Currently, the construction step distance requirements for the Ma Bai Shan Tunnel site are as follows: for Grade II surrounding rock sections, the distance from the base plate to the face is 200m, and the distance for the secondary lining is 300m; for Grade III surrounding rock sections, the distance from the invert to the face is 90m, and the distance for the secondary lining is 120m. However, due to the utilization of large-scale mechanized equipment on-site, the space required for a complete mechanical construction operation line is relatively large. The original step distance conditions cannot meet the construction requirements. It is necessary to moderately expand the current construction step distance based on the actual situation of on-site monitoring and measurement and the space requirements of large-scale mechanized equipment. The specific step distance optimization schemes for different rock grades in this numerical simulation are detailed in Table 4 and Table 5:

Table 4 Setting of Safety Step Distances for Grade II Surrounding Rock

working condition	Base plate distance/m	Second liner distance /m
Actual walking distance in Mabai Mountain	200	300
Step program I	250	350
Step program II	300	400

Table 5 Setting of Safety Step Distances for Grade III Surrounding Rock

working condition	Base plate distance /m	Second liner distance /m

Actual walking distance in Mabai Mountain	120	200
Step program I	200	300
Step program II	300	400

4.1 Analysis of Surrounding Rock Monitoring and Measurement Results

The stable final value curves of the arch crown settlement and horizontal convergence for five cross-sections in the Grade III surrounding rock section, obtained from on-site monitoring, are shown in Figure 3:

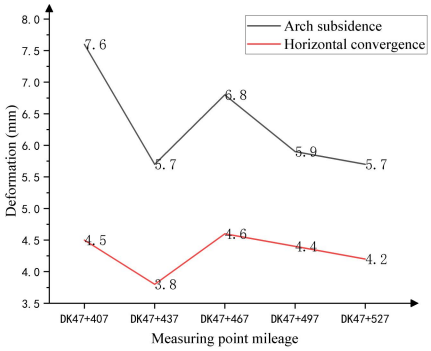

Figure 3 Final Value Curves of Arch Crown Settlement and Horizontal Convergence Deformation for Grade III Surrounding Rock

Combining the results shown in Figure 3, the cumulative settlement deformation of the arch crown for Grade III surrounding rock is not greater than 8mm, and the cumulative deformation of horizontal convergence is not greater than 5mm. The final values at monitoring points show minimal fluctuations, indicating stability. For Grade II surrounding rock, based on on-site monitoring data, its deformation pattern is consistent with Grade III surrounding rock, but with slightly smaller final values. The cumulative settlement of the arch crown deformation is not greater than 6mm, and the cumulative convergence of horizontal deformation is not greater than 3mm. The overall monitoring data of the surrounding rock indicates stability, and the deformation of the rock has not reached the deformation limits of Grade II and Grade III surrounding rocks. This provides favorable conditions for expanding the construction step distance.

4.2 Simulation Results of Step Optimization for Grade II Surrounding Rock

With regard to the influence of different base plate and second lining step distance on the deformation of Class II surrounding rock and the force on the supporting structure, the analyses of the deformation of the tunnel and the force on the initial support in combination with the simulation results are concluded as follows:

4.2.1 Surrounding rock displacement analysis

For different step distances in Grade II surrounding rock, the arch crown settlement and horizontal convergence curves for monitoring cross-sections are shown in Figure 4 and Figure 5:

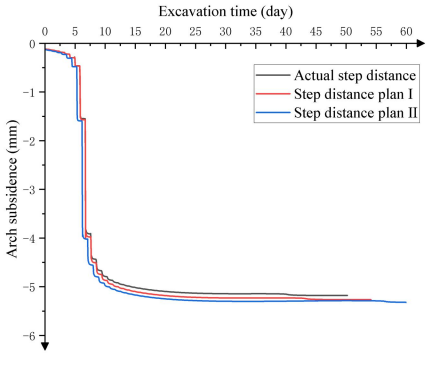

Figure 4 Comparison Curve of Arch Subsidence

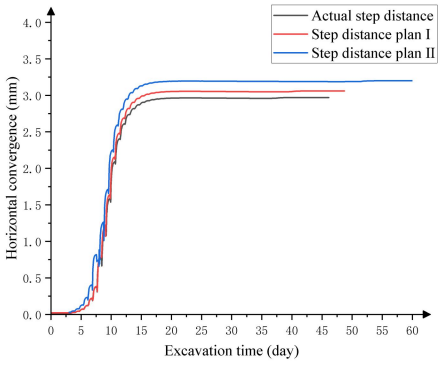

Figure 5 Comparison Curve of Horizontal Convergence

1) According to Figure 4, it is evident that under different safety step distances, the settlement of the tunnel arch shows a characteristic of initial settlement followed by stabilization. However, with the increase in the calculated safety step distance, the stable final value of tunnel arch settlement also increases. In the case of the Ma Baishan Tunnel under actual step distance conditions, the settlement of the arch is 5.18mm. From a safety perspective, this value meets the

requirements for on-site construction safety. For Step Distance Scheme 1, the arch settlement is 5.26mm, and for Step Distance Scheme 2, it is 5.32mm, which is the maximum value in this calculation. From the perspective of arch settlement, the simulation results under the three step distance conditions still fall within the deformation limit of a Class II surrounding rock tunnel, demonstrating that they all meet the safety construction requirements at the site.

2) According to Figure 5, it is observed that the horizontal convergence of the tunnel monitoring section exhibits a characteristic of initial increase followed by stabilization under different safety step distances. However, as the calculated safety step distance increases, the stable value of tunnel horizontal convergence also increases. In the case of the Ma Baishan Tunnel under actual step distance conditions, the horizontal convergence is 2.97 mm, meeting the requirements for safe on-site construction. For Step Distance Scheme 1, the horizontal convergence is 3.06mm, and for Step Distance Scheme 2, it is 3.20mm, with the maximum horizontal convergence occurring under Step Distance Scheme 2. From the perspective of horizontal convergence, the results under three schemes demonstrate that they meet the safety requirements for on-site construction of a Class II surrounding rock tunnel.

4.2.2 Initial support stress analysis

The initial support stress of the tunnel under different conditions for Class II surrounding rock are shown in Figure 6 to 8:

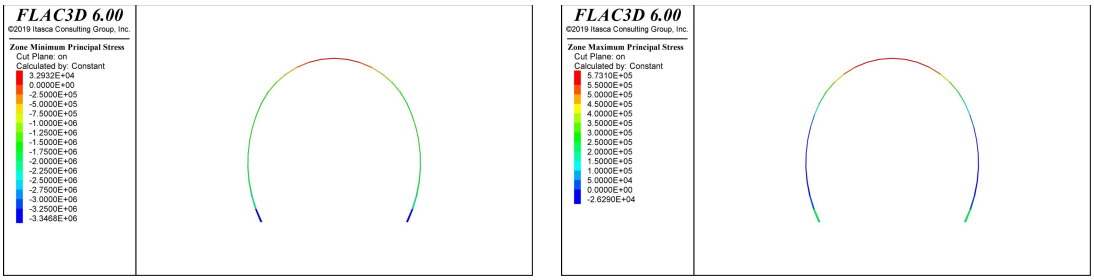

(a) Maximum Principal Stress Map (b) Minimum Principal Stress Map

Figure 6 Initial Support Stress Diagram for Actual Step Distance Conditions

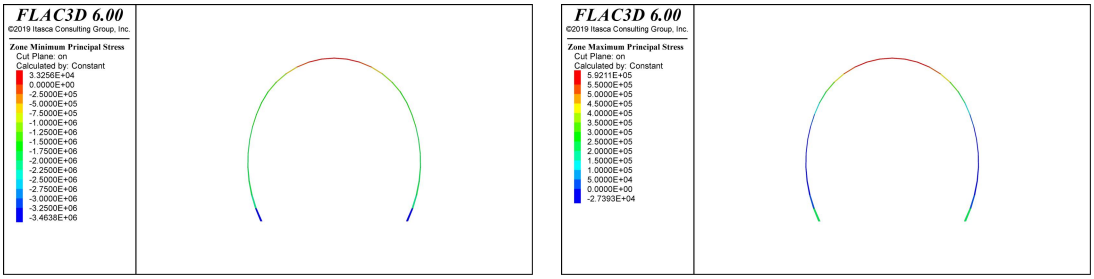

(a) Maximum Principal Stress Map (b) Minimum Principal Stress Map

Figure 7 Initial Stress Diagram for Step Distance Scheme I

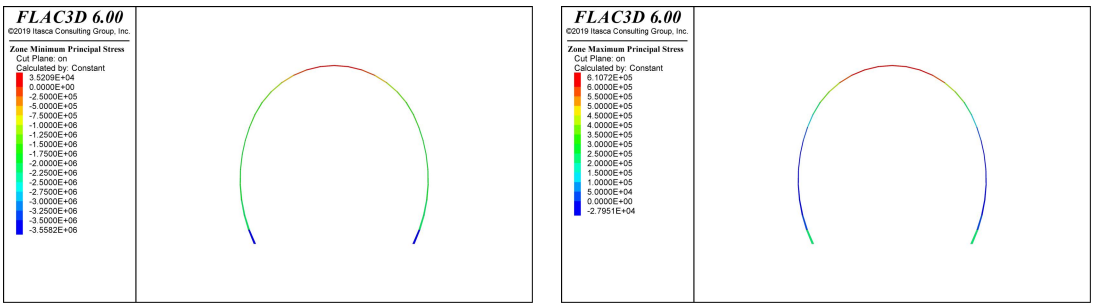

(a) Maximum Principal Stress Map (b) Minimum Principal Stress Map

Figure 8 Initial Stress Diagram for Step Distance Scheme II

According to Figure 6 to 8, it is observed that as the safety step distance increases, there is a slight increase in both the maximum and minimum principal stresses in the initial support structure of the tunnel. Under actual step distance conditions in the Ma Baishan Tunnel, the maximum compressive stress is 3.35 MPa, and the maximum tensile stress is 0.57 MPa, representing the minimum values in the simulation results and meeting the safety requirements for on-site construction. For Step Distance Scheme 1, the initial support's maximum compressive stress is 3.46 MPa, and the maximum tensile stress is 0.59 MPa. Under Step Distance Scheme 2, the initial support's maximum compressive stress is 3.56 MPa, and the maximum tensile stress is 0.61 MPa. In Step Distance Scheme 2, the initial support experiences the maximum load, but these values still fall within the ultimate stress range of C25 concrete, ensuring the safety of the initial support structure.

4.3 Simulation Results of Step Optimization for Grade III Surrounding Rock

In consideration of different construction step distance conditions for Class III surrounding rock, combined with the computational simulation results, an analysis of the deformation and initial support stress situations in Class III surrounding rock is provided, and the conclusions are as follows:

4.3.1 Analysis of surrounding rock displacement

Under different step distance conditions for Class III surrounding rock, the curves depicting the tunnel arch settlement and horizontal convergence for the monitoring section are presented in Figure 9 and Figure 10, respectively.

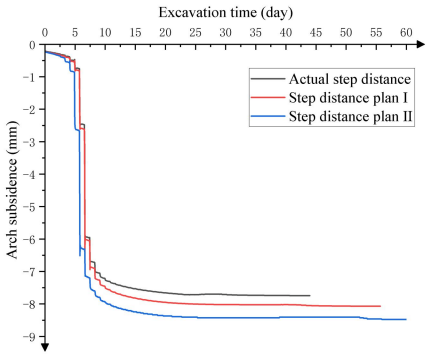

Figure 9 Comparison Curve of Arch Subsidence

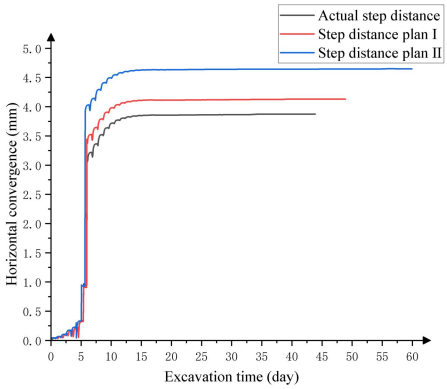

Figure 10 Comparison Curve of Horizontal Convergence

1) As can be seen from the Figure 9, it is evident that under different safety step distances, the tunnel's arch settlement exhibits characteristics similar to those observed in Class II surrounding rock conditions. Specifically, for the Ma Baishan Tunnel under actual step distance conditions, the arch settlement is 7.74mm. For Step Distance Scheme 1, the arch settlement is 8.06mm, and for Step Distance Scheme 2, it is 8.47mm, with the maximum arch settlement occurring under Step Distance Scheme 2. From the perspective of arch settlement, all three schemes are considered sufficient to meet the safety requirements for on-site construction.

2) As depicted in Figure 10, it is evident that under different safety step distances, the horizontal convergence of the tunnel monitoring section exhibits a characteristic of initial increase followed by stabilization, consistent with the convergence features observed in Class II surrounding rock. However, as the calculated safety step distance increases, the stable value of tunnel horizontal convergence also increases. Specifically, for the Ma Baishan Tunnel under on-site step distance conditions, the horizontal convergence is 3.87mm. For Step Distance Scheme 1, the horizontal convergence is 4.13mm, and for Step Distance Scheme 2, it is 4.65mm. From the perspective of horizontal convergence, all three schemes are deemed sufficient to meet the safety requirements for on-site construction.

4.3.2 Initial support stress analysis

Tunnel initial stresses under different working conditions of Class III surrounding rock are shown in Figure 11 to 13:

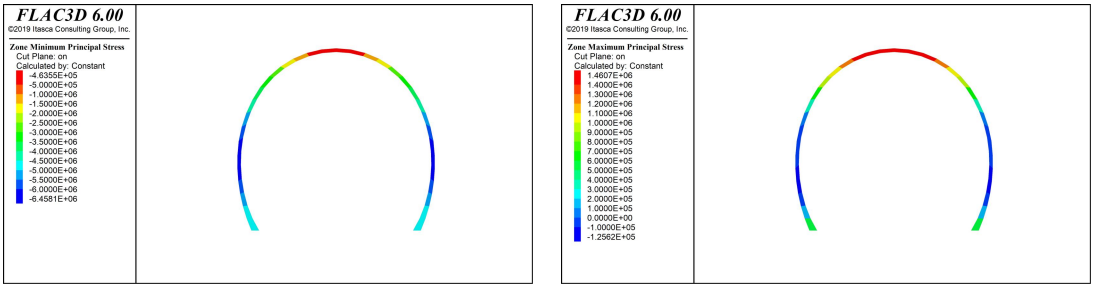

(a) Maximum Principal Stress Map (b) Minimum Principal Stress Map

Figure 11 Initial Support Stress Diagram for Actual Step Distance Conditions

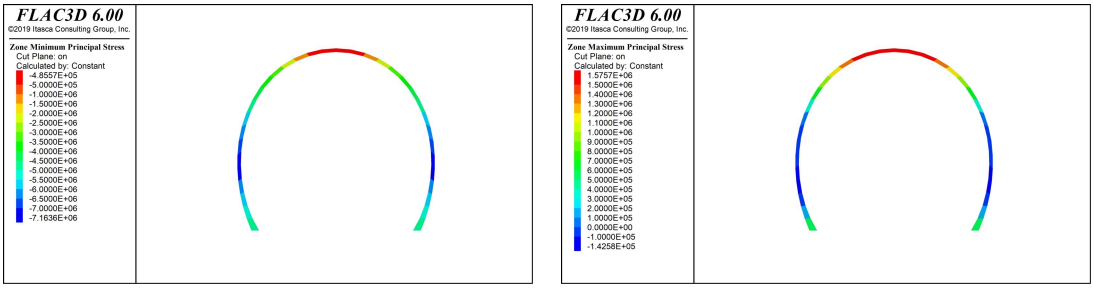

(a) Maximum Principal Stress Map (b) Minimum Principal Stress Map

Figure 12 Initial Stress Diagram for Step Distance Scheme I

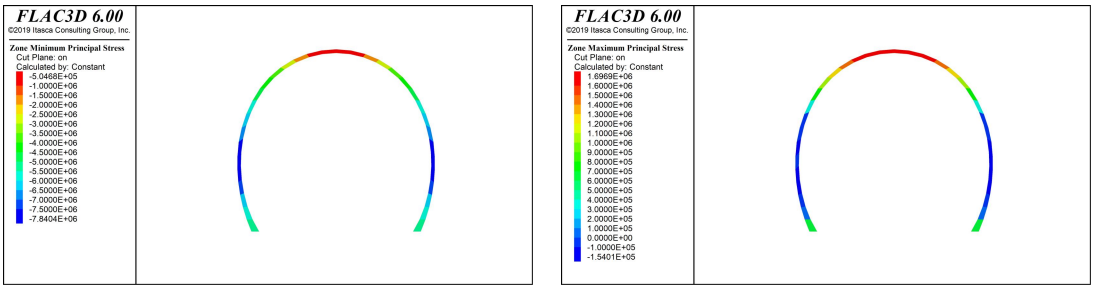

(a) Maximum Principal Stress Map (b) Minimum Principal Stress Map

Figure 13 Initial Stress Diagram for Step Distance Scheme II

According to Figure 11 to 13, it is evident that with the increase in safety step distance, both the maximum and minimum principal stresses in the tunnel's initial support structure experience a certain degree of increment. Specifically, for the Ma Baishan Tunnel under actual step distance conditions, the maximum compressive stress is 6.46 MPa, and the maximum tensile stress is 1.46 MPa. For Step Distance Scheme 1, the initial support's maximum compressive stress is 7.16 MPa, and the maximum tensile stress is 1.58 MPa. Under Step Distance Scheme 2, the initial support's maximum compressive stress is 7.83 MPa, and the maximum tensile stress is 1.69 MPa. In Step Distance Scheme 2, the initial support experiences the maximum load, but these values still fall within the ultimate stress range of C25 concrete, achieving the goal of safe construction.

4.4 Determination of Mechanized Construction Step Distances

As shown in Figure 14, to achieve mechanized and rapid construction of the single-lane tunnel in the hard rock body of Ma Baishan, large-scale mechanized equipment such as three-wall rock drilling trolleys are used to carry out mechanized excavation of the whole operation line, and the configuration of the main machinery and equipment is shown in Table 6:

Figure 14 Three-Arm Rock Drill Dolly

Table 6 Configuration Table for Mechanized Construction Equipment

serial number	operating line	Name of equipment/machinery	Brand/Model/Specification	quantities	note
1		Fully computerized three-armed rock drill	ZYS113	1	Walking, rock drilling operations, charging operations
2	scoop out	Full Section Excavation Bench	self-restraint	1	Excavation, support
3		wind-powered rock drill	YT28	20	Excavation drilling, Anchor drilling
4	shipment	Loaders (side discharge)	ZC50	2	mount a ballast
5	support	abutment	self-restraint	1	Initial support
6	spray concrete	Concrete wet sprayer	Tiejian Heavy Industry HPS3016SW /30m³/h	1	Supporting concrete spraying
7	a vault	a pierced trestlework	self-restraint	1	Arch construction
8	anti-drainage	Watertight Sheet Bench	self-restraint	2	Waterproof layer construction
9	second lining	Second lining cart	Zhuozhou Machinery Factory/12m	2	Lining Concrete Pouring

Considering the current machinery configuration, it is evident that the existing construction step distance conditions are insufficient to meet the requirements of the current mechanized construction across the entire line. Based on on-site monitoring data and numerical simulation results, it has been observed that for Class II and Class III surrounding rock, appropriately increasing the construction step distance does not significantly impact on the deformation of the surrounding rock and the stress on the tunnel support structure. This adjustment does not compromise the safety of on-site construction. Therefore, integrating the numerical simulation results with the practical requirements for the space needed in large-scale mechanized construction, the construction step distance for the base plate in Class II and Class III surrounding rock is ultimately adjusted to 300m, and the second lining step distance is adjusted to 400m.

5 CONCLUSION

This paper updates and optimizes the safety step distance for large-scale mechanized construction of the main tunnel of Ma Baishan Tunnel with Class II and Class III surrounding rocks. The main conclusions are as follows:

1) In terms of the deformation of the surrounding rock in the tunnel, it can be observed that, under the same rock classification, as the safety step distance increases, the settlement of the vault initially increases and then stabilizes. Similarly, the horizontal convergence initially increases and then remains stable. Both tunnel arch settlement and horizontal convergence show a slight increment with the enlargement of safety step distance.

2) In terms of the stresses on the support structure of the tunnel, the maximum compressive stresses on the Class II surrounding rock support structure are mainly distributed at the left and right footwalls of the tunnel due to stress concentration. The maximum compressive stresses on the Class III surrounding rock support structure are mainly located at the sidewalls. The maximum tensile stresses occur at the arch shoulders of the tunnel. With an increase in safety step distance, there is a slight increase in the maximum compressive and tensile stresses on the tunnel support structure.

3) The calculations show that the deformation of the tunnel surrounding rock and the force of the supporting structure will increase to a certain extent under the increased step spacing of Class II and III surrounding rock, but when the construction step spacing reaches the maximum, the deformation of the tunnel has not yet reached the limiting deformation value of the Class II and III surrounding rock, and the force of the supporting structure is also within the limiting stress range of C25 concrete. The support structure is still in a safe state. Therefore, the construction step distance for the base plate in Class II and Class III surrounding rock is adjusted to 300m, and the second lining step distance is adjusted to 400m, facilitating the subsequent implementation of large-scale mechanized construction.

COMPETING INTERESTS

The authors have no relevant financial or non-financial interests to disclose.

FUNDING

This research was funded by the China Railway Corporation Science and Technology Research and Development Programme Subject, grant number P2018G048, the Natural Science Foundation of Hebei Province, grant number E2021210124, and the Department of Education Natural Science Projects of Hebei Province, grant number ZD2019034.

REFERENCES

[1] HENCHER S R. The Glendoe Tunnel Collapse in Scotland. Rock Mechanics and Rock Engineering, 2019, 52(10): 4033-55.
[2] KITCHAH F, BENMEBAREK S, DJABRI M. Numerical assessment of tunnel collapse: a case study of a tunnel at the East–West Algerian highway. Bulletin of Engineering Geology and the Environment, 2021, 80(8): 6161-76.
[3] HONG Q, LAI H, LIU Y. Failure analysis and treatments of collapse accidents in loess tunnels. Engineering Failure Analysis, 2023, 145: 107037.
[4] HUANG F, ZHAO L, LING T, et al. Rock mass collapse mechanism of concealed karst cave beneath deep tunnel. International Journal of Rock Mechanics and Mining Sciences, 2017, 91: 133-8.
[5] OU G-Z, JIAO Y-Y, ZHANG G-H, et al. Collapse risk assessment of deep-buried tunnel during construction and its application. Tunnelling and Underground Space Technology, 2021, 115: 104019.
[6] FU H, XU W, WU Y. Research on the Influence of Tunnel Invert Excavation on the Rheological Deformation of Different Levels of Surrounding Rock. Applied Sciences, 2023, 13(12): 6960.
[7] Liao Haokui. Analysis of a soft rock subway tunnel collapse accident and optimization of construction safety step. South China University of Technology, 2022.
[8] WANG Q, IN Q, JIANG B, et al. Mechanized construction of fabricated arches for large-diameter tunnels. Automation in Construction, 2021, 124: 103583.
[9] KRAUZE K, BOŁOZ Ł, MUCHA K, et al. The mechanized supporting system in tunnelling operations. Tunnelling and Underground Space Technology, 2021, 113: 103929.
[10] Tong K. Research on the optimization of full-section excavation and construction step of Xinhua Tunnel. Shandong University, 2019.

[11] Hao Junming. Optimization study of step spacing for large-scale mechanized rapid construction of single-line tunnels. Railway Construction Technology, 2021(04): 115-118+130.
[12] Wang Hai-Zhou. Calculation Method of Safety Steps for Tunnel Xinao Method Construction. Lanzhou Jiaotong University, 2015.
[13] SHI Jiyao, WANG Yue. Analysis of the influence of arch step distance and step length on the stability of large section tunnels with soft rock. Tunnel Construction, 2017, 37(04): 428-434.
[14] Zhou Xueliang. Tunnel enclosure deformation monitoring and inverse analysis of enclosure parameters. Hefei University of Technology, 2007.
[15] Staudtmeister K, Rokahr R B .Rock mechanical aspects for the design of caverns in rock salt formations for the storage of compressed natural gas//Application of Computer Methods in Rock Mechanics—— International Symposium on Application of Computer Methods in Rock Mechnics & Engineering, 1993.

Eurasia Journal of Science and Technology
ISSN: 2663-1016
DOI: https://doi.org/10.61784/ejst3060

MULTI-FUNCTIONAL DRYING RACK DESIGN BASED ON INTERNET OF THINGS

JiaXin Luo*, Shuo Yang
School of Business, Guilin University Of Electronic Technology, Guilin, 541004, Guangxi Zhuang Autonomous Region, China.
Corresponding Author: JiaXin Luo, Email: 879471242@qq.com

Abstract: Intelligent home products are emerging, for the southern region of the climate is humid clothing easy to mold and bacteria, sudden changes in the weather can not collect clothes in time, the different orientation of the house leads to uneven light clothes, clothes for a long time without storage by the second pollution, this paper designs a QINHEALTH CH32V307 as the main control chip, combined with the temperature and humidity sensors, light sensors, humidity sensors to collect the environmental parameters and Bluetooth module, with automatic lifting, chain rotation, drying sterilization and other functions, users can monitor the clothes drying through APP intelligent, automated, multi-functional intelligent clothes airer. Supplemented with Bluetooth module, the multi-functional intelligent drying rack with automatic lifting, chain rotary, drying sterilization and other functions, realizes the intelligentization and automation of clothes drying, and the user can monitor the drying environment parameters and the state of clothes drying through APP. With the advantages of intelligence, automation and environmental protection, this drying rack provides convenience for contemporary urban life, meets the drying needs of different weather in different areas, and fills in the gaps for the smart home system.
Keywords: Smart clothes drying rack; Sensor; Automatic storage; Smart home; Artificial intelligence

1 INTRODUCTION

With the rapid change of science and technology, people's pace of life is significantly accelerated, and the practicality and intelligent requirements for daily necessities are also increasing, so the demand for smart home systems is constantly rising. Especially in the southern region of China, as the climate is mostly dark and humid, which brings considerable challenges to clothes drying, not only drying difficulties, but also easy to lead to moldy clothes[1] . Traditional drying methods are increasingly unable to meet modern people's pursuit of convenient, efficient and comfortable living due to poor ventilation, low automation levels and difficulties in adapting to complex and changing weather conditions.

In recent years, a large number of scholars at home and abroad have conducted relevant research on intelligent clothes drying racks. Based on STC89C52 microcontroller, scholars such as Xu Dongxue and Wei Fang designed an outdoor intelligent drying rack[2] which can dry clothes intelligently according to the weather change, it emphasizes the importance of the combination of hardware selection and software programming, which is of great significance to promote the development of intelligent drying rack technology. Scholars, such as Mr. Gan, Mr. Mu and other scholars designed an intelligent drying rack system with STM32 microcontroller as the main body[3]. The rack structure is simple, which solves the problems of high cost, complicated structure and difficult maintenance. Zhang Wei scholars proposed the optimization design of automatic rain control drying rack algorithm based on Arduino, which provides reference value for improving the automatic rain control system[4] . These researches provide important reference value for the intelligent drying rack designed in this paper, but for the existing intelligent drying rack there are problems such as single function, high energy consumption, and low degree of automatic control.

Therefore, this paper researches and designs an innovative multifunctional intelligentized clothes drying rack, which uses Qinheng CH32V307 as the main control chip and integrates temperature and humidity sensors, light sensors and other environmental monitoring devices, and is able to collect the surrounding environmental parameters in real time. When the weather conditions are detected to be unfavorable for clothes drying, the system will automatically activate the hood lifting mechanism and activate the drying and sterilization functions to ensure that the clothes can reach the ideal drying state in the shortest possible time while preventing the growth of mold[5] , as shown in Figure 1.

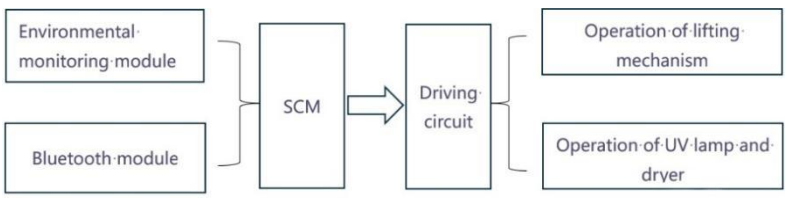

Figure 1 System Design Principle

2 SYSTEM HARDWARE DESIGN

2.1 Main Control Chip

This product uses the full-featured Qinheng CH32V307 as the main control chip, as shown in Figure 2.

Figure 2 CH32V307 Chip

2.2 Temperature and Humidity Sensors

The temperature and humidity sensor used is the DHT11 digital temperature and humidity sensor. The DHT11 digital temperature and humidity sensor is a temperature and humidity composite sensor containing a calibrated digital signal output, which applies dedicated digital module acquisition technology and temperature and humidity sensing technology to ensure that the product has a high degree of reliability and excellent long-term stability. The sensor consists of a resistive humidity sensing element and an NTC temperature sensing element, and is connected to a high performance 8-bit microcontroller. It has the advantages of excellent quality, ultra-fast response, strong anti-interference ability, cost-effective and so on, so it meets the requirements of temperature and humidity detection in this system.DHT11 adopts single-bus communication, i.e., there is only one data line to transmit the data, and the single-bus usually needs to be connected to an external pull-up resistor so that the state is high when the bus is idle. One pin of the microcontroller is connected to the data communication pin interface DATA for communication, as shown in Figure 3.

Figure 3 DHT11 Digital Temperature and Humidity Sensor

2.3 Temperature and Humidity Sensors

The raindrop sensor is made of high-quality FR-04 double-sided material with an extra-large area of 5.0 x 4.0 cm and a nickel-plated surface, which provides superior performance in terms of resistance to oxidation, conductivity, and longevity. The sensor can be used for monitoring various weather conditions, detecting whether it is raining and the size of the rainfall through the window, and converting it into a digital signal (DO) and analog signal (AO) output. This allows people to determine whether there is rain according to the high and low level of the output, and can also connect to the analog interface, which can detect the size of the rain, as shown in Figure 4.

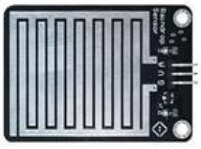

Figure 4 Raindrop Sensor

2.4 Light Intensity Sensor

The light intensity sensor uses a photoresistor module to detect light intensity. Inside the photoresistor module, the photoresistor is made of semiconductor material. The photoresistor utilizes the photoelectric effect of semiconductors, and its resistance value is inversely proportional to the light intensity. The photoresistor is very sensitive to ambient light, the stronger the light, the lower the resistance value, with the increase in light intensity, the resistance value decreases rapidly. Photoresistor module analog output AO can be connected to the AD module, through the AD

conversion, microcontroller AD acquisition can be obtained from the environmental light intensity of the precise value, and then according to the size of the value to determine the light intensity, as shown in Figure 5.

Figure 5 Light Intensity Sensor

2.5 Wireless Communication Module

The wireless communication module adopts HC-05 module, a high-performance master-slave integrated Bluetooth serial module, which can be paired with various computers with Bluetooth function, Bluetooth hosts, cell phones and other smart terminals. The advantages of this module are sensitive, easy to develop and cost-effective. When our cell phone APP is paired with the Bluetooth module, the microcontroller and the cell phone can communicate with each other, as shown in Figure 6.

Figure 6 Wireless Communication Module

2.6 Drying Systems

The module adopts the PTC heater it uses the fan to drum the air flow through the PTC electric heating element forced convection, as the main heat exchange mode, this high efficiency and excellent drying effect, fast warming and power consumption is small, with automatic thermostat function, there is a malfunction can be automatically disconnected, high security, and the PTC element generally has a waterproof function, as shown in Figure 7.

Figure 7 PTC Element

2.7 Weight Sensing

The weight sensor will record the weight of the clothes when they are hung up, and the intelligent sensing system will judge whether they are wet or dry, and the clothes will reduce their weight in the process of drying, and will remain unchanged after reaching a certain level. The gravity sensor judges whether the weight remains unchanged for a period of time, and if so, the clothes are judged to be dry, as shown in Figure 8.

Figure 8 Weight Sensor

2.8 Chain slewing system

Chain drive to achieve the clothes drying process of yin and yang conversion is the core system of this project, by the main control chip control motor driven chain to achieve directional timing fixed distance turnover, thus significantly improving the utilization of natural light and natural wind on the balcony, speeding up the speed of clothes drying at the same time, cleaner and more environmentally friendly. Its main working principle is. By the environment detection module to determine the current environment suitable for clothes drying, or by the cell phone to send a signal, the main control chip control motor to start working, the motor drives the gear and chain to complete the meshing, through the cell phone to set the turnover cycle and drying length, the chain drives the drying hooks in the hanger slots to achieve the balcony yin and yang side of the conversion cycle, as shown in Figure 9.

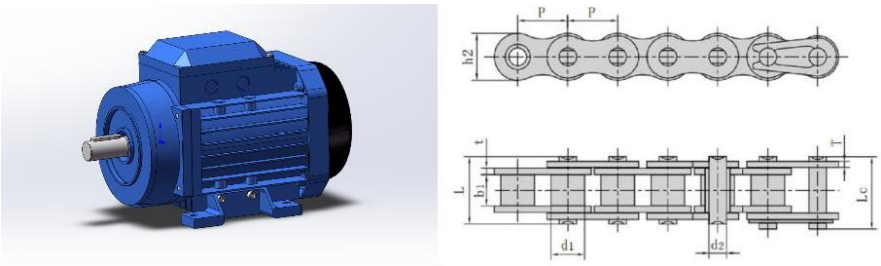

Figure 9 Schematic Diagram of the Motor and Chain Used

3 PRODUCT SOFTWARE DESIGN

3.1 Intelligent Automatic Mode

This product can be combined with the environment monitoring module, weight detection module feedback environment and clothing information, to realize the complete automation of clothing drying intelligent, drying is completed automatically lower the hood to achieve the temporary storage of clothing.

3.2 APP Remote Control Mode

Users can observe the clothes drying situation in real time through the cell phone APP, and adjust the working status of the drying rack remotely at any time[6] .

3.3 Remote Control Mode

In order to solve the situation that some elderly people have difficulty in using intelligent collection, this product can also use the simplified operation of the remote control to the product related remote control operation.

4 PRODUCT FUNCTION AND BASIC MODELS

4.1 Hanger Lifting System

Through the motor traction traction rope, both sides of the scissor frame to maintain the balance of the hanger, to achieve the hanger lifting and lowering, convenient for people to hang or remove the clothes on the hanger, at the same time after the rise of the hanger is also visually for the balcony to provide more space for indoor lighting.

4.2 Hood Lifting

When the weight detection system judges that the clothes are finished drying, the hood is automatically lowered to prevent the clothes from being polluted twice; when the environment monitoring module judges that the current environment is not suitable for drying, the system automatically lowers the hood and opens the drying system to avoid bacteria breeding and odor.

4.3 Chain Slewing System

Our products through the motor driven gears and chains to achieve clothing in the balcony yin and yang side of the cycle of rotation, so that the balcony yin and yang side of the clothes drying speed is the same, to solve the yin and yang side of the uneven drying of clothing problems. At the same time, it improves the utilization rate of natural resources such as sunlight and natural wind in the balcony, which is more energy- saving and green and environment-friendly than direct drying.

4.4 Drying Systems

In order to solve the user in the south wind days or rainy season and other cloudy and wet weather clothing is difficult to dry, easy to breed bacteria acidic and smelly problem, this drying rack using fans and sterilization ultraviolet lamps on the failure to dry the clothes in time for drying sterilization treatment, to ensure that the quality of the clothes drying (See Figure 10 and 11).

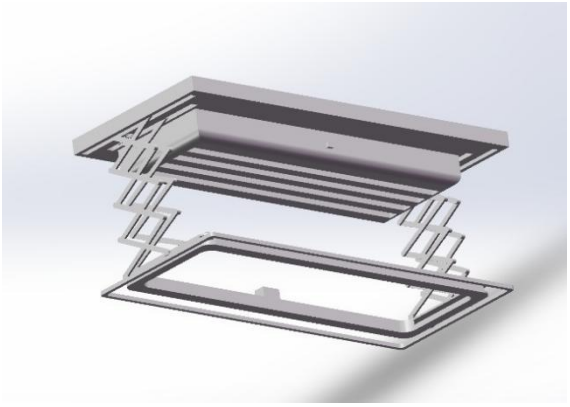

Figure 10 Unfolding of Drying Rack

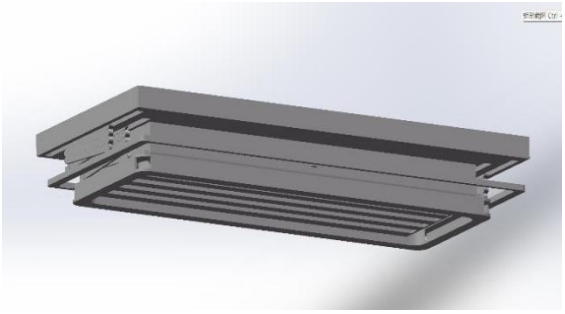

Figure 11 Drying Rack Storage

5 PRODUCT INNOVATION POINTS

This product cleverly combines the functions of drying, sterilizing and air-drying, and realizes the complete intelligence and automation of household drying racks through the environment detection module and Bluetooth system. In order to adapt to the big climate difference between north and south of China, such as rainy season and south wind weather, insufficient sunlight resources, air humidity, frequent precipitation, clothes drying will encounter long-term not dry, breeding bacteria, discoloration and mildew. As well as the user's residential floors and houses facing different directions lead to differences in lighting, clothes on different sides of different humidity and other issues.

5.1 Environmental Monitoring Systems

Through the temperature and humidity sensor, raindrop sensor, light sensor and other environmental monitoring modules, this product can monitor the clothes drying situation, outdoor weather conditions, etc. in real time through the cell phone APP, and can realize the complete intelligent automation of the clothes drying process through the main control chip.

5.2 Weight Monitoring System to Determine Whether Drying is Complete or Not

For users who have good drying environment and do not need to use the dryer, we have added a weight detection module, when the clothes are hung on the drying rack, the weight detection module automatically records an initial weight, when the weight of the clothes is reduced to a certain value and does not fall for a long time when the clothes calculate a final weight, the main control chip calculates the standard index of dryness of the clothes according to the two values, and when the index reaches 70-90%, the main control chip determines that the clothes have been dried. When this index reaches 70%-90%, the main control chip judges that the clothes have been dried, and transmits the message of clothes drying completion to the user's cell phone through the wireless communication module, and automatically lowers the garment cover to realize the temporary storage of clothes. If the index does not reach 70%, it will judge that the clothes are not dry, lower the hood and turn on the dryer for drying, until the index reaches 70% and the humidity in the hood is not higher than 40%, then the clothes will be judged dry.

5.3 Chain Slewing System

The use of motor-driven chain, through the main control chip to control the motor direction, timing, fixed- distance slewing so as to realize the clothing balcony small area of limited sunlight resources, can be faster to make the clothes drying. At the same time, compared with direct drying of clothes, it can increase the utilization rate of sunlight, natural wind and other clean energy.

6 CONCLUSION

According to the different weather conditions around the world, for the traditional drying racks with poor ventilation effect, low automation degree, to cope with the complex and changing climate and other problems and facing the rise of lazy economy, the multi-functional intelligent drying racks designed by QINHENG CH32V307 chip as the main control chip, combined with temperature and humidity sensors, raindrop sensors, light intensity sensors, and weight sensor are conducive to the timely collection of weather data, and the dryer and UV lamp can be opened to assist drying and sterilization. Under the environment not suitable for drying, the hood is lowered to realize clothing storage, and the dryer and ultraviolet light are opened to assist in drying and sterilization. This product is cleverly equipped with a fan and a sterilization ultraviolet light, which provides timely sterilization and drying treatment for the clothes, prevents bacteria from breeding and producing bad smells, and broadens the use of the product to increase the product's cost-effectiveness. In terms of intelligent remote control, this drying rack uses Bluetooth module to connect with cell phone or use the remote control to manually adjust or select the intelligent mode of the drying rack, and the drying rack automatically completes the whole process of clothes drying. Compared with the various brands of drying racks on the market, this product greatly improves the intelligence of the clothes drying process, adding convenience to modern urban life.

FUNDING

This work was financially supported by 2024 Guangxi Zhuang Autonomous Region Student Entrepreneurship and Innovation Program: Muyang Technology - Smart balcony new choice (202410595102X) fund.

CONFLICT OF INTEREST

The authors have no relevant financial or non-financial interests to disclose.

REFERENCES

[1] Yao Jia, Wang Youyou, Wu Aihua. Design and Implementation of a New Intelligent Clothes Drying Device. Science and Technology Information, 2019, 22(16): 30-33.
[2] Xu Dongxue, Wei Fang, Xing Chunxiao, et al. Design of a New Intelligent Telescopic Air-drying Hanger. Xinjiang Agricultural Mechanization, 2022, (04): 17-19.
[3] Gan Jiayi, Mu Wenjing. Design and Implementation of Intelligent Drying Hanger System Based on Singlechip. Heilongjiang Science, 2024, 15(04): 138-140.
[4] Zhang Wei, Optimization algorithm design of automatic rain control clothes hanger based on Arduino. Chinese Journal of Integrated Circuits, 2023, 32(06): 58-61.
[5] Zhang Weiwei. Design and Implementation of an Intelligent Clothes Hanger. Electronic Technology, 2022, 51(05): 210-211.
[6] Yang Xianbin. Design of Intelligent Clothes Hanger Based on Internet of Things. Value Engineering, 2023, 42(32): 77-79.

Eurasia Journal of Science and Technology
ISSN: 2663-1016
DOI: https://doi.org/10.61784/ejst3062

PERCEIVED DISCRIMINATION AND DEPRESSION AMONG ECONOMICALLY DISADVANTAGED COLLEGE STUDENTS: THE MEDIATING ROLE OF STRESS AND SELF-ESTEEM

ShuangLe Fu[1,2], Bin Liu[3*], Li Zhu[4]
[1]*School of Elderly Care Services and Management, Nanjing University of Chinese Medicine, Nanjing 210023, Jiangsu, China.*
[2]*School of Aging Industry, Nanjing University of Chinese Medicine, Nanjing 210023, Jiangsu, China.*
[3]*JiangSu Provincial Academy of Social Sciences, Nanjing 210004, Jiangsu, China.*
[4]*School of Social and Behavioral Sciences, Nanjing University, Nanjing 210023, Jiangsu, China.*
Corresponding Author: Bin Liu, Email: binziliu@163.com

Abstract: A growing of research suggests a clear positive correlation between perceived identity discrimination and depression. However, the various intermediary processes behind this connection have not been adequately studied. The purpose of this study was to investigate the relationship between perceived discrimination and depression among economically disadvantaged college students, as well as the mediating role of stress and self-esteem. An online questionnaire was distributed to collect data. The sample consisted of 896 students from economically disadvantaged families from 22 universities. Descriptive statistics and Pearson correlation analysis were performed using stata (16.0) and structural equation modeling (SEM) was performed by Mplus (8.0). The results showed that identity discrimination was positively correlated with stress and depression in college students with family economic difficulties. Stress and self-esteem mediated the relationship between identity discrimination and depression among poor students, and the perceived stress caused by discrimination had a negative impact on self-esteem, thereby reinforcing depression; These findings are of great significance for the prevention and intervention of depression in college students with economically disadvantaged. This study focused on the impact of perceived identity discrimination on depression among economically disadvantaged college students, with stress and self-esteem acting as mediating factors. It reflects the potential risks brought by the funding project to the financially disadvantaged college students, and provides a basis for the implementation of the university funding policy and the active intervention of the mental health of the economically disadvantaged college students.
Keywords: Perceived discrimination; Depression; Economically disadvantaged; Stress; Self-esteem

1 INTRODUCTION

According to the data of the National Student Financial Aid Development Report (2021),[1] there are 8.7094 million college students in China who need to apply for national financial aid to help them complete their studies, accounting for about 20% of the total number of college students that year. The current funding system requires economically disadvantaged college students to complete the identification of financially disadvantaged students in order to receive financial aid, collectively referred to as "economically disadvantaged students," similar to an identity label. This economic disadvantage can take a toll on their mental health. Previous research has shown that children from financially disadvantaged families are more likely to be disadvantaged in college than students from financially well-off families.[2,3] They may have a strong sense of inferiority, excessive inferiority, excessive self-esteem and so on, compared with other students.[4] In addition, their paranoid, social withdrawal and social aggression scores were significantly higher than those of non-poor students.[5] The identity label of poor students often brings stigma and discrimination to them, making them feel different from others and even suffer some unfair treatment.

Discrimination based on class is more widespread among economically disadvantaged college students, and these students are more stressed than others owing to their families' financial challenges in affording college.[6,7] They experience a change in their identity after applying for financial aid, and the discrimination and self-stigma attached to their identity label lead to poor physical and mental health.[8,9] Studies have shown that perceived discrimination puts economically disadvantaged college students at potential threats, the most obvious of which is depression.[10,11] While previous studies have shown that discrimination and individual depression are highly correlated, [12-14] few of these studies have specifically focused on perceived status-based discrimination among economically disadvantaged college students. Therefore, the purpose of this study was to investigate how perceived discrimination affects the mental health of economically disadvantaged college students. In addition, we wanted to look at the role of stress and self-esteem in mediating perceived discrimination and depression among economically disadvantaged college students.

1.1 Perceived Discrimination and Depression

Perceived discrimination is an important predictor of self-assessed mental health,[13] and self-reported levels of discrimination are more likely to cause harm to individuals than actual adverse situations. Perceived discrimination

affects self-rated health status,[15] and discrimination is associated with higher crime rates.[16] Current research on discrimination and depression focuses on race,[17-19] gender,[20] and heterosexuality,[21] using Risk models confirm that multiple forms of discrimination are associated with a higher risk of depressive symptoms.[22] Among them, identity labels are more likely to make people perceive discrimination and express mental distress.[23] The impact of perceived discrimination on vulnerable groups is larger, and the negative impact on their well-being is particularly significant.[14] It is possible to argue that the negative impact of perceived discrimination on individual mental health is critical. Perceived discrimination is more widespread among socially disadvantaged persons, which may explain some of the relationship between disadvantaged social position and mental health.[24]

1.2 The Mediating Role of Stress

Stress is related to external events experienced by people, which may exceed the individual's ability to bear and even induce mental or physical illness.[25] Identity affiliation is directly related to an individual's mental health and can also interact with stressors, and identity characteristics can contribute to a certain degree of stress and distress. Individuals with complex self-identities are less likely to be depressed when faced with stress, while individuals with problems with self-identity are more likely to experience stress that further damages or threatens their self-perception and psychological state. In existing studies, exposure to stressors is an important predictor of depression,[26,27] and college students who are economically disadvantaged are more likely to experience stress, and these stressors increase depression in all groups and anxiety symptoms, but this effect is particularly severe in groups that have previously suffered financial hardship.[28,29] Previous research has demonstrated a significant relationship between stress and depression in economically disadvantaged college students, with perceived discrimination increasing stressor exposure and vulnerability to stress, which in turn leads to symptoms of depression,[30] higher depressive symptoms are a direct result of stress caused by poverty.[31] According to the findings, perceived persistent discrimination was linked to greater stress and depression. Combining these studies, we hypothesized that stress may be a mediating factor linking perceived discrimination and depression in college students with financially disadvantaged families.

1.3 The Mediating Role of Self-Esteem

Discrimination has been linked to depression and low self-esteem in studies examining the consequences of perceived discrimination on mental health.[32,33] Members of stigmatized groups may have lower self-esteem, yet self-esteem has been shown to mitigate discrimination-pain correlations.[34] Low self-esteem and depression are also tightly associated, as low self-esteem may lead to depression,[35] depression can destroy self-esteem,[36] and the influence of self-esteem on depression is substantially larger than the effect of depression on self-esteem.[37] Individuals with high vulnerability to self-esteem have higher responses to discrimination and higher levels of depression.[38] The involvement of self-esteem as a mediator in the pathways of perceived discrimination and psychological stress has also been shown.[32,39,40] Furthermore, prospective studies have shown that people at risk of developing depressive symptoms following life stress show more unstable self-esteem than those without risk.[41] Self-esteem instability interacts with perceived stress variability and depressive mood variability,[35,42] and self-esteem plays a role in moderating social exclusion responses.[43] Based on the above studies, we hypothesized that self-esteem may be a mediating factor linking perceived discrimination and depression among college students with financial disadvantages.

1.4 The Present Study

As noted above, few studies have explicitly focused on the mental health effects of economically disadvantaged college students' perceived discrimination because of their status, and the mediating role of stress and self-esteem in this relationship requires further research. In contrast, research on perceived discrimination has focused on categories (race, gender, heterosexuality, etc.) and groups (psychiatric, physical disabilities, immigrants, single mothers, etc.). Most of the research has focused on the social support and group identification that financially disadvantaged college students bring to apply for grants, while the stigma and discrimination that this identification entails have been overlooked. To address this research gap and better conduct financial aid for disadvantaged college students to reduce negative effects, the purpose of this study was to look at the influence of perceived discrimination on depression among economically disadvantaged college students, as well as the role of stress and self-esteem in mediating this process. Based on our analysis of the literature, we suggest the following hypotheses:

H1: In college students from economically disadvantaged backgrounds, perceived discrimination is a strong predictor of depression.

H2: The link between depression and perceived discrimination is mediated by stress.

H3: The relationship between perceived discrimination and depression is mediated by self-esteem.

H4: Stress and self-esteem as mediators of perceived discrimination and depression among economically disadvantaged college students.

2 MATERIAL AND METHODS

2.1 Data and Participants

The data used in this study is based on the "Tao Students Panel Survey" (TSPS) student aid program. The survey was launched in 2018 by a research team from Nanjing University. It conducts a questionnaire survey on college students funded by the Jiangsu Tao Shing Pee Education Foundation from March to May every year, aiming to understand their development after receiving the funding. The data used this time comes from a May 2022 survey of seniors who had received financial aid for four consecutive years. The foundation has cooperative relations with 22 universities in Jiangsu Province, China. The foundation sponsors 200 students in each school each year and 50 in each grade from freshman to senior year. These sponsored students were selected based on three screenings: first, their household registration was in rural areas; second, their families could not afford their college expenses due to financial difficulties; and third, they had certain plans for their future. Those who pass these conditions are selected to become members of the program and receive 5,000 RMB of financial aid each year from the beginning of the first year to the end of the senior year. If a student's family's financial situation improves during the process, funding for him will be stopped. Affected by the control of the COVID-19 epidemic in Chinese universities, the research team did not have the right to enter each university to conduct on-site investigations. Hence, the survey took the form of an online questionnaire. Participants were invited to fill out a questionnaire based on the email addresses they left when applying for funding. The purpose of the investigation and research is fully explained in the email, and the answering session can only be entered after obtaining their informed consent. The ethics committee approved the protocol for this study of the investigator's university. The procedures used in this survey follow the Declaration of Helsinki principles. A total of 1050 questionnaires were sent out, and 896 were recovered, with an effective recovery rate of 85.3%. Participants included 312 (34.82%) men and 584 (65.18%) women. Participants ranged in age from 19 to 26, with an average age of 22.56. 707 (78.91%) participants had siblings, and 653 (72.88%) were first-generation college students in their families, with an average annual family income of no more than 40,000 RMB. Table 1 shows descriptive data for the study sample.

Table 1 Demographic Characteristics of Participants (N = 896)

	Frequency (N) / M	Percentage (%) / S.D.
Gender		
Male	312	34.82%
Female	584	65.18%
Age	M=22.565	S.D.=0.912
Only child		
Yes	189	21.09%
No	707	78.91%
First Generation College Student		
Yes	653	72.88%
No	243	27.12%
Family income	M=3.851	S.D.=2.596

Abbreviations: M, means; SD, standard deviations

2.2 Measurement

2.2.1 Perceived discrimination

Responses to the questionnaire "Do you feel discriminated against at school because of your identity as an economically disadvantaged student?" were used to assess perceived discrimination by economically disadvantaged university students. This question was aimed to illustrate the impact that challenging student status has on individuals by emphasizing the prejudice that comes with the status classification. The responses ranged from '1=never' to '5=always' on a 5-point Likert scale. The higher the score, the greater the level of discrimination experienced by economically disadvantaged university students.

2.2.2 Perceived stress

The 4-item Perceived Stress Scale (PSS-4) was used to assess stress,[44] and respondents were asked to report how much control they had over important things in their lives in the previous month, confidence in dealing with difficulties, and whether events are going the way they want (eg: how often have you felt that things were going your way in the last month?). Answers are on a scale from 0 (never) to 4 (very often). The PSS-4 score is obtained by adding the scores for the four questions, with the second and third questions being reversed. The highest score for this measure is 16. The PSS-4's Cronbach's alpha in this study was 0.698.

2.2.3 Self-esteem

The Rosenberg (1979) Self-Esteem Scale (RSES),[45] which consists of 10 questions with five positive and five negative statements (for example, "I believe that I have a number of nice attributes. "), was used in this study to gauge respondents' overall judgments of self-esteem (eg, "I feel I do not have much to be proud of."). Response scores on the 4-point Likert scale range from 1 (strongly disagree) to 4 (strongly agree) (completely agree). The RSES's Cronbach's alpha in this study was 0.857.

2.2.4 Depression

This study used the 20-item CESD scale for depression testing,[46] which asked participants to report how often they felt and behaved during the past week, including 16 negative items (eg, "I feel alone." "I don't sleep well." "I feel like my life is a failure.") and 4 positive items (eg, "I am happy." "My life is meaningful."), answered on a scale from 0 (rarely or none of the time) to 3 (most or all of the time), with 4 positive items for reverse scoring. The higher the score after the items are added together, the stronger the degree of depression. In this study, the Cronbach's alpha for CESD was 0.931.

2.2.5 Covariates

In our study, we also controlled for the following covariates: gender, age, only child, first-generation college students, and family income. Gender (0=male, 1=female); age in years; only child (0=no, 1=yes); first-generation college students (0=yes, 1=no); household income was a continuous variable in tens of thousands.

2.3 Data Analysis

First, descriptive statistics for all key variables, including frequency, mean, standard deviation, and percentage, were performed in Stata 16.0, followed by a Pearson correlation analysis of the interrelationships between all key variables in the study. Second, SEM analysis was performed using Mplus8.0.[47] After establishing the impact of perceived discrimination on depression, we include stress and self-esteem as mediating factors to examine the significance of the direct effect of perceived discrimination on depression. In this study, we used the following metrics to evaluate model fit, (1) a value of $\chi 2/df$ less than 5 was considered "reasonable".[48] (2) The Tucker-Lewis index (TLI) and the comparative fit index (CFI) are both larger than 0.90.[49] (3) The approximation's root mean square error (RMSEA) is less than 0.06,[50] and (4) SRMR (standardized root mean square residual error) is less than 0.08.[51] The above five indices are all used to evaluate the fit of the model. In addition, for estimate, we employed 95% percentile confidence intervals based on 5000 bootstrap samples and bias-corrected 95% bootstrap confidence intervals (CI). When the 95% CI value did not contain zero, the mediation effect was statistically significant.[52]

3 RESULT

3.1 Preliminary Analyses

The mean, standard deviation, and bivariate correlations for all major variables in this investigation were shown in Table 2. According to the correlation results, perceived discrimination was positively connected with sadness ($r=0.247$, $p<0.001$), stress ($r=-0.164$, $p<0.001$), and negatively correlated with self-esteem ($r=-0.194$, $p<0.001$) of economically disadvantaged college students. These findings provide support for our hypothesis to test mediation effects.

Table 2 Key Variable Descriptive Statistics and Correlations (N = 896)

	Range	M	S.D.	1	2	3	4
Perceived discrimination	1-5	1.540	0.745	1			
Stress	0-4	2.496	0.470	0.090***	1		
Self-esteem	1-4	2.880	0.347	-0.194***	-0.206***	1	
Depression	0-3	0.929	0.476	0.247***	0.336***	-0.589***	1

Note: *** is p< 0.001, ** is p< 0.05, * is p< 0.01
Abbreviations: M, means; S.D., standard deviations

3.2 Mediation Analysis

The structural model, as illustrated in Figure 1, exhibits the influence of perceived discrimination on depression. The fitting index of the structural model is $\chi 2/df=1.537$, $p<0.001$, CFI=0.990, TLI=0.979, RMSEA=0.024, SRMR=0.025, indicating that the fitting effect of the model is good. Perceived discrimination had a significant direct effect on depression ($\beta=-0.077$, $P<0.001$). As a result, this investigation supports Hypothesis 1. In economically disadvantaged college students, perceived discrimination had a beneficial influence on depression.

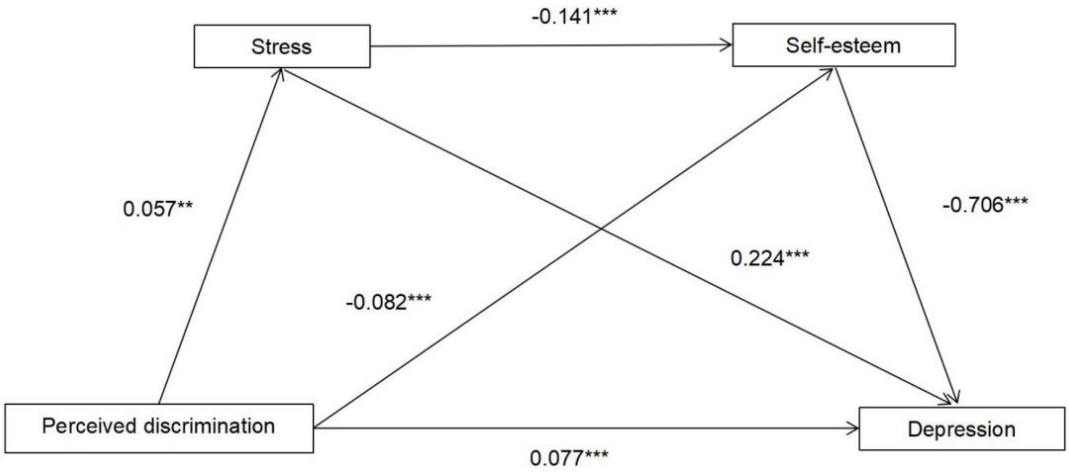

Figure 1 Result of Structural Model

Note: Standardized estimates. Covariate coefficients including gender, age, only child, first-generation college students, and household income are not shown in the figure. Significant paths are indicated with asterisks; *** is p< 0.001, ** is p< 0.05, * is p< 0.01

Moreover, in order to investigate the mediating impacts of stress and self-esteem, the study looked at the direct effects of perceived discrimination on depression as well as the indirect effects via stress and self-esteem mediation pathways (Table 3). The results show that perceived discrimination can directly (β=0.121, 95%CI=[0.043, 0.110]) and indirectly (β=0.120, 95%CI=[0.052, 0.102]) affect the economic difficulties of college students depression. This leads in a total effect size of (β=-0.240, 95%CI=[0.113, 0.195]). The mediation model revealed that the indirect effect of perceived discrimination mediated by stress on depression was considerable. The mediation model revealed that the indirect effect of perceived discrimination mediated by stress on depression was significant (β=0.020, 95%CI=[0.004, 0.023]). Hypothesis 2 was supported. Furthermore, the indirect effect of perceived discrimination mediated by self-esteem on depression was significant (β=0.091, 95%CI=[0.036, 0.083]). Hypothesis 3 is supported. Finally, the indirect effect of perceived discrimination mediated by stress and self-esteem on depression was significant (β=0.009, 95% CI=[0.002, 0.011]). Therefore, Hypothesis 4 was supported by this study.

Table 3 Standardization's Mediated Path Effects

Model pathways	Estimate	S.E	95% CI
Total Effect	0.240	0.033	[0.113, 0.195]
Direct effects	0.121	0.027	[0.043, 0.110]
Total Indirect Effect	0.120	0.020	[0.052, 0.102]
PD→Stress→Depression	0.020	0.007	[0.004, 0.023]
PD→SE→Depression	0.091	0.019	[0.036, 0.083]
PD→Stress→SE→Depression	0.009	0.004	[0.002, 0.011]

Note: standardized estimating of 5000 bootstrap sample.
Abbreviations: PD, perceived discrimination; SE,self-esteem; CI, confidence interval.

4 DISCUSSION

The purpose of this study was to look at the impact of stress and self-esteem in the relationship between perceived discrimination and depression among economically disadvantaged college students. The results of the study are consistent with our expectations, that is, perceived discrimination positively predicts depression in college students from disadvantaged families, and stress and self-esteem have a strong mediation influence on perceived discrimination and depression.

First, the findings suggest that perceived discrimination can harm the mental health of economically disadvantaged college students, which is consistent with earlier research.[3,6] Receiving financial help, in particular, may identify and stigmatize people, causing them to feel discriminated against. And the more intense their feeling of discrimination, the more depressed they will become. Economic inequities in colleges will make economically disadvantaged college students more stressed. Their family background, consumption habits, and identification characteristics will cause them to feel isolated from the people around them, as well as psychological resistance, making it much simpler for them to feel discriminated against.[30] At the same time, this discrimination is accompanied by stress, which contributes to their depression. Due to the economic disadvantage of their family, some students choose part-time jobs and loans to help

them finish their studies to relieve financial pressure, but these measures are more likely to increase their pressure.[53,54] This study supports the hypothesis of a stress-mediated mediating effect, confirming that perceived discrimination causes more stress and that more stress causes more depression. As a result, assisting economically disadvantaged college students in reducing psychological stress is a feasible measure to prevent depression among economically disadvantaged college students. This highlights the importance of economic disadvantage, which can lead to psychological distress.

Second, this study demonstrated the important links between perceived discrimination, stress, self-esteem, and depression as well as the mediating function that self-esteem played between perceived discrimination and depression. This study concluded that self-esteem is both a mediator of perceived discrimination and depression, and a mediator of stress and depression, and stress is a mediator of perceived discrimination and self-esteem. Our hypothesis is supported by the involvement of self-esteem as a mediator. Specifically, people who perceive strong discrimination negatively affect their self-esteem and increase their depression. Perceived discrimination can also increase an individual's depression by increasing their stress, causing damage to their self-esteem. Numerous studies have shown that receiving funding can relieve their financial pressure.[55,56] But requiring them to demonstrate why they are poor to qualify for funding, and making their poor status public creates discrimination. The process of obtaining financial aid can also bring psychological stress, and the exposure to their privacy can create feelings of inferiority and hurt the self-esteem of economically disadvantaged college students. Despite the fact that several studies have found a direct or indirect relationship between perceived discrimination and sadness, less attention has been paid to difficult students who already have family financial problems and received financial aid, and stress and self-esteem have not been used as mediators between perceived discrimination and depression. As a result, this study examines the influence of perceived discrimination on the depression of economically disadvantaged college students, with a focus on the discrimination and stress caused by economic disadvantage, and employs stress and self-esteem as mediators. There is also a lack of such research in the literature on the negative effects of financially disadvantaged college students' post-funded status transition. The results of this study can also help to fund policymakers, college administrators, and economically disadvantaged college students to take steps to reduce the pressures of the poor student status, improve their self-esteem, reduce the sense of discrimination caused by this status, and ultimately Relief of depression in economically disadvantaged college students.

5 LIMITATIONS AND FUTURE RESEARCH DIRECTIONS

It is necessary to note several significant study limitations. First of all, this study relies on the self-reports of economically disadvantaged college students regarding their perceptions of discrimination as poor students and has a relatively small measurement dimension of perceived discrimination. Although the experience of perceived discrimination is largely a subjective one, future research must establish a more varied method of measuring perceived discrimination to improve it. Second, the cross-sectional design of the study makes it challenging for us to analyze the relationship between variables in the model, even though the study's data pertains to financially disadvantaged college students who have received financial aid for four years. If more conclusions about the causal relationships and pathways between perceived discrimination, stress, low self-esteem, and depression are required, longitudinal tracking data should also be included. The third feature is that the questionnaires are distributed electronically. There is a lack of supervision in answering the questions, and the filling may be easily influenced by uncontrollable interference.

6 CONCLUSIONS

This study examines the association between perceived discrimination, stress, self-esteem, and depression among economically disadvantaged college students, therefore broadening the impact of identity discrimination on economically disadvantaged college students. The findings support the direct impact of felt discrimination on depression in economically disadvantaged college students, emphasizing the importance of stress and self-esteem in the relationship between perceived discrimination and depression . The connections between perceived discrimination and stress, self-esteem, and depression demonstrate how perceived discrimination affects depression. The present study reflects the unintended consequences of financial aid, and the identification tag attached to financial aid can bring certain psychological distress to economically disadvantaged college students. Considering these potential influencing factors, these findings can provide valuable insights into how to better finance the well-being of economically disadvantaged college students, alleviate their psychological distress, and adopt positive psychological interventions. Relieving the pressure of college students with financial difficulties and enhancing their self-esteem can play a positive preventive role. In the process of funding, a multi-faceted support system is established, which is not limited to providing material assistance, but also guides them to correctly deal with economic disadvantages. Further studies are needed to improve the mental health of financially disadvantaged college students and to explore how to address the negative impact of receiving financial aid on financially disadvantaged college students to better consolidate financial aid outcomes.

COMPETING INTERESTS

The authors have no relevant financial or non-financial interests to disclose.

FUNDING

This work was funded by Jiangsu Education Department(2023SJYB0323); School of Elderly Care Services and Management(School of aging industry), Nanjing University of Chinese Medicine (2024YLFWYGL009).

REFERENCES

[1] Ministry of Education of the People's Republic of China. CHina student financial aid development report, 2021. Available from: https://m.gmw.cn/baijia/2021-09/17/35172741.html. Accessed October 10, 2023.
[2] Walpole M. Socioeconomic status and college: How SES affects college experiences and outcomes. Review of Higher Education, 2003, 27: 45-73.
[3] Drotos SM, Cilesiz S. Shoes, dues, and other barriers to college attainment: Perspectives of students attending high-poverty, Urban high schools. Education and Urban Society, 2016, 48: 221-244.
[4] Li CS. The manifestations and countermeasures of the psychological problems of impoverished college students. Higher Engineering Education Research, 2002, 6: 49-51.
[5] Li XH. Reflections on Mental Health Education for the Poor Students. China Higher Education Research, 2001, 12: 64-65.
[6] Goodman E, Amick BC, Rezendes MO, et al. Adolescents' understanding of social class: a comparison of white upper middle class and working class youth. Journal of Adolescent Health, 2000, 27: 80-83.
[7] Goodman E, McEwen BS, Dolan LM, et al. Social disadvantage and adolescent stress. Journal of Adolescent Health, 2005, 37: 484-492.
[8] Kalisova L, Michalec J, Hadjipapanicolaou D, et al. Factors influencing the level of self-stigmatisation in people with mental illness. International Journal of Social Psychiatry, 2018, 64: 374-380.
[9] Schomerus G, Angermeyer M. Stigma and its impact on help-seeking for mental disorders: What do we know? Epidemiologia E Psichiatria Sociale, 2008, 17: 31-37.
[10] Yu QY. Mediating roles of rejection sensitivity and depression in the relationship between perceived discrimination and aggression among the impoverished college students. Chinese Journal of Clinical Psychology, 2018, 6: 1100-1103.
[11] Li DP, Xu L, Bao ZY, et al. Family financial strain and adolescents' depression: The effects of perceived discrimination and parent-adolescent attachment. Psychological Development and Education, 2015, 6: 342-349.
[12] Gayman MD, Barragan J. Multiple Perceived Reasons for Major Discrimination and Depression. Society and Mental Health, 2013, 3: 203-220.
[13] Monk EP. The cost of color: Skin color, discrimination, and health among African-Americans. American Journal of Sociology, 2015, 121: 396-444.
[14] Schmitt MT, Branscombe NR, Postmes T, et al. The consequences of perceived discrimination for psychological well-being: A meta-analytic review. Psychological Bulletin, 2014, 140: 921-948.
[15] Finch BK, Hummer RA, Kol B, et al. The role of discrimination and acculturative stress in the physical health of mexican-origin adults. Hispanic Journal of Behavioral Sciences, 2001, 23: 399-429.
[16] Joanna LW, Sophie MA, Myles ID, et al. The protective role of ethnic identity for urban adolescent males facing multiple stressors. Journal of Youth and Adolescence, 2014, 43: 1728-1741.
[17] Andrade N, Ford AD, Alvarez C. Discrimination and latino health: A systematic review of risk and resilience. Hispanic Health Care International, 2021, 19: 5-16.
[18] Hooker K, Phibbs S, Irvin VL, et al. Depression among older adults in the united states by disaggregated race and ethnicity. The Gerontologist, 2019, 59: 886-891. DOI: 10.1093/geront/gny159.
[19] Karlsen S, Nazroo JY. Relation between racial discrimination, social class, and health among ethnic minority groups. American Journal of Public Health, 2002, 92: 624-631.
[20] Mishel E. Discrimination against queer women in the U.S. workforce: A résumé audit study. Socius, 2016.
[21] Meyer IH. Prejudice, social stress, and mental health in lesbian, gay, and bisexual populations: Conceptual issues and research evidence. Psychological Bulletin, 2003, 129: 674-697.
[22] Vargas SM, Huey SJ, Miranda J. A critical review of current evidence on multiple types of discrimination and mental health. American Journal of orthopsychiatr, 2020, 90: 374-390.
[23] Xin M, Luo S, She R, et al. Negative cognitive and psychological correlates of mandatory quarantine during the initial COVID-19 outbreak in China. American Psychologist, 2020, 75: 607-617.
[24] Kessler RC, Mickelson KD, Williams DR. The prevalence, distribution, and mental health correlates of perceived discrimination in the United States. Journal of Health and Social Behavior, 1999, 40: 208-230.
[25] Dohrenwend BP. The role of adversity and stress in psychopathology: Some evidence and its implications for theory and research. Journal of Health and Social Behavior, 2000, 41: 1-19.
[26] Bolger N, DeLongis A, Kessler RC, et al. Effects of daily stress on negative mood. Journal of Personality and Social Psychology, 1989, 57: 808-818.
[27] Rudenstine S, McNeal K, Schulder T, et al. Depression and anxiety during the COVID-19 pandemic in an urban, low-income public university sample. Journal of Traumatic Stress, 2021, 34: 12-22.
[28] Gili M, Roca M, Basu S, et al. The mental health risks of economic crisis in Spain: Evidence from primary care centres, 2006 and 2010. European Journal of Public Health, 2013, 23: 103-108.

[29] Henninger WR, Luze G. Poverty, caregiver depression and stress as predictors of children's externalizing behaviours in a low-income sample. Child & Family Social Work, 2014, 19: 467-479.
[30] Pearlin LI, Menaghan EG, Lieberman MA, et al. The stress process. Journal of Health and Social Behavior, 1981, 22: 337-356.
[31] McDonald A, Thompson AJ, Perzow SED, et al. The protective roles of ethnic identity, social support, and coping on depression in low-income parents: A test of the adaptation to poverty-related stress model. Journal of Consulting and Clinical Psychology, 2020, 88: 504-515.
[32] Cassidy C, O'Connor RC, Howe C, et al. Perceived discrimination and psychological distress: The role of personal and ethnic self-esteem. Journal of Counseling Psychology, 2004, 51: 329-339.
[33] Mereish EH, N'cho HS, Green CE, et al. Discrimination and depressive symptoms among black American men: Moderated-Mediation effects of ethnicity and self-esteem. Behavioral Medicine, 2016, 42: 190-196.
[34] Crocker J, Major B. Social stigma and self-esteem—The self-protective properties of stigma. Psychological Review, 1989, 96: 608-630.
[35] Roberts JE, Kassel JD, Gotlib IH. Level and stability of self-esteem as predictors of depressive symptoms. Pers Personality and Individual Differences, 1995, 19: 217-224.
[36] Sowislo JF, Orth U. Does low self-esteem predict depression and anxiety? A meta-analysis of longitudinal studies. Psychological Bulletin, 2013, 139: 213-240.
[37] Franck E, De Raedt R. Self-esteem reconsidered: Unstable self-esteem outperforms level of self-esteem as vulnerability marker for depression. Behaviour Research and Therapy, 2007, 45: 1531-1541.
[38] Meier LL, Semmer NK, Hupfeld J. The impact of unfair treatment on depressive mood: The moderating role of self-esteem level and self-esteem instability. Personality and Social Psychology Bulletin, 2009, 35: 643-655.
[39] Corning AF. Self-esteem as a moderator between perceived discrimination and psychological distress among women. Journal of Counseling Psychology, 2002, 49: 117-126.
[40] Fischer AR, Holz KB. Perceived discrimination and women's psychological distress: The roles of collective and personal self-esteem. Journal of Counseling Psychology, 2007, 54: 154-164.
[41] Gable SL, Nezlek JB. Level and instability of day-to-day psychological well-being and risk for depression. Journal of Personality and Social Psychology, 1998, 74: 129-138.
[42] Rosenberg M. Self-concept from middle childhood through adolescence. In: Suls J, editors. Psychological perspectives on the self, Vol. 3. Hillsdale NJ: Erlbaum, 1986: 107-136.
[43] Leary MR. Responses to social exclusion: Social anxiety, jealousy, loneliness, depression, and low self-esteem. Journal of Social and Clinical Psychology, 1990, 9: 221-229.
[44] Cohen S, Kamarck T, Mermelstein R. A global measure of perceived stress.Journal of Health and Social Behavior, 1983, 24: 385-396.
[45] Rosenberg M. Conceiving the Self. New York, NY: Basic Books, 1979.
[46] Radloff LS. The CES-D scale: A self-report depression scale for research in the general population. Applied Psychological Measurement, 1977, 1: 385-401.
[47] Cheung MW-L. Multivariate meta-analysis as structural equation models. Structural Equation Modeling, 2013, 20: 429-454.
[48] Schumacker RE, Lomax RG. A beginner's guide to structural equation modeling, Second edition. Mahwah, NJ: Lawrence Erlbaum Associates, 2004.
[49] Bentler PM. Comparative fit indexes in structural models. Psychological Bulletin, 1990, 107: 238-246.
[50] Steiger JH. Point estimation, hypothesis testing and interval estimation using the RMSEA: Some comments and a reply to Hayduk and Glaser. Journal of Consumer Psychology, 2000, 7: 149-162.
[51] Iacobucci D. Structural equations modeling: Fit Indices, sample size, and advanced topics. The American journal of orthopsychiatry, 2010, 20: 90-98.
[52] Preacher KJ, Hayes AF. Asymptotic and resampling strategies for assessing and comparing indirect effects in multiple mediator models. Behavior Research Methods, 2008, 40: 879-891. DOI: 10.3758/brm.40.3.879.
[53] Carney C, McNeish S, McColl J. The impact of part time employment on students' health and academic performance: A scottish perspective. Journal of Further and Higher Education, 2005, 29: 307-319.
[54] Cooke R, Barkham M, Audin K, et al. Student debt and its relation to student mental health. Journal of Further and Higher Education, 2004, 28: 53-66.
[55] Loyalka P, Song Y, Wei J. The distribution of financial aid in China: Is aid reaching poor students? China Economic Review, 2012, 23: 898-917.
[56] Wang X, Liu C, Zhang L, et al. Does financial aid help poor students succeed in college? China Economic Review, 2013, 25: 27-43.

Eurasia Journal of Science and Technology
ISSN: 2663-1016
DOI: https://doi.org/10.61784/ejst3063

DIFFERENCES IN PRODUCTION AREA AFFECT BACTERIAL AND FUNGAL COMMUNITY STRUCTURE IN *PANAX NOTOGINSENG* RHIZOSPHERE

Yang Lou[1,2], YiNing Wang[3],Hui Liu[4], ZiLong Zhang[1*]
[1]*School of Chinese Materia Medica, Beijing University of Chinese Medicine, Beijing 100029, China*
[2]*Institute of Medicinal Plant Development, Chinese Academy of Medical Sciences, Peking Union Medical College, Beijing 100094, China.*
[3]*College of Horticulture, China Agricultural University, Beijing 100193, China.*
[4]*Luquan Agricultural and Rural Bureau of Economic Crops Technology Extension Station, Kunming 651500, China*
Corresponding Author: ZiLong Zhang, Email: zhangzilong76@163.com

Abstract: *Panax notoginseng* is a well-known Chinese herb that is used worldwide. Studies on the factors affecting the quality of *Panax notoginseng* have mainly focused on the physical and chemical properties of the soil, with little reference to the differences in the microbial structure of different production areas. The goal of this work was to explore the diversity and structure of rhizosphere microbial communities of *Panax notoginseng*. To do this, *Panax notoginseng* rhizosphere soil samples were collected from ten production areas in China, and the 16SrRNA and internal transcribed spacer (ITS1) sequences were analyzed by Illumina high-throughput sequencing technology. The results revealed similar species composition of fungal and bacterial communities in the different producing areas, but significant variation in the abundances of some dominant flora. Redundancy analysis showed that environmental factors explained 41.3% of the fungal community and 45.7% of the bacterial community. Among all samples, the beneficial fungus Chaetomium was the most abundant with an average abundance of 19.65%. We detected significant enrichment of some root rot pathogens, including Ilyonectria, Fusarium, and Pseudomonas, in samples from Wenshan City and Yunnan Province. In summary, the results reveal differences in the structure of rhizosphere soil microbial community of *Panax notoginseng* in different production areas. The results of this study show that there are differences in the structure of rhizosphere soil microbial community of *Panax notoginseng* in different producing areas and some rhizosphere microbes may be related to rhizosphere rot. The results of this work should be beneficial to the agricultural development of *Panax notoginseng* and can provide a theoretical basis for the control of diseases and pests during cultivation of this important plant.
Keywords: *Panax notoginseng*; Microbial community; Rhizosphere; Root rot; Regional differences

1 INTRODUCTION

Sanqi [*Panax notoginseng* (Burkill) F. H. Chen] is a valuable Chinese herbal medicine endemic to Southwest China, which can be used for the treatment of cardiovascular diseases, inflammation, various kinds of body pains, internal and external bleeding caused by wounds and injuries [1], and is popular within the global market. Due to the special growing environment of Panax ginseng, there are fewer wild resources, and it mainly relies on cultivation to meet the market demand. Currently, the cultivation area of Panax pseudoginseng has been expanded from Wenshan City, Yunnan Province, a localized production area, to ten regions, including Jingxi City, Guangxi Province, and Panzhou City, Guizhou Province. In the process of cultivation, it was found that long-term large-scale intensive cultivation of *Panax notoginseng* made the continuous soil diseases increasingly serious, which seriously affected the quality of *Panax notoginseng* [2,3]. Among them, the soil-borne disease root rot has caused the most serious damage to panax pseudoginseng in cultivated areas in China. Root rot prevents plant roots from absorbing and transporting nutrients such as water, CO_2 and inorganic salts in the soil, thus affecting the healthy growth of plants. The field symptoms of the disease often manifest in the early stage of the aboveground part of the plant with incorrect leaf color, wilting of leaves, yellowing and shedding of leaves and rotting of the underground part of the plant, which can lead to a 5-70% reduction in yield or even extinction of the harvest. Therefore this also hinders the industrialization of this valuable medicinal herb[4].

Inter-root of medicinal plants is a special micro-ecosystem of plant-soil-microbe interaction[5]. The plant root system provides nutrients for the inter-root microorganisms to meet their growth needs by secreting secretions such as sugars, proteins, organic acids, and a variety of secondary metabolites, which in turn affects the composition and diversity of the inter-root microbial community. At the same time, inter-root microorganisms can also affect plant growth by synthesizing various hormones and compounds or improving the soil environment[6,7].. Some studies have shown that the accumulation of harmful soil-borne pathogens is an important factor contributing to root rot. the study by Lixia Tian et al. found that increased relative abundance of the pathogenic fungi Gibellulopsis and Gibberella was associated with the onset of root rot in western ginseng. Meanwhile, a study reported that root rot disrupted the P. cyrtonema rhizosphere microbial community and reduced diversity [8], suggesting that root rot affects the inter-root microbial community and function. There are a variety of microorganisms in the inter-root soil, including beneficial, harmful and

neutral microorganisms, which may interact with Panax pseudoginseng roots and thus affect the growth and health of *Panax pseudoginseng* [9]. Root rot disease has become a bottleneck for the development of the *Panax notoginseng.* The effective components and quality of medicinal materials cultivated in different regions can vary, and this difference is closely related to rhizosphere microorganisms [10]. At present, the factors affecting the quality of *Panax notoginseng* mainly focus on climatic factors and soil factors, in which the physical and chemical properties of soil are the main research factors, and the research on soil microbial diversity is less. The effective components and quality of medicinal materials cultivated in different regions can vary, and this difference is closely related to rhizosphere microorganisms [10]. Microbial characteristics, such as inter-root microbial abundance, composition, and diversity, are potentially valuable indicators of soil quality [11]. Therefore, the objectives of this study were to compare the composition and diversity of the inter-root microbial communities of Panax notoginseng in ten cultivation areas. Characterization of the pathogenic and probiotic flora of these different areas can guide microbial approaches to control root rot and improve the quality and yield of Panax notoginseng for improved industrial production.

2 MATERIALS AND METHODS

2.1 Sampling locations

Yunnan Province is the major growing area of *Panax notoginseng* in China, so inter-root soil samples were collected from eight separate cultivation areas in Yunnan Province, as well as one each from cultivation areas in Guangxi Province and Guizhou Province, for a total of 10 locations (Table 1). The *Panax notoginseng* cultivated in these areas were all the same variety, and all plants had been cultivated for three years using the same cultivation methods.The physico-chemical properties of the soil from different origins are shown in Table 2. The longitude and latitude data of these producing areas were obtained from the "National geographic information resource directory service system" website and ArcGis 2.0 software was used to obtain the climate factor data for these sites, as listed in Table 1.

Table 1 Basic Information of P. Notoginseng Growing Areas

Number	Producing area	Environmental Factor							
		bio1	bio2	bio3	bio4	bio5	bio6	bio7	bio8
BS	Laojiezi Village, Pupiao Town, Longyang District, Baoshan City, Yunnan Province	14.9	23.1	48	11.2	75	99.19	25.54	1388
GX	Liangbiao Village, Xinjing Town, Jingxi City, Guangxi Province	19.9	22.2	36	8.2	84	106.43	23.09	720
GZ	Tiechang Village, Danxia Town, Pangzhou City, Guizhou Province	14.8	23.8	39	9.4	82	104.55	25.64	1783
KM	Changhu Town, Shilin County, Kunming City, Yunnan Province	15.2	22.5	46	10.4	84	103.24	24.42	1905
LX	Xiaosama Village, Xiangyang Township, Luxi County, Honghe Prefecture, Yunnan Province	17.6	23.2	45	10.6	79	103.88	24.33	2078
QJ	Dawulong Villager Group, Wulong Village, Caiyun Town, Shizong County, Qujing City, Yunnan Province	14.3	23.1	43	10.1	84	103.98	25.6	1868
WS	Baishapo Village, Kaihua Town, Wenshan City, Wenshan Prefecture, Yunnan Province	17.4	20.7	42	8.7	78	104.13	23.41	1390
XC	Lin Anchong Village, Wangjiatang Village Committee, Xichou County, Wenshan Prefecture, Yunnan Province	17.0	20.7	40	8.4	82	104.49	23.32	1073
XSBN	Xing Volcano, Mengman Town, Menghai County, Xishuangbanna Prefecture, Yunnan Province	19.4	23.3	53	12.4	84	100.1	21.56	1805
YS	Huilong Base, Huilong Community, Pingyuan Town, Yanshan County, Wenshan Prefecture, Yunnan Province	17.2	21.7	45	9.9	80	103.7	23.75	1476

bio1: annual mean temperature (℃), bio2: annual difference in temperature (℃), bio3: isothermality (%), bio4: daily difference in mean temperature (℃),bio5: seasonal variation of precipitation (%), bio6: longitude (°E), bio7: latitude (°N), bio8: altitude (m)

Table 2 Physico-Chemical Properties of Soils of Different Origins

Number	pH	Organic matter (g/kg)	Alkaline-hydrolyzed N (mg/kg)	Available P (mg/kg)	Available K (mg/kg)
BS	6.59	25.63	139.42	15.76	212.94
GX	4.86	43.3	123.41	48.81	203.70
GZ	5.98	52.01	125.23	13.80	51.82
KM	5.50	33	158.20	34.20	110.97
LX	6.34	14.33	325.10	11.60	316.80
QJ	6.57	38.83	123.29	34.67	220.25
WS	5.49	16.19	58.27	94.87	129.95
XC	6.59	31.77	150.99	28.50	84.42
XSBN	5.51	48.43	71.21	2.88	189.47
YS	5.46	16.6	92.51	36.87	181.62

2.2 Sample Collection

Soil samples were collected in October 2019 using a five-point sampling method at each site of 1-2 acres in size and then mixed/homogenized. Healthy and disease-free plants with uniform growth were selected, and soil was collected 0-0.5 cm away from the root/ rhizome as the rhizosphere soil sample. The soil samples of *Panax notoginseng* from each area were collected and put into self-sealing bags and then stored in the freezer at -20℃ in the laboratory before sample processing.

2.3 DNA Extraction and Sequencing

According to the manufacturer's instructions, the MN NucleoSpin 96 Soil kit was used to extract DNA from samples. The soil fungal ITS1 regions were amplified with primers of 5'-CTTGGTCA TTTAGAGGAAGTAA-3' and 5'-GCGCGTTCTT--CATCGATGC-3', and the soil bacteria V3-V4 regions of the 16S rRNA gene were amplified using primers 5'-CTTGGTCA TTTAGAGGAAGTAA-3' and 5'-GCGCGTTCTTCATCGATGC-3'. Sequencing was completed by Beijing Biomarker Technologies Co, Ltd. using the Illumina MiSeq sequencing platform.

2.4 Data Analysis

The sequencing data were analyzed using the cloud platform of Biomark Technology. Briefly, analysis included effective tag acquisition, OTU clustering, alpha diversity analysis, beta diversity analysis, species richness analysis, and redundancy of correlation analysis. Using Flash V1.2.7, the software performs overlapping PCR assembly on the reading length of each sample to obtain the original label. Trimmomatic V0.33 software was used to filter the assembled original labels to obtain high-quality clean labels, Uchime V4.2 software was used to identify and remove chimeras, and uclust in QIIME V1.8.0 software was used to cluster the effective tags with 97% similarity and then classify and label the operational classification units (OTUs). The representative sequences of OTUs were compared with the microbial reference database to obtain the taxonomic information of species corresponding to each OTU. Next, the community composition of each origin sample was determined at multiple levels (phylum, class, genus), and species abundance tables at different taxonomic levels were generated using QIIME software. Histograms of species distribution of samples at each taxonomic level were plotted using R language tools to determine the similarity of species abundance among samples. Using Mothur V1.3.0 software, the species richness index (Chao1) and the species diversity index (Shannon) were determined for bacterial and fungal communities of the different samples. Additionally, the species diversity of the inter-root microbial community of *Panax notoginseng* of a single origin was studied by alpha diversity analysis. Using QIIME software, principal coordinate analysis (PCoA) was carried out according to Bray Curtis distance, and principal component analysis (PCoA) plots were drawn using R language tools to compare the magnitude of differences in species diversity (community composition and structure) among the different groups through beta diversity analysis. In addition, linear discriminant analysis (LDA) effect size (LEfSe) was used to detect significantly different taxa with differential abundances (LDA scores greater than 3.0, ($P < 0.01$). Microbial community with statistically significant differences between groups were identified by between-group difference significance analysis. One-way analysis of variance (ANOVA) was performed using SPSS (20.0) software to test for significant differences in the relative abundances of taxonomic taxa, and a value of $P < 0.05$ was considered statistically significant. Using the species-sample data to do DCA analysis, the first axis data of Lengths of gradient in the analysis result is less than 3.0, and the RDA is selected Redundancy analysis (RDA) was used to assess the effects of environmental factors on the composition of inter-rooted microorganisms, to distinguish potential influences of temperature, precipitation, and latitude and longitude.

3 RESULTS

To investigate potential microbial variation in different cultivation sites, inter-root soil samples were collected from eight separate *Panax notoginseng* cultivation areas in Yunnan Province, as well as one sample each from cultivation areas in Guangxi Province and Guizhou Province, for a total of 10 sampling locations (Table 1).

3.1 Driving Factors of the Panax Notoginseng Rhizosphere Microbial Community

Redundancy analysis (RDA) showed that there was a correlation between rhizosphere soil microorganisms and environmental factors of climate, longitude, latitude and altitude. The RDA results are presented in Figure 1. Solid arrow rays represent different environmental factors. The longer the ray, the greater the influence degree of the factor. A blue dashed arrow ray indicates the affected species. The relationship between rays is represented by the angle, where an acute angle represents a positive correlation and an obtuse angle represents a negative correlation. Rda1 and rda2 axes represent the two variables with the largest degree of interpretation, and the abscissa and ordinate values respectively represent the degree of interpretation of the two ranking axes to the environment. The greater the sum of the two, the greater the ability to explain the environmental community structure and species distribution.

Ten genera of fungi were related to environmental factors: Chaetomium, Cladosporium, Fusarium, Ilyonectria, Mortierella, Plectosphaerella, Penicillium, Pseudonymnoascus, Tetraclaudium, and Trichoderma. RDA showed that the isotherm of bio3 and the daily range of average temperature of bio4 had the greatest impact on the rhizosphere fungal community. Mortierella, Trichoderma, and Ilyonectria were positively correlated with bio3 and bio4, and the other seven genera were negatively correlated with these two factors. The first axis could explain 23.8% of all information,

the second axis could explain 17.5%, for a cumulative amount of interpretation information of 41.3% (Figure 1a).
Ten genera of bacteria were related to environmental factors, including Sphingomonas, Pseudomonas, Novosphingobium, Rhodanobacter, Burkholderia-Caballeronia-Paraburkholderia, Allorhizobium-Neorhizobium-Pararhizobium-Rhizobium, Sphingobium, Lelliottia, Arthrobacter, and Streptomyces. RDA showed that the annual average temperature of bio1 and the latitude of bio7 had the greatest impacts on the rhizosphere bacterial community. Sphingomonas was negatively correlated with bio1 and positively correlated with bio7, and the other nine genera were positively correlated with bio1 and negatively correlated with bio7. The first axis can explain 26.9% of all information and the second axis can explain 18.8%, for a cumulative amount of interpretation information of 45.7% (Figure 1b). Therefore, the first two axes well reflect the relationship between diseases and soil factors.

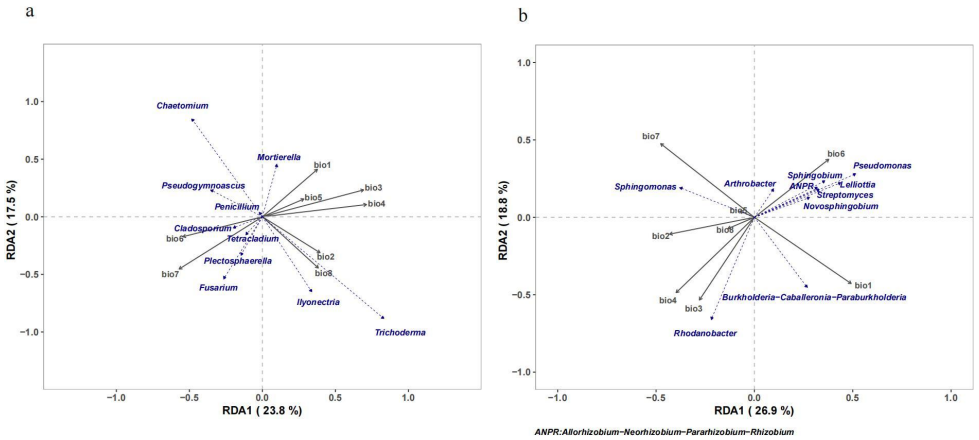

Figure 1 RDA Diagram of Inter-Root Microorganisms and Environmental Factors. (a) and (b) Represent the Fungal and Bacterial Communities, Respectively

3.2 Fungal Community Composition

We sequenced the fungal ITS1 region in the 30 soil samples (three samples from each of the ten production areas) and obtained a total of 9,259,728 pairs of reads. After paired end comparison, mass filtration, and chimera deletion, about 250,000 effective tags were generated for each sample, and 431 fungal OTUs were identified, with a sequence similarity of 97%. The number of fungal OTUs detected for BS, GX, GZ, KM, LX, QJ, WS, XC, XSBN and YS were 158, 205, 292, 201, 314, 164, 284, 259, 302 and 158, respectively. The distributions of fungal OTUs were evaluated at different classification levels.
The sequences revealed three main fungal phyla, Ascomycota (52.56% ~ 97.75%), Mortierellomycota (0.13% ~ 39.72%), and Basidiomycota (0.32% ~ 4.98%), accounting for more than 75%. However, the ten samples diff ered in the relative abundances of these major fungal species. Ascomycota was the highest content category in the ten groups, and its relative abundance Xsbn was significantly lower than that in other groups (ANOVA, $P < 0.05$). The relative abundance of Mortierellomycota was significantly higher in QJ than that in other grou ps (ANOVA, $P < 0.05$).There were significant differences in the relative abundances of Basidiomycota in GZ and other groups (ANOVA, $P < 0.05$) (Figure 2a). At the class level, the highest average relative abundances were Sordariomycetes (69.90%), Mortierellomycetes (10.16%), and Leotiomycetes (6.09%), with Sordariomycete s the dominant class inall ten groups (Figure 2b). At the genus level, Chaetomium was the most abundant ge nus in the ten groups, but exhibited a different distribution in each group, with significantly higher relative ab undance of Chaetomium in GX compared to that in other groups (ANOVA, $P < 0.05$). There were other diffe rences, with Plectosphaerella significantly higher in XC than in other groups (ANOVA, $P < 0.05$), Mortierella significantly higher in QJ (ANOVA, $P < 0.05$), and Ilyonectria and Fusarium more abundant in WS (ANOVA, $P < 0.05$) (Figure 2c).

3.3 Bacterial Community Composition

We sequenced the V3-V4 region of bacterial 16SrRNA in the 30 soil samples (three samples from each of the ten production areas) and obtained a total of 5,300,226 reads. After assembly and filtration, paired end alignment, mass filtration, and deletion of chimeras, an average of 120,000 effective tags were generated for each sample. A total of 1570 bacterial OTUs were identified, with a sequence similarity of 97%. The numbers of bacterial OTUs detected were 1400, 1397, 1418, 1376, 1346, 1409, 1359, 1302, 1210 and 1217 for BS, GX, GZ, KM, LX, QJ, WS, XC, XSBN and YS, respectively. The distributions of bacterial OTUs were analyzed at different classification levels.
The sequencing revealed ten main bacterial phyla, accounting for 99% of the whole bacterial community. Proteobacteria, Actinobacteria, and Acidobacteria were the most abundant, accounting for respectively 37.81% ~ 85.42%, 2.44% ~ 40.21%, and 1.33% ~ 21.57% of the total sequences of the groups. Actinobacteria exhibited the highest abundance in GX, with a significantly higher relative abundance in GX and a significantly lower abundance in LX (ANOVA, $P <$

0.05). Of the other groups, proteobacteria is the most abundant, and was highest in LX ($P < 0.05$) (Figure 2d). At the class level, Gammaproteobacteria (28.35%), Alphaproteobacteria (25.88%), Actinobacteria (13.90%), and Acidobacteria (6.97%) were the most abundant (Figure 2e). Arthrobacter was identified as the most abundant genus for the ten sites, but the distribution varied for the different locations. The abundance of Arthrobacter was significantly higher in GX than in other locations (ANOVA, $P < 0.05$) and that of Sphingomonas was significantly higher in KM than in other locations (ANOVA, $P < 0.05$). The relative abundance of Burkholderia-caballeronia-paraburkholderia was significantly higher in LX than that in other groups (ANOVA, $P < 0.05$). The relative abundance of Sphingobium was significantly higher in XC than that in other groups (ANOVA, $P < 0.05$) and that of Pseudomonas was significantly higher in WS than that in other groups (ANOVA, $P < 0.05$) (Figure 2f).

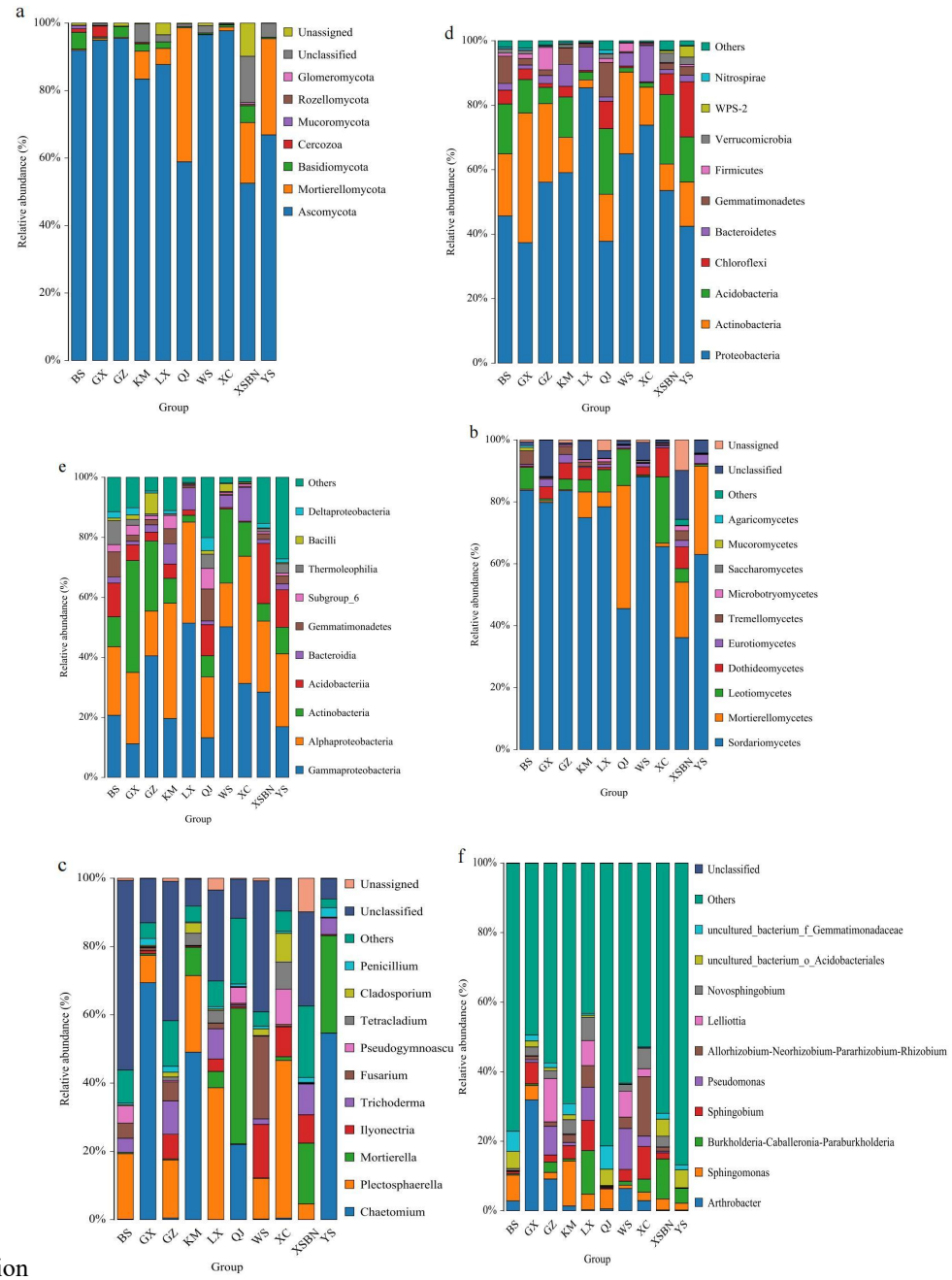

Figure 2 Composition and Structure of Fungal and Bacterial Communities in ten P. Notoginseng Origins. (a), (b) and (c) Represent Phylum, Class and Genus Level Of Fungi, Respectively. (d), (e) and (f) Represent Phylum, Classr and Genus Level of Bacteria, Respectively. The Top 10 Relative Abundances are Shown, and the Remaining Abundances are Indicated as 'Others'

3.4 Diversity Analysis of Fungi and Bacteria

To investigate the diversity at the different sites, the species richness (Chao1 index) and diversity (Shannon index) of soil rhizosphere microorganisms were calculated for the ten cultivation areas, as shown in Figure 3. The difference in the Chao1 index and Shannon index results may be due to the uneven distribution of species. The Chao1 index measures species abundance, or the number of species, and the Shannon index measures species diversity. The fungi

species richness was relatively high for GZ, LX, and XSBN and relatively low for BS, QJ, and YS. The diversity of fungi in the rhizosphere soil samples significantly varied for the different producing areas. Compared with other groups, the species diversity level of XSBN was the highest and that of GX was the lowest (ANOVA, $P < 0.05$). Between BS and YS α, there was no significant difference in diversity (ANOVA, $P > 0.05$) (Figure 3a). For bacteria, the species richness of YS was significantly lower than that of other regions, and the diversity level of QJ was significantly higher than that of other regions (ANOVA, $P < 0.05$) (Figure 3b). Overall, the Chao1 and Shannon index values were significantly higher for bacteria than for fungi (ANOVA, $P < 0.01$).

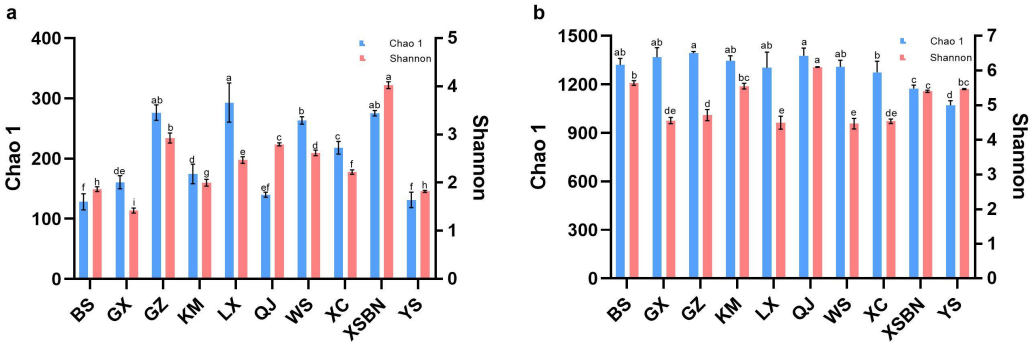

Figure 3 The Chao 1 (Species Richness) and Shannon (Species Diversity) Index Values of Fungal (a) and Bacterial (b) Communities for the Ten P. Notoginseng Sites. Different Lower Case Letters in the Figure Indicate Significant Differences (P <0.05) in the Numbers of Sequences between Origins

The differences in fungi and bacteria from different producing areas were compared by PCoA analysis of Bray Curtis distance matrix. According to the PCoA diagram, the ten sites were roughly divided into four quadrants according to the diversity of fungi, with obvious separation. YS is the only member of its group; BS, XC, WS, LX, and GZ formed a group; GX and KM formed a group; and XSBN and QJ were grouped. About 51.45% of the observed changes can be explained by the first two principal coordinates (Figure 4a). The PCoA diagram of bacteria is presented in Figure 4b. The 10 locations were roughly divided into four groups according to bacterial diversity, with obvious separation between the groups. Among them, BS, QJ, GX, and KM formed a group; XSBN and YS clustered as a group; GZ, WS, and XC formed a group; and LX is the sole member of a separate group. About 53.04% of the observed changes can be explained by the first two principal coordinates (Figure 4b). In conclusion, the PCoA diagrams of fungi and bacteria allow the grouping of samples from the ten producing areas, indicating differences in the rhizosphere microbial community in the different producing areas.

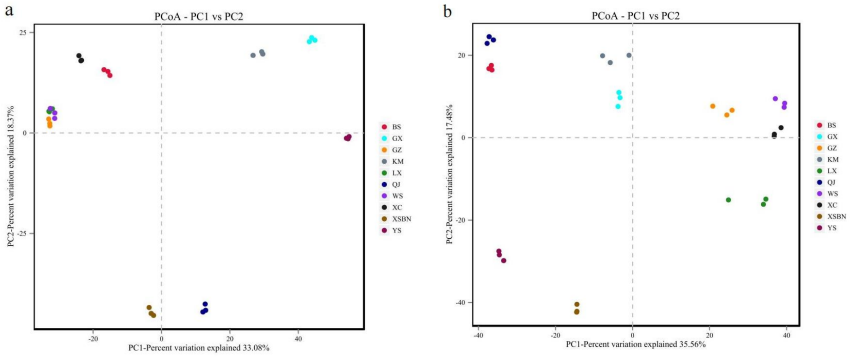

Figure 4 PCoA Diagram of Fungi (a) and Bacteria (b) from Different Origins

3.5 Linear Discriminant Analysis (LDA) Effect Size (LEfSe) Analysis of Microbial Community

To obtain more information about the variation in rhizosphere bacterial and fungal communities, we used LEfSe (Linear discriminant analysis effect size) to identify differential abundance taxa with LDA scores higher than 3.0 or 4.0 in the ten locations. The circle in the evolutionary cladistic diagram represents the classification level from phylum to species, moving from inside to outside. The diameter size of the small circles is proportional to the relative abundance size, different colors indicate different subgroups, and different colored nodes indicate microbial groups that play an important role in the subgroup represented by that color.

LEfSe analysis of rhizosphere fungi with LDA scores higher than 3.0 showed 190 significantly different abundant taxa for the ten sites. Among them, 58 groups have different abundances in XSBN, especially Archaeorhizomycetaceae, Desmazierella, Nigrospora, Sporobolomyces, and Saitozyma. The most abundant fungal groups in GX were

Chaetomium, Endophora, and Apiotrichum; Hannaela and Papiliotrema were obviously enriched in KM; Staphylotrichun-coccosporum was significantly enriched in LX; Mortierella-samyensis and Mortierella-alpina were obviously enriched in QJ; Barnettozyma was obviously enriched in WS; Plectosphaerella, Pseudoeurotiaceae, Tetraclaudium, and Cladosporium were enriched in XC; and Mucor, Guehomyces, and Minimedusa were obviously enriched in YS (Figure 5a).

LEfSe analysis of rhizosphere bacteria with LDA scores higher than 4.0 identified 163 significantly different abundant taxa for samples from the ten sites. Among them, 32 groups were present at different abundances in YS, including Elsterales and Micropepsales, Acidobacteriales, uncultured-bacterium-c-TK10, uncultured-bac-terium-c-AD3, and uncultured-bacterium-p-WPS-2. The most abundant bacterial taxa in BS, GX, LX, WS, and XSBN, respectively, were Gaiellales, Micrococcaceae, Burkholderia-caballeronia-paraburkholderia, Xanthomonadaceae, and Subgroup-2. Streptomycethales, Bacillales and Leliottia were significantly enriched in GZ; Caulobacterales and Sphingomonas were significantly enriched in KM; Gemmatimonadales, Ktedonobacterales and uncultured-bacterium-c-subgroup-6 were significantly enriched in QJ; Rhizobiaceae and Falvobacteria were significantly enriched in XC (Figure 5b).

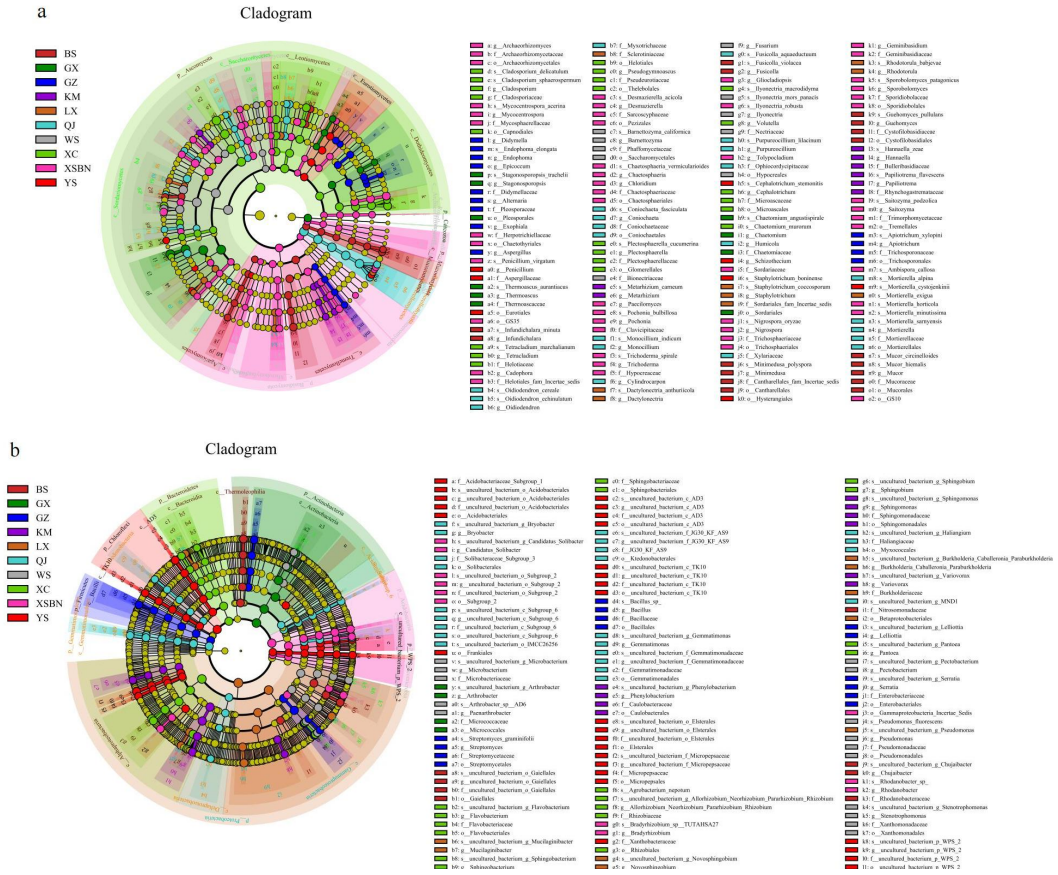

Figure 5 LEfSe Analysis Showing the Diferent Taxon among P. Notoginseng Origins Rhizospheres for Fungi (a) and Bacteria (b)

3.6 Pathogenic and Beneficial Fungal and Bacterial Abundances

We further evaluated the pathogenic fungal genera (Plectosphaerella, Ilyonectria, Fusarium, Penicillium), pathogenic bacterial genera (Sphingomonas, Sphingobium, Pseudomonas, Lelliottia), and beneficial fungal genera (Chaetomium, Mortierella, Trichoderma, Pseudogymnoascus) of the inter-rhizosphere soil samples from the ten sites. We also identified the beneficial fungal genera (Chaetomium, Mortierella, Trichoderma, Pseudogymnoascus), and beneficial bacterial genera (Arthrobacter, Burkholderia-Caballeronia-Paraburkholderia) in terms of relative abundances (Table 3). The most abundant fungus was Plectosphaerella (mean abundance 16.81%), and the abundances of pathogenic bacteria Sphingomonas, Sphingobium, Pseudomonas, and Lelliottia did not vary significantly (ANOVA, $P > 0.05$). Ilyonectria, Fusarium, and Pseudomonas were significantly higher in abundance in WS than the other sites (ANOVA, $P < 0.05$). The average abundance of beneficial fungus Chaetomium was as 19.65%, and abundances of Chaetomium and Arthrobacter were significantly enriched in GX (ANOVA, $P < 0.05$). At YS, the presence of five pathogenic bacteria was almost negligible (ANOVA, $P \leq 0.05\%$), but the abundances of beneficial genera were relatively high.

Table 3 Relative Abundance of Pathogenic and Beneficial Bacteria in Ten Origins(%)

Producing area	BS	GX	GZ	KM	LX	QJ	WS	XC	XSBN	YS

	Plectosphaerella	19.18	7.99	16.98	22.42	38.60	0.21	11.89	46.20	4.60	0.02
Pathogenic fungal genera	Ilyonectria	0.01	0.83	7.22	0.36	3.67	0.53	15.70*	8.77	8.30	0.31
	Fusarium	4.46	0.78	5.58	0.10	1.66	0.50	24.24*	0.62	0.22	0.02
	Penicillium	0.54	2.03	1.75	0.27	0.69	0.75	0.81	0.63	1.41	2.77
	Sphingomonas	7.43	4.12	1.88	12.95	4.48	5.73	0.97	2.45	3.17	1.94
Pathogenic bacterial genera	Sphingobium	0.66	6.14	2.00	3.79	8.66	0.27	3.40	9.37	1.77	0.01
	Pseudomonas	0.16	0.79	8.29	0.92	9.53	0.23	11.78*	3.02	0.46	0.05
	Lelliottia	0.02	0.11	12.45	0.21	7.20	0.03	7.45	2.25	0.04	0.01
	Chaetomium	0.16	69.40*	0.50	49.07	0.05	22.00	0.20	0.45	0.03	54.68
	Mortierella	0.37	0.54	0.31	8.29	4.76	39.72	0.13	1.10	17.81	28.53
Beneficial fungal genera	Trichoderma	4.14	0.08	9.77	0.06	8.84	0.42	1.59	0.09	8.99	4.84
	Pseudogymnoascus	4.99	0.18	0.46	0.04	0.03	4.70	0.12	10.34	0.01	0.01
	Arthrobacter	2.84	31.91*	9.16	1.38	0.32	0.57	6.40	2.91	0.25	0.23
Beneficial bacterial genera	Burkholderia-Caballeronia-Paraburkholderia	0.35	0.49	3.01	0.62	12.53	0.18	1.14	3.76	11.50	4.27

*Signifcant at the 0.05 probability level.

4 DISCUSSION

4.1 Variation in Rhizosphere Microbial Community Structure for Different Cultivation Areas

Analysis of the fungal and bacterial community composition of rhizosphere samples from ten Panax notoginseng-producing areas revealed similar species, but there were differences abundance of some dominant flora. These findings suggest that different habitats affect the composition of the rhizosphere microbial community. For example, Arthrobacter was enriched in GX and Pseudomonas was enriched in WS. Lina et al. also identified Pseudomonas and Arthrobacter as dominant flora in the rhizosphere soil of Panax notoginseng [12]. Interestingly, the fungus Tetraclaudium was significantly enriched in XC, and has been shown to be beneficial to the host [13]. The probiotics Pseudourotiaceae and Cladosporium were also significantly enriched in XC. The results reveal significant differences in the rhizosphere soil microorganisms of different Panax notoginseng production areas. Microbial diversity can be affected by many factors, such as plant varieties [14], planting years [15], and environmental factors [16]. In this study, all soil samples were collected from areas where the same variety of Panax notoginseng was cultivated for three years, so the influence of plant varieties and planting years can be excluded. Therefore, the observed rhizosphere microbial diversity may be explained by environmental factors. RDA showed that more than 40% of the overall changes in fungal and bacterial community composition were explained by environmental factors. The seasonal variation of precipitation exhibited little impact on the microbial community structure, consistent with little variation in this parameter for the test locations. As a direct living environment for microorganisms, the influence of soil on the distribution of microbial communities is obvious, and this study found that climatic factors, latitude and longitude, and altitude can also explain the differences in the distribution of microbial communities in Panax pseudoginseng well. The inter-root microorganisms were closely related to the soil and plant growth conditions, while the altitude, latitude and longitude had an effect on the physicochemical properties of the soil, the regional climate as well as the plant growth, which further drove the microbial distribution, therefore, although latitude, longitude and altitude could not directly act on the microorganisms, their effects on the microorganisms were multifaceted [17,18]. In addition, the number of bacterial OTUs was higher than that of fungi for all producing areas, with higher Chao1 and Shannon index values for bacteria than those for fungi. Compared with fungal communities, bacterial communities may be more resistant and resilient to environmental interference [19].

4.2 Rhizosphere Microorganisms Related to Root Rot of Panax Notoginseng

Microbial diversity and richness play key roles in the sustainable development of soil health, ecosystem function, and plant growth [20]. Changes in the inter-root microbial community are thought to be the main cause of the high mortality of Panax notoginseng in continuous cropping systems [21]. Typically, a richer microbial community composition has a greater ability to suppress pathogens [22]. Highly diverse microbial communities have stronger functional redundancy and transboundary associations [21,23]. Reduced microbial diversity was found in the inter-root soil of diseased

cyrtonema [24] and banana [25], and higher microbial diversity was found in healthy sugar beets [26] and peppers [27]. In this study, we detected fungi and bacteria including root rot pathogens and beneficial microorganisms that control disease and promote nutrient supply. This information is valuable for the development of sustainable disease management strategies, such as those using biocontrol agents [28]. The rhizomes are used for many medicinal plants, and 70% of these plants are limited by continuous cropping [29]. WS is a main production area for Panax notoginseng, with a cultivation history of at least 400 years, with a growth cycle that is generally at least three years. A large amount of chemical fertilizers and pesticides are applied during cultivation, and this can cause continuous cropping soil diseases, such as an imbalance of the microbial community, allelopathy, and self-toxicity [30]. Our test results confirmed significantly higher abundances of root rot pathogens Ilyonectria, Fusarium, and Pseudomonas in WS than those in other producing areas, which suggests that the long-term cultivation of WS has increased the risk of disease. Li et al. found that the enrichment of Arthrobacter in soils with high yield may contribute to the increase of *Panax notoginseng* yield [31]. In the present study we found that Chaetomium and Arthrobacter are abundant in the origin and they promote healthy growth of *Panax notoginseng*.Therefore, the regulation of rhizosphere microbial community may help overcome the obstacles of continuous cropping and can improve the yield of medicinal plants by improving the soil environment. Beneficial microorganisms do not directly act on pathogenic bacteria to reduce the occurrence of root rot, but increase the number of other beneficial microbial flora in the soil to antagonize pathogenic microorganisms and reduce disease [32]. Currently, there is no effective means to control continuous cropping obstacles, the application of chemical pesticides can reduce the incidence of root rot of Panax pseudoginseng, but it leads to the problem of pesticide residues. Li et al. suggest that the application of antagonistic microbial agents may be part of a safer and more environmentally friendly biocontrol strategy [33]. Therefor, future research should study the structure and function of rhizosphere soil microorganisms to determine strategies to regulate the crop rhizosphere habitat to ensure high yield and high quality for continued sustainable development of *Panax notoginseng*.

COMPETING INTERESTS

The authors have no relevant financial or non-financial interests to disclose.

FUNDING

This work is supported by the National Natural Science Foundation of China general project "Study on the Authenticity Markers of *Panax notoginseng* Based on Multi-source Information Fusion" (Grant No. 82274090).

REFERENCES

[1] Sun H X, Qin F, Ye Y P. Relationship between haemolytic and adjuvant activity and structure of protopanaxadiol-type saponins from the roots of Panax notoginseng. Vaccine, 2005, 23(48-49): 5533–5542. DOI: https://doi.org/10.1016/j.vaccine.2005.07.036.

[2] Yang J, Guan H, Liu D, et al. Study on mechanism of Sanqi (Panax notoginseng F.H.Chen) replant failure and its alleviation technology. North. Hortic.2016, 14: 160–167. DOI: https://doi.org/10.11937/bfyy.201614040.

[3] Qiao Y J, Gu C Z, Zhu H T, et al. Allelochemicals of Panax notoginseng and their effects on various plants and rhizosphere microorganisms. Plant diversity, 2020, 42(5): 323–333. DOI: https://doi.org/10.1016/j.pld.2020.04.003.

[4] Wen Yongjun, Huang Huang, Ma Zhonggang, et al. Illumina high throughput sequencing to analyze the diversity of Rhizosphere Soil and endophytic fungi of healthy Panax notoginseng and Panax notoginseng with root rot. Food and fermentation technology, 2020, 56(06): 22-30.

[5] Zhi min Lin, MUHAMMAD, Umar Khan, et al. Types of crop allelopathy: research status and prospects in China. Chinese Journal of ecological agriculture (Chinese and English), 2022, 30(03): 343-355.

[6] Babalola OO. Benefcial bacteria of agricultural importance. Biotechnol Lett, 2010, 32: 1559–1570. DOI: https://doi.org/10.1007/s10529-010-0347-0

[7] Fei Z, Wang J, Zhang K, et al. Regulation of photosynthetic material production by inter-root microbial extinction and metabolic pathways in sorghum under different nitrogen application patterns. Scientific reports, 2022, 12(1): 6755. DOI: https://doi.org/10.1038/s41598-022-10969-4

[8] Pang Z, Mao X, Xia Y, et al. Multiomics Reveals the Effect of Root Rot on Polygonati Rhizome and Identifies Pathogens and Biocontrol Strain. Microbiology spectrum, 2022, 10(2): e0238521. DOI: https://doi.org/10.1128/spectrum.02385-21.

[9] Qu Q, Li Y, Zhang Z, et al. Efects of S-metolachlor on wheat (Triticum aestivum L.) seedling root exudates and the rhizosphere microbiome. J Hazard Mater, 2021, 411: 125137. DOI: https://doi.org/10.1016/j.jhazmat.2021.125137.

[10] Sang Y, Xiao Y. Analysis and reflection on the current situation of informatization construction in tertiary tcm hospitals in china. Journal of Physics: Conference Series, 2021, 1774(1): 012004 (8pp).

[11] Romaniuk R, Giuffré L, Costantini A, et al. Assessment of soil microbial diversity measurements as indicators of soil functioning in organic and conventional horticulture systems. Ecol Indic, 2011, 11: 1345–1353.

[12] Lina F U, Wang Y, Wang X, et al. The study on microbial diversity of rhizosphere in continuous cropping system of panax notoginseng. Journal of Yunnan Agricultural University(Natural Science), 2018.
[13] Hilton S, Picot E, Schreiter S, et al. Identification of microbial signatures linked to oilseed rape yield decline at the landscape scale. Microbiome, 2021, 9(1): 19. DOI: https://doi.org/10.1186/s40168-020-00972-0.
[14] Wu L, Wang J, Wu H, et al. Comparative Metagenomic Analysis of Rhizosphere Microbial Community Composition and Functional Potentials under Rehmannia glutinosa Consecutive Monoculture. International journal of molecular sciences, 2018, 19(8): 2394. DOI: https://doi.org/10.3390/ijms19082394.
[15] Tang B, Dong Y, He M, et al. Effects of different planting years of healthy Panax notoginseng on the rhizosphere microbial community in Wenshan of Yunnan province. Microbiol, 2020, 9: 2857–2866. DOI: https://doi.org/10.13344/j.microbiol.china.200192.
[16] Zhou Z, Wang C, Luo Y. Meta-analysis of the impacts of global change factors on soil microbial diversity and functionality. Nature communications, 2020, 11(1): 3072. DOI: https://doi.org/10.1038/s41467-020-16881-7.
[17] Xiong W J, H Zhu, J B Li, et al. Spatiotemporal distribution patterns and drivers of bacterial communitiesin the rhizosphere and bulk soil under an Abies fabri forest on Gongga Mountain. Chinese Journal of Applied and Environmental Biology, 2021(05):1130-1138. DOI:10.19675/j.cnki.1006-687x.2021.02037.
[18] ZI Haiyun, JIANG Yonglei, CHENG Xiaomao, et al. Microbial extracellular enzyme activity in the rhizosphere soil of ancient wild tea trees at different altitudes in the Qianjiazhai Reserve. Chinese Journal of Applied and Environmental Biology, 2020, 26: 1087-1095.
[19] Uroz S, Buée M, Deveau A, et al. Ecology of the forest microbiome: Highlights of temperate and boreal ecosystems. Soil Biol Biochem, 2016, 103:471–488. DOI: https://doi.org/10.1016/j.soilbio.2016.09.006.
[20] Morales M E, Iocoli G A, Villamil M B, et al. Effect of winter cover crops on the soil microbiome: a systematic literature review. Revista Argentina de microbiologia, 2022, 54(1): 57–70. DOI: https://doi.org/10.1016/j.ram.2021.02.008
[21] Wagg C, Schlaeppi K, Banerjee S. et al. Fungal-bacterial diversity and microbiome complexity predict ecosystem functioning. Nat Commun, 2019, 10: 4841. DOI: https://doi.org/10.1038/s41467-019-12798-y.
[22] Hu Y, Qiu L, Zhang Z, et al. Control of Streptomyces alfalfae XY25T over clubroot disease and its effect on rhizosphere microbial community in Chinese cabbage field trials. Front Microbiol, 2021, 12: 641556.
[23] Gao M, Xiong C, Gao C, et al. Disease-induced changes in plant microbiome assembly and functional adaptation. Microbiome, 2021, 9(1): 187. DOI: https://doi.org/10.1186/s40168-021-01138-2.
[24] Pang Z, Mao X, Xia Y, et al. Multiomics Reveals the Effect of Root Rot on Polygonati Rhizome and Identifies Pathogens and Biocontrol Strain. Microbiology spectrum, 2022, 10(2): e0238521. DOI: https://doi.org/10.1128/spectrum.02385-21.
[25] Liu Y, Zhu A, Tan H, et al. Engineering banana endosphere microbiome to improve Fusarium wilt resistance in banana. Microbiome, 2019, 7: 74.
[26] Kusstatscher P, Zachow C, Harms K, et al. Microbiome-driven identification of microbial indicators for postharvest diseases of sugar beets. Microbiome, 2019, 7:112.
[27] Mendes LW, Raaijmakers JM, de Hollander M, et al. Influence of resistance breeding in common bean on rhizosphere microbiome composition and function. ISME J, 2018, 12: 212–224.
[28] Chaudhary V, Prasanna R, Nain L, et al. Bioefficacy of novel cyanobacteria-amended formulations in suppressing damping off disease in tomato seedlings. World Journal of Microbiology & Biotechnology, 2012, 28(12): 3301-3310.
[29] Wu H. A commentary and development perspective on the consecutive monoculture problems of medicinal plants. CHINESE JOURNAL OF ECO-AGRICULTURE, 2020, 28(6).
[30] Tan Y, Cui Y, Li H, et al. Rhizospheric soil and root endogenous fungal diversity and composition in response to continuous Panax notoginseng cropping practices. Microbiological research, 2017, 194: 10–19. DOI: https://doi.org/10.1016/j.micres.2016.09.009.
[31] Li M, Chen Z, Qian J, et al. Composition and function of rhizosphere microbiome of Panax notoginseng with discrepant yields. Chinese medicine, 2020, 15: 85. DOI: https://doi.org/10.1186/s13020-020-00364-4.
[32] Wu X, Guo S, Jousset A, et al. Bio-fertilizer application induces soil suppressiveness against fusarium wilt disease by reshaping the soil microbiome. Soil Biology & Biochemistry, 2017, 114: 238-247. DOI: https://doi.org/10.1016/j.soilbio.2017.07.016.
[33] Li J J, Yang L, Miao C P, et al. Impact of rhizosphere microorganisms on arsenic (As) transformation and accumulation in a traditional Chinese medical plant. Environmental science and pollution research international, 2021, 28(43): 60923–60934. DOI: https://doi.org/10.1007/s11356-021-14500-6.

Eurasia Journal of Science and Technology
ISSN: 2663-1016
DOI: https://doi.org/10.61784/ejst3064

HEAVINESS UNDER THE GOLDEN CROWN

DongQiao Chen
The Experimental High School Attached to Beijing Normal University, Beijing 100032, China.
Corresponding Email: 25180082@qq.com

Abstract: In Henry IV Part Two, Shakespeare explores the complexities of kingship, revealing the profound responsibilities and burdens that accompany the crown. This paper examines the qualities essential to being a great king, as portrayed in the play. These include an understanding of kingship as not just a symbol of power and wealth but as a heavy burden requiring immense personal sacrifice, a willingness to change one's character to fulfill the demands of leadership, and a commitment to justice and law above personal interests. Through the character development of Prince Henry, who matures into King Henry V, the play illustrates the importance of self-awareness, transformation, and moral integrity in effective leadership. By contrasting Henry's earlier carefree behavior with his later dedication to justice, Shakespeare emphasizes the role of a ruler as both a servant of the state and an upholder of laws.
Keywords: Kingship; Shakespeare; Leadership; Justice; Transformation

1 INTRODUCTION

The concept of kingship has been a recurring theme in literature, especially in the works of William Shakespeare. The role of a king is often portrayed as one of great power and authority, but also one that comes with immense responsibilities. Some believe that a responsible king should have the ability to get things done, while others argue that being feared by his people is more important [1]. In the play "Henry IV Part Two," Shakespeare delves into the complexities of what it takes to be a great king. The most important factors include having a profound understanding of the identity as king, the willingness to make changes in one's personality in order to rule effectively, and the ability to see justice as a crucial evaluation in society [2]. This paper will explore these qualities in detail, using examples from the play to illustrate how Shakespeare portrays the ideal king [3].

1.1 Historical Context of Shakespeare's Kingship

The historical context of Shakespeare's time provides a rich backdrop for understanding his portrayal of kingship. The Renaissance period, during which Shakespeare wrote, was marked by significant political and social changes. The concept of the "divine right of kings" was still prevalent, suggesting that monarchs were appointed by God and thus held absolute power. However, this idea was increasingly challenged by the emerging ideals of humanism and the rule of law. Shakespeare's plays often reflect these tensions, exploring the balance between power and responsibility, authority and justice [4].
During the Renaissance, there was a revival of classical ideas, including the concept of the "ideal ruler" as described by thinkers like Machiavelli and Plato. Machiavelli's "The Prince" argued that a ruler must be willing to do whatever is necessary to maintain power, even if it means acting immorally. In contrast, Plato's "Republic" emphasized the importance of moral integrity and the common good. Shakespeare's portrayal of kingship in "Henry IV Part Two" suggests a nuanced perspective that balances these two extremes. While power is essential, it must be tempered by a deep sense of responsibility and an understanding of the burdens that come with it [5].

1.2 The Play "Henry IV Part Two"

"Henry IV Part Two" is the second part of Shakespeare's historical tetralogy, which includes "Richard II," "Henry IV Part One," and "Henry V." The play continues the story of Prince Henry (Hal), who evolves from a carefree youth into a responsible ruler [6]. This transformation is central to the play's exploration of leadership and governance. By examining the qualities essential to being a great king, Shakespeare offers valuable insights into the nature of effective leadership and the importance of moral integrity in governance.

2 THE QUALITIES ESSENTIAL TO BEING A GREAT KING

2.1 A King Needs to Have a comprehensive Cognition of the Identity of Kingship

2.1.1 The burden of power

The role of a king is often romanticized as one of power, wealth, and privilege. However, Shakespeare's portrayal of kingship in "Henry IV Part Two" reveals a much more complex reality. A king is not merely a symbol of authority but also a bearer of immense responsibility. This is evident in the character of Prince Henry, who undergoes a profound transformation as he comes to understand the true nature of kingship [7].

In one of the most poignant scenes of the play, Prince Henry, believing his father to be dead, takes the crown prematurely. King Henry IV, still alive, confronts his son with the words: "You are eager for a power which will one day overwhelm you." This moment serves as a turning point for Prince Henry, who begins to realize that the crown is not a mere ornament but a heavy burden. The king's words highlight the idea that power, while attractive, comes with significant responsibilities that can weigh heavily on a ruler.

Prince Henry's understanding of kingship deepens as he reflects on the nature of the crown. He describes it as "a polished symbol of distress; a golden object of worries, that keeps the eyelids open wide, forced to face night after night without sleep." This metaphor encapsulates the idea that the responsibilities of a king are relentless and often sleepless. It suggests that the joy of power and wealth is overshadowed by the burden of decision-making and the need to ensure the well-being of the kingdom [8].

2.1.2 Historical and literary context

Shakespeare's portrayal of kingship is rooted in the historical context of the Renaissance, a time when the role of the monarch was both revered and scrutinized. The Renaissance saw a revival of classical ideas, including the concept of the "ideal ruler" as described by thinkers like Machiavelli and Plato. Shakespeare, drawing on these traditions, presents a nuanced view of kingship that emphasizes the importance of self-awareness and sacrifice.

For example, Machiavelli's "The Prince" argues that a ruler must be willing to do whatever is necessary to maintain power, even if it means acting immorally. However, Shakespeare's portrayal of kingship in "Henry IV Part Two" suggests a different perspective. While power is essential, it must be balanced with a deep sense of responsibility and an understanding of the burdens that come with it. This view aligns more closely with the humanist ideals of the Renaissance, which emphasized the importance of moral integrity and the common good.

2.1.3 The role of the crown in Shakespeare's works

Shakespeare's exploration of kingship is not limited to "Henry IV Part Two." Throughout his historical plays, he repeatedly examines the complexities of power and responsibility. In "Richard II," for example, Shakespeare portrays a king who fails to understand the burdens of his position, leading to his downfall. In contrast, "Henry V" shows a king who embodies the qualities of an ideal ruler, combining strength with compassion and justice.

By examining these different portrayals of kingship, Shakespeare provides a rich tapestry of leadership styles, each with its own strengths and weaknesses. In "Henry IV Part Two," the focus is on Prince Henry's journey towards understanding the true nature of kingship. This journey is central to the play's exploration of leadership and governance, as it highlights the importance of self-awareness and personal sacrifice.

2.2 Great Leaders Needs to Have the Willingness and Faith to Change Himself in order to Show Worthwhile of the Kingship

2.2.1 The transformation of prince Henry

The journey from prince to king is not merely a change in title but a transformation of character. This is exemplified in the character of Prince Henry, who begins the play as a carefree and irresponsible young man. His early associations with Falstaff and his band of rogues highlight his youthful indiscretions and lack of seriousness towards his future role.

King Henry IV, recognizing the potential danger of his son's behavior, criticizes him, saying, "It's very rare that a bee will make a new nest in a dead animal's carcass. Likewise, I will be very surprised if Hal ever leaves behind his companions." This metaphor suggests that Prince Henry's current environment is corrupting him, and that he must break away from it to fulfill his destiny as a great king.

The turning point for Prince Henry comes when he ascends to the throne as King Henry V. His first test comes in the form of Falstaff, who, unaware of the change in Henry's character, greets him enthusiastically, expecting to benefit from their old friendship. However, King Henry V's response is clear and decisive: he denies any previous acquaintance with Falstaff, thereby signaling a complete break from his past behavior.

This act of disavowal is significant because it demonstrates King Henry V's commitment to justice and the rule of law. Falstaff, a character known for his opportunism and self-interest, represents the antithesis of the values required of a king. By rejecting Falstaff, Henry V shows that he is willing to put aside personal loyalties for the greater good of the kingdom. This transformation highlights the idea that a great leader must be willing to change themselves in order to fulfill the responsibilities of their position.

2.2.2 The concept of self-fashioning

Shakespeare's portrayal of this transformation is rooted in the Renaissance concept of "self-fashioning," a term coined by Stephen Greenblatt to describe the process by which individuals shape their identities through their actions and choices. Prince Henry's journey from a carefree youth to a responsible king is a prime example of self-fashioning, as he consciously chooses to shed his old identity in favor of one that is more aligned with the demands of kingship.

This idea of self-fashioning is not only relevant to the character of Prince Henry but also to the broader context of Renaissance literature and culture. During this period, there was a growing emphasis on the importance of personal development and the cultivation of virtues. Writers like Erasmus and Thomas More explored the idea that individuals could shape their own destinies through education, self-reflection, and moral choices. Shakespeare's portrayal of Prince Henry's transformation reflects these ideals, suggesting that true leadership requires both personal growth and a commitment to the greater good.

2.2.3 The Role of mentorship and guidance

Prince Henry's transformation is not only a result of his own self-awareness but also the influence of his father, King Henry IV. The relationship between father and son is central to the play, as it highlights the importance of mentorship and guidance in shaping a future king. King Henry IV, despite his own flaws, serves as a role model for his son, emphasizing the importance of responsibility and duty.

This theme of mentorship is also evident in the character of the Chief Justice, who plays a significant role in Prince Henry's development. The Chief Justice's unwavering commitment to justice and the rule of law serves as a powerful example for the young prince. By interacting with these influential figures, Prince Henry learns the importance of integrity and the need to put the interests of the kingdom above his own.

2.3 Lastly, a King Needs to Recognize the Importance of Justice, and the Fact that King Can Never Go Beyond Law

2.3.1 The theme of justice in "Henry IV Part Two"

The theme of justice is central to Shakespeare's portrayal of kingship. A great king must not only understand the burden of power but also recognize the importance of upholding the law. This is exemplified in the relationship between Prince Henry and the Chief Justice.

When Prince Henry ascends to the throne, he initially accuses the Chief Justice of imprisoning him. However, the Chief Justice responds by reminding him that no one, not even the prince, is above the law. This confrontation forces Prince Henry to confront the reality that justice must be impartial and that even the crown cannot exempt him from the rules he is sworn to uphold.

Ultimately, Prince Henry, now King Henry V, recognizes the importance of the Chief Justice's role and asks him to continue in his position. He says, "You did arrest me, and for that I ask you to continue in your role, remembering this: you must always be as brave, just, and impartial as you have been with me." This statement marks a significant moment in Henry's development as a king. He acknowledges that justice is not merely a tool of power but a fundamental principle that must guide his rule.

2.3.2 Historical and literary context

Shakespeare's emphasis on justice reflects the Renaissance fascination with the rule of law and the idea of a just society. The works of thinkers like Thomas More and Erasmus, who wrote extensively on the subject of governance and justice, influenced Shakespeare's portrayal of kingship. By highlighting the importance of justice, Shakespeare suggests that a great king must be both a servant of the state and an upholder of the law.

The historical context of the Renaissance also plays a crucial role in understanding Shakespeare's portrayal of justice. During this period, there was a growing emphasis on the importance of legal institutions and the rule of law. The Renaissance saw the rise of constitutionalism, which argued that even monarchs were subject to the law. This idea was a significant departure from the earlier notion of the divine right of kings, which suggested that monarchs were above the law.

Shakespeare's "Henry IV Part Two" reflects these historical debates. By portraying Prince Henry's journey towards understanding the importance of justice, Shakespeare suggests that true leadership requires a commitment to the rule of law. This idea is particularly relevant in the context of Renaissance political thought, which emphasized the importance of a just and equitable society.

2.3.3 The role of justice in effective governance

The theme of justice is not only central to Shakespeare's portrayal of kingship but also to the broader context of effective governance. A just society is one in which the rule of law is upheld, and where individuals are treated fairly and impartially. By emphasizing the importance of justice, Shakespeare suggests that a great king must prioritize the well-being of his subjects over his own interests.

This idea is particularly relevant in the context of Renaissance political thought, which emphasized the importance of a just and equitable society. Writers like Thomas More and Erasmus argued that the primary role of a ruler was to serve the common good, rather than to pursue personal power or wealth. Shakespeare's portrayal of Prince Henry's transformation reflects these ideals, as he evolves from a self-centered youth into a ruler who understands the importance of justice and the rule of law.

3 CONCLUSION

Being a great king requires more than just the title or the trappings of power. It demands a deep understanding of the responsibilities that come with the crown, the willingness to transform oneself to meet the demands of leadership, and a commitment to justice and the rule of law [9]. Shakespeare's "Henry IV Part Two" provides a compelling exploration of these themes through the character development of Prince Henry, who evolves into the wise and just King Henry V. By examining the qualities essential to kingship, Shakespeare offers valuable insights into the nature of effective leadership and the importance of moral integrity in governance [10].

Shakespeare's portrayal of kingship in "Henry IV Part Two" is not only relevant to the historical context of the Renaissance but also to contemporary discussions about leadership and governance [11]. The qualities that Shakespeare identifies as essential to being a great king—self-awareness, transformation, and a commitment to justice—are timeless ideals that remain relevant in any era. By exploring these themes through the character of Prince Henry, Shakespeare

provides a powerful reminder that true leadership requires both personal sacrifice and a dedication to the greater good [12].

COMPETING INTERESTS

The authors have no relevant financial or non-financial interests to disclose.

REFERENCES

[1] Anderson K. Performing kingship: Theatricality in Henry V. Shakespeare Performance Studies, 2025, 12(2): 77-95.
[2] Green L. The evolution of leadership in Shakespeare's Henriad. Journal of Renaissance Culture, 2022, 18(4): 89-102.
[3] Robinson M. War and kingship in Shakespeare's historical tetralogies. Early Modern Studies Journal, 2025. 15(1): 33-49.
[4] Smith J. The politics of power in Shakespeare's history plays. Renaissance Drama Quarterly, 2024, 39(3): 201-218.
[5] Turner P. Shakespeare's royal metaphors: Power and imagery in the Henriad. Studies in English Literature, 2023, 45(2): 141-162.
[6] Wilson T. Honor and identity in Shakespeare's Henry IV. Journal of Early Modern Drama, 2021, 10(1): 45-64.
[7] Baker R. The historical narratives in Shakespeare's histories. Comparative Literature Review, 2023, 8(4): 201-220.
[8] Hall C. Gender and authority in the Henriad. Shakespeare Studies Quarterly, 2024, 17(2): 88-107.
[9] Peterson H. Theatrical adaptation and political critique in Henry V. Drama in Context, 2023, 12(3): 55-72.
[10] Morgan E. The concept of kingship in Renaissance drama. Historical Perspectives on Literature, 2022, 19(2): 34-50.
[11] Clarke D. Shakespeare's use of historical sources in the Henriad. Textual Analysis Journal, 2021, 7(1): 101-116.
[12] Edwards F. The interplay of power and morality in Henry V. Journal of Shakespearean Studies, 2023, 14(4): 222-238.

Eurasia Journal of Science and Technology
ISSN: 2663-1016
DOI: https://doi.org/10.61784/ejst3065

PERFORMANCE OPTIMIZATION STRATEGY FOR CARBON FIBER REINFORCED ALUMINUM MATRIX COMPOSITES

YiXian Yang
School of Materials Science and Engineering, Changchun University of Technology, Changchun 130012, Jilin, China.
Corresponding Email: 20220129@stu.ccut.edu.cn

Abstract: Carbon fiber reinforced aluminum matrix composites (Cf/Al) are highly sought after for their exceptional strength, modulus, and light weight, making them ideal for aerospace and automotive applications. However, the inherent differences in physical and chemical properties between carbon fibers and the aluminum matrix present significant challenges for achieving optimal interfacial bonding, ultimately limiting the composite's performance. This paper investigates strategies to enhance the interface in Cf/Al composites, with a particular focus on carbon fiber copper plating and wettability improvement methods. Experimental data analysis demonstrates the effectiveness of these methods in improving interfacial bonding and wettability, leading to enhanced overall mechanical properties, electrical conductivity, and corrosion resistance of the composites. The research underscores the critical role of interface optimization in unlocking the full potential of Cf/Al composites for broader applications in high-performance engineering sectors. Additionally, this paper explores various liquid-phase composite preparation processes, including diffusion bonding, pressure impregnation, and pressure less infiltration, comparing their advantages and limitations in terms of efficiency, cost, and composite properties. This review concludes by emphasizing the significance of interface optimization and highlighting the potential for further research in areas such as mechanism understanding, systematic studies, process optimization, environmental friendliness, and long-term performance stability to advance the field of high-performance composite materials.
Keywords: Electroless plating; Cf/Al; Composite material; Wettability

1 INTRODUCTION

Carbon fiber-reinforced aluminum composites are popular in aerospace and automotive manufacturing. They have excellent mechanical properties and are lightweight. However, issues at the interface between the carbon fiber and aluminum matrix, like low wettability and different thermal expansion coefficients, limit their performance. Researchers have developed many surface treatment techniques and liquid phase composite preparation processes to improve interfacial bonding. These include electroless copper plating and diffusion bonding. This paper will review these strategies, with a focus on carbon fiber copper plating and wettability improvement techniques. The review aims to provide a reference for the research and application of carbon fiber aluminum matrix composites.

Carbon fiber-aluminum matrix composites have great potential for use in many fields. They combine the high strength and modulus of carbon fibers with the light weight and corrosion resistance of aluminum matrices. However, interfacial issues restrict their performance. The carbon fiber has low surface energy, which leads to poor wettability with aluminum. This results in insufficient interfacial bonding strength and affects the overall performance of the composite material. To overcome these challenges, researchers have explored various surface treatment techniques, such as chemical copper plating and composite material addition, to improve the interfacial bonding and wettability of carbon fiber and aluminum matrix. This paper will focus on these optimization strategies to provide a valuable reference for the research and application of carbon fiber aluminum matrix composites. Applying these techniques enhances the mechanical properties of the composite material. Adding carbon fiber increases the hardness of the aluminum matrix composite by 14%–22%. Chemical copper plating increases the hardness by an additional 23%–26%. Copper plating also raises the material's tensile strength by about 15% and its elastic modulus by about 10% [1]. It also improves its electrical conductivity and corrosion resistance. Electroless copper plating treatment increases the interfacial bond strength of a carbon fiber-aluminum matrix composite by about 50% compared to an untreated sample. It also raises the electrical conductivity by about 20% [2]. Current research has made progress in optimizing the interface, improving performance, and expanding applications of carbon fiber-aluminum matrix composites. However, more research is needed in areas such as mechanism understanding, systematic studies, further application expansion, process optimization, environmental friendliness, and long-term performance stability.

2 STRATEGIES FOR ENHANCING CARBON FIBER ALUMINUM COMPOSITES

2.1 Liquid-Solid Preparation Technique

Liquid-solid forming technology is a key process in making carbon fiber-aluminum matrix composites. It is gaining interest for its cost-effectiveness and ability to create parts with complex shapes.

Stir casting is a method for uniformly dispersing carbon fibers in liquid aluminum or its alloys. This is achieved by mechanical stirring. The method includes full liquid, semi-solid, and stir casting. Stir casting has advantages such as

simplicity, low cost, and high productivity. It also allows for secondary processing. Experiments have shown that the content of carbon fibers significantly affects the mechanical properties of the composite material. When the content reaches 8wt%, the tensile strength and yield strength reach 219MPa and 171MPa respectively, and the elongation is 9.3%, which is the peak performance. However, beyond a certain threshold, increasing the carbon fiber content to 10wt% leads to a decrease in the material's strength to 209MPa and 189MPa. Additionally, the elongation decreases to 8.2%. [3]. An excessively high carbon fiber content can lead to poor dispersion and affect the material properties. We can improve the dispersion of carbon fibers and interfacial bonding by optimizing parameters. These parameters include stirring speed, time, mold preheating temperature, and pouring temperature.

Squeeze casting is a process where liquid aluminum metal is forced into a pre-heated carbon fiber preform by applying external mechanical pressure. After solidification, a composite material is formed. This method is cost-effective and suitable for mass production. The right pressure improves the wettability between the carbon fiber and aluminum metal. This reduces the interfacial reaction and makes the structure of the composite material more compact and uniform. To obtain the best composite properties, key parameters such as extrusion pressure, holding time, and preform preheating temperature can be optimized. The vacuum hot pressing method involves using a furnace called OTF-1200X-VHP4. This furnace applies high pressure in a vacuum. It allows for precise control of parameters like pressing temperature, pressure, and time. This precision helps create high-quality carbon fiber reinforced aluminum matrix composites. Orthogonal experiments have led to the discovery of the best hot pressing process parameters. These parameters include a hot-pressing temperature of 510°C, a hot-pressing time of 180 minutes, and a hot-pressing pressure of 15 MPa. Under these conditions, the tensile strength and density of the resulting composite reached 286.98 MPa and 99.92%, respectively [4], showing excellent mechanical properties.

The hot pressing and diffusion method is a key solid state forming technology for preparing carbon fiber-aluminum matrix composites. The process utilizes high temperatures and pressures. These conditions create an atomic-level bond between the carbon fiber and the aluminum matrix. This bonding strengthens the interface connection. As a result, the material's strength, corrosion resistance, and wear resistance all improve. The process includes steps such as pretreatment, layering, mixing, hot pressing and post-processing. The pretreatment stage is key for carbon fiber and aluminum matrix bonding. It involves surface treatment and precise control of temperature, pressure, and time. Experiments show that at a 45% carbon fiber volume fraction, the composite's tensile strength is 856MPa at room temperature and 774.7MPa at 350°C. Its tensile modulus is 204.3GPa at room temperature and 197.3GPa at 350°C. The average density is 98.86%, the interface bonding is good, and the Al_4C_3 content, a reaction product at the interface, is low [5]. The data indicate that the hot press diffusion method can enhance the properties of carbon fiber-aluminum matrix composites. This is achieved by optimizing the process parameters. It offers an effective method to produce high-performance, low-cost composites.

Stir casting, squeeze casting, and hot press diffusion are methods for carbon fiber-aluminum composites. Stir casting is cost-effective for mass production but has challenges with dispersion and bonding. Squeeze casting provides a uniform structure with good wettability but requires precise parameter control. Hot pressing and diffusion offer strong interfacial bonding but are energy-intensive and costly. Choosing the right method depends on performance needs, cost, and efficiency.

2.2 Liquid-Phase Composite Preparation Technique

Carbon and aluminum differ significantly in physical and chemical properties like melting points and thermal expansion coefficients. These differences make direct composite challenging and demand special preparation processes. Presently, the liquid phase composite preparation processes for carbon fiber-aluminum matrix composites fall into three categories: diffusion bonding method, pressure impregnation method, and pressure less infiltration method.

Diffusion bonding is a pressurized heating treatment method used in a vacuum environment. It arranges carbon fibers and aluminum foil layer by layer to prevent unwanted interfacial reactions. The heating temperature is controlled below the melting point of the aluminum substrate. Diffusion bonding joins the substrate and carbon fibers, resulting in carbon fiber-aluminum matrix composites. These composites have a controlled reinforcement phase distribution, high density, and excellent mechanical properties. High equipment costs and slow forming speeds restrict mass production. Nevertheless, research demonstrates that adjusting parameters such as hot-pressing temperature, time, and pressure can improve composite performance. The bonding strength of acid- and alkali-treated carbon fibers to the aluminum substrate can exceed 1.5 times that of untreated carbon fibers. Vacuum heating treatment effectively removes gases and impurities at the interface, increasing the interfacial bonding strength to over 1.2 times that of untreated composites. Experiments show that at the optimal hot-pressing temperature of 560°C, with a duration of 35 minutes and a pressure of 30 MPa, the Al_4C_3 content in the prepared composite material is only 1.3%. This further demonstrates that the properties of the composite material can be significantly improved through precise adjustment of the process parameters [6].

Pressure impregnation is a method for preparing composites. It is used for items like sheets, rods, and tubes in various sizes. Aluminum is pressed into preheated carbon fiber preforms using hydraulic pressure. This method controls the density and volume fraction of the reinforcement phase to optimize properties. However, high pressure can damage the carbon fibers and impact the mechanical properties. Preheating and lubrication can be used to prevent damage. Preheating makes the carbon fibers softer, while lubrication reduces friction. Experiments show that adjusting process parameters and pre-treatment measures can enhance composite performance. For instance, preheating the carbon fiber

preform at 600°C, infiltrating at 780°C, and infiltrating at a pressure of 1.5MPa followed by rapid cooling with water led to the best properties in the carbon fiber-aluminum matrix composite. The material showed no defects like porosity. The flexural strength exceeded 1400 MPa, the specific strength and specific are 667 (MPa·cm^3/g) and 110 (GPa·cm^3/g), respectively. The longitudinal thermal expansion coefficient is (0–2) × 10^{-6}/°C, and the transverse thermal expansion coefficient is (17–20) × 10^{-6}/°C [7].

The twin-roll casting process is a new method for preparing carbon fiber-aluminum matrix composites. It has the advantages of being continuous and efficient, and is expected to enable mass production. By reasonably selecting process parameters such as the casting speed and pouring temperature, the thickness, density and wettability of the composite material can be controlled. At a volume fraction of 6.8% carbon fiber, the composite material achieved a tensile strength of 137.1MPa. This is a 182% increase from the matrix's tensile strength. Furthermore, it was found that the composite material's interface structure could be improved by heat treating it in a vacuum atmosphere, which may further enhance its performance. After interface optimization, the tensile strength of the composite material reached 155.6MPa [7]. The process parameters of this technology are complex to control and require further research and optimization to achieve more efficient mass production.

Diffusion bonding, pressure impregnation, and double roll casting are primary methods for fabricating carbon fiber-aluminum composites, each with unique traits and uses. Diffusion bonding, in a vacuum, bonds the materials through controlled heating and time, resulting in high-density, mechanically strong composites, but it's costly and slow. Pressure infiltration uses external pressure to push aluminum into preheated carbon fiber preforms. It can fit various sizes but may damage fibers with excessive pressure. Double roll casting is a new and efficient method for mass production. However, it requires precise parameter control. Choosing the right method involves considering factors such as efficiency, cost, and composite properties.

3 INTERFACE OPTIMIZATION FOR CARBON FIBER ALUMINUM COMPOSITES

3.1 Carbon Fiber-Reinforced Aluminum with Copper Plating

Copper plating causes solid solution strengthening and second phase strengthening. Cu-Cf/Al composite with 1% carbon content is harder and more ductile than Cf-Al material. The copper-carbon fiber composite has high hardness due to the SPS sintering process. Copper atoms from the carbon fiber's copper plating can diffuse into the aluminum matrix during this process. This diffusion leads to solid solution strengthening, which significantly increases the composite's hardness. Intermetallic compounds such as AlCu and Al_2Cu may also form at the carbon fiber interface. These compounds contribute to a second-phase strengthening effect in the composite material. As the carbon fiber content increases, the strengthening effect becomes more pronounced [8]. As shown in Table 1. Intermetallic compounds such as AlCu and Al_2Cu are formed in Cu-Cf/Al composites. These compounds are distributed as fine particles. They are positioned between the carbon fibers and the aluminum matrix. Their presence strengthens the composite. Additionally, they increase the hardness of the composite material [8].

Table 1 Vickers Hardness of The Sample (HV)

Sample	Vickers hardness (HV)
AL	41.03
0.5%Wt C_f/Al	47.24
1.0%Wt C_f/Al	50.18
0.5%Wt Cu-C_f /Al	58.35
1.0%Wt Cu-C_f /Al	63.12

Copper plating strengthens the interface bonding by completely surrounding the carbon fiber. This enhances the bond between the matrix and the carbon fiber and improves wettability. After copper plating, the carbon fiber surface is covered with a copper layer, preventing chemical reactions with the aluminum substrate. This reduces contact between them, leading to improved bonding between the reinforcement and the matrix metal. The result is a high-quality interface structure and bonding strength. The original carbon fiber surface is smooth, but copper plating forms a uniform and dense copper layer on it. This prevents direct contact between the carbon fiber and the aluminum substrate, avoiding interface reactions. Copper plating significantly improves interfacial bonding by creating a copper layer on the carbon fiber surface. The copper layer enhances wettability and promotes bonding between the carbon fiber and the aluminum substrate. A tight interface bond, such as the one shown in Figure 1, is beneficial. It allows for the effective transfer of loads. These loads are between the carbon fiber and aluminum matrix. This transfer improves the overall performance of the composite [9].

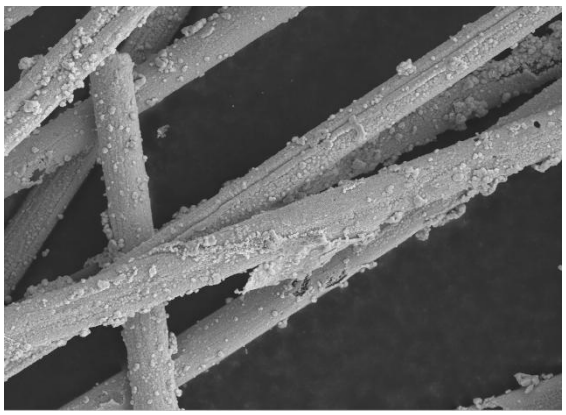

Figure 1 Microstructure of Carbon Fiber Coated with Copper

Carbon fiber copper plating technology is a reinforcement phase modification method that significantly impacts the mechanical properties of composite materials. Studies show that copper plating on carbon fiber surfaces improves the interfacial bonding between fibers and the resin matrix. This, in turn, enhances the overall performance of the composite material. The copper plating layer optimizes the interfacial structure and reduces defects, thereby increasing bond strength. This stronger bond allows for more effective load transfer, maximizing the reinforcing effect of carbon fibers. As a result, the composite material's ductility, fatigue resistance, and impact resistance improve. In the composite material, carbon fibers are evenly dispersed within the resin matrix, creating a strong interfacial bond. The addition of copper-plated carbon fibers helps to effectively distribute external loads throughout the composite material, preventing stress concentration. When an external force acts on the composite material, the copper-plated carbon fibers can withstand some of the load. They then transfer this load to the resin matrix via the interface. This mechanism of load distribution not only enhances the ductility of the composite material but also improves its fatigue resistance and impact resistance. Figure 2 shows the fracture morphology of C_f-Cu/Al with a carbon content of 1%. Pull-out phenomena in fracture morphology are relatively rare. This indicates that the carbon fiber can effectively bear and disperse the load. This prevents material damage under external forces when the composite material is subjected to tensile load. The load dispersion mechanism improves the ductility of the composite material. It also enhances its fatigue resistance and impact resistance [10].

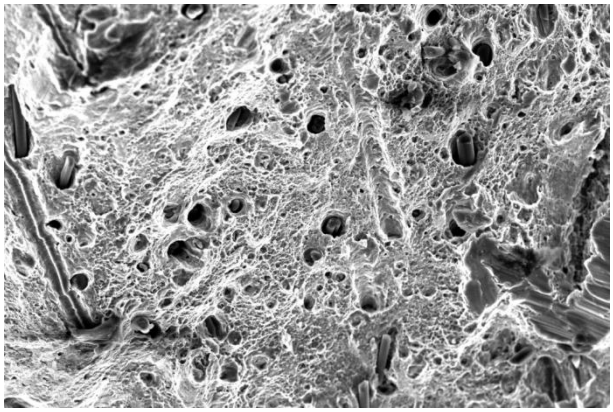

Figure 2 C_f-Cu/Al with 1% Carbon Content

3.2 Improve Wettability of Composite Materials

Wettability is the ability of a liquid to spread over a solid surface and form a stable contact angle. It is an important parameter for evaluating the interaction between a liquid and a solid interface. In carbon fiber reinforced aluminum matrix composites, wettability is a key factor determining the interfacial bond strength and the overall material performance. Good wettability helps the liquid form a uniform and dense coverage on the solid surface. This enhances the interfacial bond. It also improves the mechanical and durability properties of the material. The contact angle is an important parameter for measuring wettability. The smaller the value, the better the wettability of the liquid on the solid and the stronger the interaction between the two. Contact angle measurement can be used to evaluate the free energy of a solid surface. It can also assess the interaction between a liquid and a solid. This provides a basis for optimizing the properties of composite materials. In practice, a contact angle meter can be used to measure the contact angle of a liquid on a solid surface. The instrument usually consists of a micro-syringe, a high-precision stage and a high-resolution camera. The liquid is dropped onto the solid surface using the micro-syringe, and the shape of the drop is captured using the camera. The contact angle is calculated using image analysis software. During the preparation of carbon fiber aluminum matrix composites, the wettability between the carbon fiber and aluminum matrix can be improved. This can be done by optimizing the surface treatment of the carbon fiber and the pre-treatment of the aluminum matrix. By doing

so, the interfacial bond strength and overall performance of the composite can be improved. [11].

Wettability is crucial for interfacial bonding in carbon fiber-aluminum matrix composites. Interfacial bonding involves the adhesive strength between the carbon fiber and the aluminum matrix. This strength directly impacts the overall performance of the composite material. It includes mechanical properties, thermal properties, and corrosion resistance. Good wettability allows the aluminum matrix to cover and penetrate the carbon fiber surface effectively. This creates a uniform and compact interface layer. The uniform interface layer provides strong mechanical interlocking and chemical bonding. It enhances the interaction between the carbon fiber and the aluminum matrix. As a result, it improves the interfacial bonding strength of the composite material. If the wettability is poor, the aluminum matrix cannot fully cover the surface of the carbon fiber. This results in voids and defects at the interface. These voids and defects weaken the interfacial bonding and reduce the performance of the composite material. In practical applications, the surface energy of the carbon fibers can be improved. Their wettability with the aluminum matrix can be enhanced by surface treatment techniques. These techniques include chemical treatment, plasma treatment, or coating technology. In addition, the wettability of the aluminum matrix with the carbon fibers can be optimized. This can be done by selecting suitable parameters for the melt infiltration process. These parameters include temperature, pressure, and time. By doing so, the quality of the interfacial bond can be improved. Wettability is a key factor affecting the interfacial bond of carbon fiber-aluminum matrix composites. By optimizing wettability, the interfacial bond strength of the composite material can be significantly improved, thereby improving its overall performance [12].

Chemical plating, plasma treatment, or coating technology can increase the surface energy of carbon fibers. These methods can also improve the wettability of the aluminum substrate to the carbon fibers. Using chemical copper plating can improve the bonding strength of the interface between the substrate and the plating and improve wettability, as shown in Figure 3 (a). For the fusion impregnation process, the wettability of the aluminum substrate to the carbon fibers can be improved. This can be done by adjusting the temperature, pressure, and time during the fusion impregnation process. A moderate increase in temperature and pressure can reduce the surface tension of the molten aluminum. This reduction promotes its spreading and penetration on the surface of the carbon fiber, as shown in Figure 3 (b). Add a small amount of surfactant or wetting agent to the aluminum matrix. This will reduce the surface tension of the molten aluminum. This can improve its wetting ability on the carbon fiber. These additives can form an intermediate layer between the molten aluminum and the carbon fiber to promote good contact between the two. Interface modification can improve the wettability and interfacial strength of the interface. This can be achieved by introducing an interface modification layer. Examples of such layers include a ceramic coating or an intermetallic compound layer. These layers are placed between the carbon fiber and the aluminum substrate. These modification layers can provide mechanical and chemical bonding to enhance the interfacial bonding. Figure 3 (c) shows the surface of the carbon fiber grafted with graphene oxide. Through the above strategies, we can effectively improve the wettability of carbon fiber aluminum matrix composites. This improvement enhances the interfacial bond strength and overall performance. The enhancement is of great significance for the application of carbon fiber aluminum matrix composites in high-end engineering fields [13].

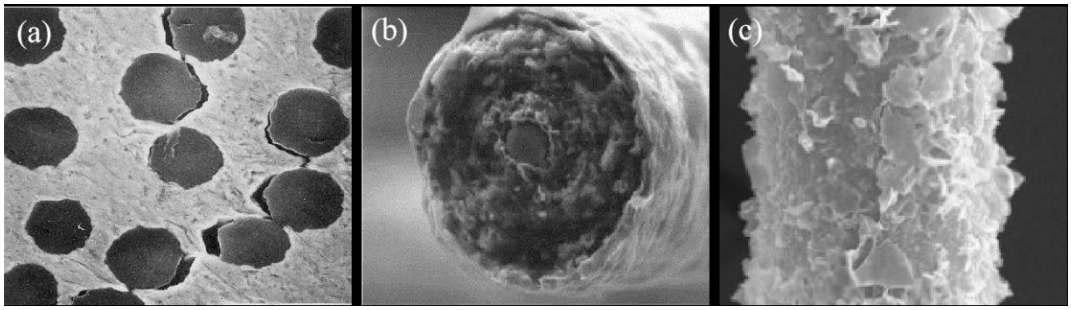

Figure 3 The Form of Carbon Fibers under Different Surface Treatments: (a) Interface between Copper-Plated Carbon Fiber and Copper Matrix; (b) Nickel-Plated Carbon Fiber 800°C Heat Treatment; (c) Graphene Oxide Grafted on a Carbon Fiber Surface

Improving wettability is a key step for optimizing material properties comprehensively. Wettability in materials science is the ability of a liquid to form a stable contact on a solid surface. It directly affects the bond strength and overall performance at the material interface. By optimizing wettability, you can significantly improve the mechanical, thermal, and chemical stability of materials. For example, in composite materials, improving fiber and substrate wettability through surface treatment technology enhances interface bonding. This improves the tensile strength and toughness of the composite material. In metal coating applications, optimizing the wettability of the coating material ensures good adhesion between the coating and the substrate. This enhances corrosion and wear resistance. In electronic materials, improving the wettability of conductive paste to the substrate can improve the conductivity and reliability of the printed circuit. In biomaterial applications, optimizing the wettability of biocompatible materials can enhance their affinity with biological tissues. This improves the biocompatibility and functionality of implantable materials. Improving wettability is an important strategy for optimizing material properties comprehensively. By precisely controlling wettability, we can effectively improve the performance of materials. This improvement applies to various application fields. It promotes

progress and innovation in materials science [14-15].

4 CONCLUSIONS

Carbon fiber reinforced aluminum matrix composites are ideal for aerospace and automotive applications. They offer high strength, modulus, and light weight. These properties are complemented by aluminum's electrical conductivity. However, there is a stark contrast in physical and chemical properties between carbon and aluminum. This includes melting points and thermal expansion coefficients. Because of this contrast, specialized preparation methods are necessary for effective compounding. Liquid-phase preparation methods are used for these composites. These methods include diffusion bonding, pressure impregnation, and pressure less infiltration. Each method has its own benefits and drawbacks. The choice of method depends on application needs and cost considerations. Improving the interface between the carbon fiber and the aluminum matrix is crucial for enhancing composite performance. Strategies like copper plating on carbon fibers and enhancing wettability can effectively increase interfacial bond strength and overall composite performance. After copper plating, the composite material shows significantly improved interfacial bond strength and fewer pull-out phenomena in fracture morphology. Techniques such as stir casting, squeeze casting, and hot-pressing diffusion are used for liquid-solid preparation. Diffusion bonding, pressure impregnation, and two-roll casting are used for liquid-phase preparation. These techniques can significantly enhance composite wettability and interfacial bonding. Advances in preparation and interface optimization are expected to expand the use of carbon fiber aluminum composites. This expansion is expected across various industries.

CONFLICT OF INTEREST

The authors have no relevant financial or non-financial interests to disclose.

REFERENCES

[1] Yang L, Cunguang C, Xinhua L, et al. Preparation and properties of carbon fiber/aluminum matrix composites. JOURNAL OF NAVALUNIVERSITY OF ENGINEERING, 2023, 35(04): 41-47.

[2] Yingdong J, Jingying H, Chunran Z, et al. Research Status of the Preparation and Alloying of Carbon Fiber Aluminum Matrix Composites. FOUNDRY TECHNOLOGY, 2024, 45(05): 494-502. DOI: 10.16410/j.issn1000-8365.2024.4049.

[3] Qichao M, Guoli F, Jinpeng H, et al. Microstructure and weldability of copper/diamond composite after electroless copper plating. ELECTROPLATING & FINISHING, 2023, 42(19): 1-7. DOI: 10.19289/j.1004-227x.2023.19.001.

[4] Shuchao W, Process Optimization and Performance Research of Carbon Fiber Reinforced Aluminum Matrix Composites for Construction. AGEING AND APPLICATION OF SYNTHETIC MATERIALS, 2023, 52(01): 83-85. DOI: 10.16584/j.cnki.issn1671-5381.2023.01.002.

[5] Yang L, Changchun C, Huan Y, et al. Investigation on microstructure and tensile properties of domestic M50J carbon fiber/aluminum matrix composites. MATERIALS REPORTS, 2022, 36(21): 130-135.

[6] Weipeng M, Baoshu Z, Nana W, et al. Study on preparation of continuous carbon fiber reinforced aluminum matrix composites by twin-roll casting technology. Composite Materials Science and Engineering, 2024, (07):105-115. DOI: 10.19936/j.cnki.2096-8000.20240728.014.

[7] Liuxin L, Xiaoying L, Ying W, et al. Progress in interface modification and application of carbon fiber reinforced resin matrix composites. Journal of Materials Engineering, 2024, 52(09): 70-81.

[8] Xu R, Haohao Z, Qian L, et al. Study on the preparation and performance of copper matrix composites reinforced coated carbon fiber. Journal of Changchun University of Technology, 2022,43(Z1): 332-340. DOI: 10.15923/j.cnki.cn22-1382/t.2022.4/5.06.

[9] Yiwei Z, Qiji C, Research Methods and Application Development of Carbon Fiber Composite Materials in the Field of Rail Transportation. Ageing and application of synthetic materials, 2024, 53(04): 92-96. DOI: 10.16584/j.cnki.issn1671-5381.2024.04.010.

[10] Yufan W, Yinhu Q, Chao M, et al. Preparation and properties of carbon nanotube electroless copper plating composite paste. Journal of Xi'an Polytechnic University, 2021, 35(05): 92-99. DOI: 10.13338/j.issn.1674-649x.2021.05.014.

[11] Yadav V, Singh S, Singh S, et al. Life cycle assessment of chemically treated and copper coated sustainable biocomposites. The Science of the total environment, 2024, 948174474.

[12] Fan H, Ouyang D, Chen X, et al. Effect of electroless copper plating on microstructure, properties and interface of MWCNT-Cu / Ti composites. Journal of Alloys and Compounds, 2024, 990.

[13] Chen C, Zhai Z, Sun C, et al. Mechanical Properties of Ti 3 AlC 2 /Cu Composites Reinforced by MAX Phase Chemical Copper Plating. Nanomaterials, 2024, 14(5).

[14] Luo L, Peipei L, Xiang L, et al. Synthesis of carbon-based Ag-Pd bimetallic nanocomposite and the application in electroless copper deposition. Electrochemical Acta, 2023, 439.

[15] Di W, Kenjiro S, Gen S. Effective Thermal Conductivity and Thermal Resistance of Electroless Copper Plated Carbon Fiber and Fe Composite. MATERIALS TRANSACTIONS, 2023, 64(2): 586-595.

Eurasia Journal of Science and Technology
ISSN: 2663-1016
DOI: https://doi.org/10.61784/ejst3066

OPTIMIZATION OF CROP PLANTING STRATEGIES BASED ON SPEARMAN-NORMAL STOCHASTIC LINEAR PROGRAMMING

ZhuoFan Yang[1*], JinTao Hu[2], XiaoHan Yang[1], XinYu Wang[3]
[1]*Computer College, Guangzhou Maritime University, Guangzhou 510725, Guangdong, China.*
[2]*Electronic and Electrical Engineering College, Zhaoqing University, Zhaoqing 526061, Guangdong, China.*
[3]*Navigation College, Guangzhou Maritime University, Guangzhou 510725, Guangdong, China.*
Corresponding Author: ZhuoFan Yang, Email: yangzhuofan@gzmtu.edu.cn

Abstract: This study considers a variety of planting conditions and uncertainties, and comprehensively analyzes and optimizes crop planting strategies to achieve profit maximization. This study is based on a detailed data set of crop planting information of a village in a mountainous area of North China in 2023, including expected sales volume, planting cost, per mu yield, and selling price. In the first phase of the study, assuming that the expected sales volume, planting cost, acre yield, and selling price of the crop remained stable as in the dataset, two scenarios were considered: excess sales were unsold and excess was sold at a 50% discount. The optimal planting scheme was solved by a simple linear programming model. In the second stage of the study, in order to solve the uncertainty and potential risk of expected sales volume, yield per mu, planting cost and selling price, a fluctuation factor is introduced, and a new objective function containing the fluctuation factor is constructed by using normal curve probability random fluctuation method. In the third stage of the study, taking into account the fungibility and complementarity among crops, as well as the correlation between expected sales volume, planting cost and selling price, Spearman correlation analysis was used to define and solve the substitution complementarity coefficient and correlation coefficient. These coefficients are introduced into the new constraints of the linear programming model to further optimize the model, and finally a more scientific and practical Spearman-Normal stochastic linear programming model is proposed to optimize crop planting strategies, which is conducive to facilitate field management, improve production efficiency, and reduce planting risks caused by various uncertainties.
Keywords: Linear programming model; Normal curve probability random fluctuation method; Spearman correlation analysis; Spearman-Normal stochastic linear programming; Optimize crop planting strategies

1 INTRODUCTION

Based on the actual situation of rural areas, making full use of the limited arable land resources and adapting to local conditions to develop organic planting industries is of great practical significance for the sustainable development of rural economies. A village in the mountainous area of North China has complex geographical conditions, low temperatures, limited arable land resources, and can only grow one crop per year [1-2]. Now, in response to the planting needs of this village, it is necessary to establish a mathematical model to optimize the crop planting plan. The main goal is to rationally arrange the planting time and plots of different crops to increase production efficiency, reduce the planting risks caused by overstocking or price fluctuations, and at the same time take into account the requirements of soil rotation and the convenience of field management [3]. In addition, future climate change, fluctuations in market demand, changes in planting costs and sales prices, and other uncertain factors also need to be considered to ensure the sustainability of crop planting and maximize economic benefits.

Carlo Filippi employed integer programming to identify the crop combination that maximizes farmers' expected profits, defining market-related factors as random variables [4]. Hengtian Ma utilized linear programming to optimize crop planting schemes under a series of constraints and employed Monte Carlo simulation to model market scenarios, thereby accounting for market uncertainties [5]. JE Annetts proposed a multi-objective linear programming model aimed at considering agricultural conditions such as market prices, potential crop yields, soil and weather characteristics to optimize profits or environmental outcomes, or both [6]. From the existing literature, it is evident that optimizing crop planting schemes under multiple factors has long been a hot topic of interest for experts and scholars. The primary approach has been to establish linear programming models or combine them with other models to consider fluctuating factors [7]. However, these research methods generally fail to take into account fluctuating factors or simulate them within the fluctuation range with equal random probabilities, lacking realistic and scientific analysis.

This paper proposes a linear programming model that constructs a new objective function containing a stochastic fluctuation factor in the normal curve probability and a constraint condition including the Spearman correlation coefficient. The Spearman-Normal Stochastic LP model considers the correlation between variables more objectively by introducing the Spearman correlation coefficient, better capturing the interdependence among variables; by introducing the normal curve probability stochastic fluctuation factor, the random probability of the fluctuation factor within the fluctuation range becomes more realistic and scientific, thereby enhancing the robustness and adaptability of the model; it more realistically reflects the complexity and uncertainty in the real world, improving the practicality of the model. This model combines the efficiency and certainty of linear programming with the methods for handling correlation and randomness, making it more practical and effective in the planning of crop planting schemes.

2 METHODOLOGY

2.1 Data Analysis

2.1.1 Description of the dataset

This study is based on the specific conditions of cultivated land in a village in the mountainous area of North China and the relevant statistics of crop planting in 2023. The dataset is available at https://www.mcm.edu.cn/html_cn/node/a0c1fb5c31d43551f08cd8ad16870444.html. The first data table provides the existing cultivated land data of the village, including the land type and area of each plot, as well as explanations of the land types, such as: flat dry land, terraced fields, and hillside land can only grow one crop per year. The second data table presents the data of crops planted in the village, including the crop name, type, and cultivated land corresponding to each crop number, as well as explanations of the crops grown on each plot, such as: flat dry land, terraced fields, and hillside land are suitable for growing one season of grain crops (except rice) per year. The third data table shows the crop planting situation in 2023, including the crops planted on each plot, the corresponding planting area, and the planting season. The fourth data table provides the relevant statistics for 2023, including the acre yield, planting cost, and selling price of each crop in the corresponding land type and planting season.

2.1.2 Data preprocessing

Using the planting and sales data of 2023 as the basic input data for the model, preprocess the per mu yield, planting cost, expected sales volume and price of different crops, as shown in Figure 1 Data preprocessing below.

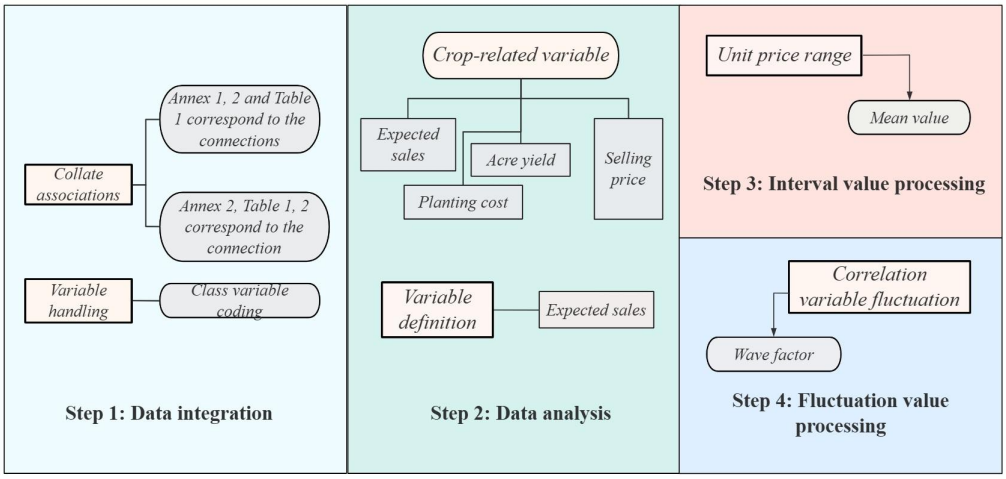

Figure 1 Data Preprocessing

By analyzing the attached table in the dataset, a data table of crop-related variables for 2023 was obtained. This table details the specific data of planting costs, acre yield, and selling prices of various crops in different plots and different seasons in 2023, for further analysis and modeling.

To facilitate the subsequent model solving, in this study, the crop types such as soybeans, black beans,..., white shiitake mushrooms, and morel mushrooms are numbered from 1 to 41 respectively, and the plots A1, A2, A3,..., F3, F4 are numbered from 1 to 50 respectively.

The related variables of crops include expected sales volume, planting cost, acre yield, and selling price. Since the dataset does not provide specific data on expected sales volume, this study adopts an ideal processing method, that is, production and sales balance. It is assumed that the total output of each crop in 2023 is equal to the expected sales volume of each crop in the future, thereby simplifying the model and providing a basic reference point for subsequent analysis and prediction. The expected sales volume of each crop is shown in Figure 2 Each crop corresponds to the total output.

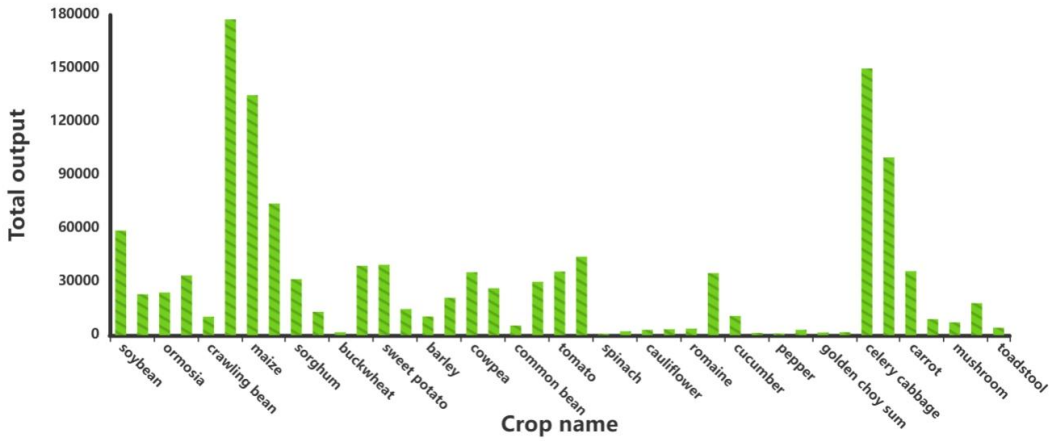

Figure 2 Each Crop Corresponds to the Total Output

This study adopts the mean approach to handle the interval data of sales unit prices, taking advantage of its characteristic of representing the central tendency to make a preliminary estimation of the data. Given that the expected sales volume, acre yield, planting cost, and sales price of crops in the dataset may all be influenced by multiple factors, which could lead to discrepancies between actual results and predictions, this study considers introducing a fluctuation factor to address the inherent uncertainties and risks in agricultural production.

2.2 Linear Programming Model

2.2.1 Model analysis

In this paper, we construct an optimal planting scheme model which seeks to maximize planting profit under various constraints. Specifically, if the total production of a crop each season exceeds the expected sales volume, the excess will be either unsalable or sold at a 50 percent discount. In order to distinguish these two sales scenarios, this study introduced an adjustment coefficient K into the objective function, so as to adjust the parameters in the objective function according to different scenarios, so as to obtain the optimal planting plan when maximizing revenue.

The constraint conditions are shown in Figure 3 Crop planting constraints, which are the constraint of season number, the constraint of total area of block number, the constraint of planting of legume crop, the constraint of repeated cropping, the constraint of crop type of plot, the constraint of special crop type and the constraint of planting area.

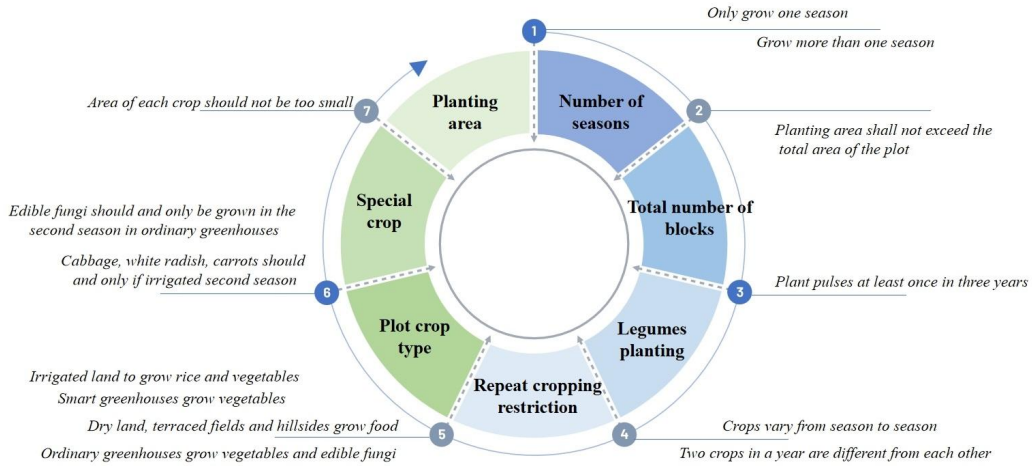

Figure 3 Crop Planting Constraints

2.2.2 Model building process

Figure 4 Linear Programming Model Building

As shown in Figure 4 Linear programming model building, the expected sales volume was first defined as the total production of each crop in 2023. A linear programming model was adopted to determine the crop planting scheme whose objective function was to maximize profit, and the constraint function was determined. The objective function contains discount coefficient K, and this study can solve the optimal planting scheme in two different situations by setting the value of K to 0 and 0.5 [8].

2.2.3 Objective function

Based on the above analysis, a linear programming model of the maximum profit from the sale of cultivated crops is established to guide the crop planting plan in future years.

Objective function:

Where $i \in \{1,2,\ldots,54\}$ indicates the plot number, $j \in \{1,2,\ldots,41\}$ denotes the crop number, $t \in \{2024,2025,\ldots,2030\}$ represents the planting year, $s \in \{1,2\}$ represents the quarter number, $q_{i,j,t,s}$ represents the actual yield of the j crop planted in the s season of the t year in the i plot, $p_{i,j,t,s}$ represents the selling price of the j crop planted in the s season of the t year in the i plot, and d_j represents the sales volume of the j crop. $e_{i,j,t,s}$ represents the cost of planting the j crop in the s season of the t year for plot i.

$$\text{Max} \sum_{t=2024}^{2030} \sum_{i=1}^{54} \sum_{s=1}^{2} \sum_{j=1}^{41} \left[\min\left(q_{i,j,t,s}, d_j\right) \cdot p_{i,j,t,s} + \max\left(0, q_{i,j,t,s} - d_j\right) \cdot K \cdot p_{i,j,t,s} - e_{i,j,t,s}\right] \tag{1}$$

Yield of each crop:

The yield of each crop is the area planted($x_{i,j,t,s}$) multiplied by the yield per acre($y_{i,j,t,s}$).

$$q_{i,j,t,s} = x_{i,j,t,s} \cdot y_{i,j,t,s}, \forall i, \forall j, \forall t, \forall s \tag{2}$$

Planting cost of each crop:

The cost of growing each crop is the area planted($x_{i,j,t,s}$) it multiplied by the cost of growing($c_{i,j,t,s}$).

$$e_{i,j,t,s} = x_{i,j,t,s} \cdot c_{i,j,t,s}, \forall i, \forall j, \forall t, \forall s \tag{3}$$

2.2.4 Constraint function

(1) Season constraints

According to the different planting characteristics of different plot types, the number of seasons is restricted:

The land types are flat dry land, hill land and terrace, that is, $i \in \{1,2,\ldots,26\}$, the plot can only grow one season of crops, that is, s = 1:

$$x_{i,j,t,1} = 0, \forall i \in \{1,2,\ldots,26\}, \forall t, \forall j \tag{4}$$

When the local type is irrigated land, ordinary greenhouses, and smart greenhouses, that is, $i \in \{27,28,\ldots,54\}$, the plot can be planted with one or two crops, i.e. s = 1 or s = 2:

$$x_{i,j,t,1} \geq 0, x_{i,j,t,2} \geq 0, \forall i \in \{27,28,\ldots,54\}, \forall t, \forall j \tag{5}$$

(2) Constraints on the total land area

The total area of crops grown in different plots cannot exceed the plantable area of the plots A_i:

$$\sum_{j=1}^{41} x_{i,j,t,s} \leq A_i, \forall i, \forall t, \forall s \tag{6}$$

(3) Planting constraints of legumes

Every plot of land needs to be fertilized at least once every three years with legumes, which are numbered j_{legumes}:

$$\sum_{t=t_0}^{t_0+2} \sum_{s=1}^{2} x_{i,j_{\text{legumes}},t,s} \geq 1, \forall i, \forall t_0 \in \{2024,2025,2026,2027,2028\} \tag{7}$$

(4) Repeated crop restriction

Crops cannot be grown consecutively in the same planting season on the same plot or in two adjacent planting seasons:

The land types are flat dry land, terraced land and hilly land, that is, $i \in \{1,2,...,26\}$,The crops planted this year and next year cannot be the same:

$$x_{i,j,t,1} \cdot x_{i,j,t+1,1} = 0, \forall i \in \{1,2,...,26\}, \forall t, \forall j \tag{8}$$

Because in mixed integer linear programming, constraints on product form are usually not allowed because the model becomes nonlinear. Therefore, this study needs to transform the constraints of this product form into a linear form. In this study, two bivariate variables $w_{i,j,t}$ and $w'_{i,j,t}$ are introduced by large M method [9].

$$x_{i,j,t,1} \leq M \cdot w_{i,j,t}, \forall i \in \{1,2,...,26\}, \forall t, \forall j \tag{9}$$

$$x_{i,j,t+1,1} \leq M \cdot w'_{i,j,t}, \forall i \in \{1,2,...,26\}, \forall t, \forall j \tag{10}$$

$$w_{i,j,t} + w'_{i,j,t} \leq 1, \forall i \in \{1,2,...,26\}, \forall t, \forall j \tag{11}$$

Which $w_{i,j,t}$ and $w'_{i,j,t}$ is a binary variable, constant M is large enough, this constraint means that if $x_{i,j,t,1} > 0$, then $w_{i,j,t} = 1$, thus $w'_{i,j,t} = 0$, then $x_{i,j,t,1}$ must be zero, and vice versa.

The block type is irrigated land, i.e. $i \in \{27,28,...,34\}$, rice cannot be planted for two consecutive years:

$$x_{i,16,t,1} \cdot x_{i,16,t+1,1} = 0, \forall i \in \{27,28,...,34\}, \forall t, \forall j \tag{12}$$

The same can be obtained by using large M method:

$$x_{i,j,t,1} \leq M \cdot w_{i,j,t}, \forall i \in \{27,28,...,34\}, \forall t, \forall j \tag{13}$$

$$x_{i,j,t+1,1} \leq M \cdot w'_{i,j,t}, \forall i \in \{27,28,...,34\}, \forall t, \forall j \tag{14}$$

$$w_{i,j,t} + w'_{i,j,t} \leq 1, \forall i \in \{27,28,...,34\}, \forall t, \forall j \tag{15}$$

When the block type is smart greenhouse, that is, $i \in \{51,52,53,54\}$, the crops planted in the second quarter of last year and the first quarter of this year cannot be the same, and the crops planted in the first quarter of this year and the second quarter of this year cannot be the same:

$$x_{i,j,t-1,2} \cdot x_{i,j,t,1} = 0, \forall i \in \{51,52,53,54\}, \forall t, \forall j \tag{16}$$

$$x_{i,j,t,1} \cdot x_{i,j,t,2} = 0, \forall i \in \{51,52,53,54\}, \forall t, \forall j \tag{17}$$

The same can be obtained by using large M method:

$$x_{i,j,t,2} \leq M \cdot w_{i,j,t}, \forall i \in \{51,52,53,54\}, \forall t, \forall j \tag{18}$$

$$x_{i,j,t+1,1} \leq M \cdot w'_{i,j,t}, \forall i \in \{51,52,53,54\}, \forall t, \forall j \tag{19}$$

$$w_{i,j,t} + w'_{i,j,t} \leq 1, \forall i \in \{51,52,53,54\}, \forall t, \forall j \tag{20}$$

$$x_{i,j,t,1} \leq M \cdot w_{i,j,t}, \forall i \in \{51,52,53,54\}, \forall t, \forall j \tag{21}$$

$$x_{i,j,t,2} \leq M \cdot w'_{i,j,t}, \forall i \in \{51,52,53,54\}, \forall t, \forall j \tag{22}$$

$$w_{i,j,t} + w'_{i,j,t} \leq 1, \forall i \in \{51,52,53,54\}, \forall t, \forall j \tag{23}$$

(5) Constraints of crop types in plots

Different plot types are suitable for different types of crops:

On flat dry land ($i \in \{1,2,...,6\}$), terraces ($i \in \{7,8,...,20\}$), hill land ($i \in \{21,22,...,26\}$), can only grow food crops ($j \in \{1,2,...,15\}$) :

$$x_{i,\text{nonfood},t,s} = 0, \forall i \in \{1,2,...,26\}, \forall t, \forall s \tag{24}$$

For irrigated land ($i \in \{27,28,...,34\}$), can only grow rice ($j = 16$) or vegetables ($j \in \{17,18,...,37\}$) :

$$\sum_{j \in \{1,2,...,15\} \cup \{38,39,40,41\}} x_{i,j,t,s} = 0, \ \forall i \in \{27,28,...,34\}, \forall t, \forall s \tag{25}$$

For ordinary greenhouses ($i \in \{35,36,...,50\}$), only vegetable crops can be planted in the first season ($j \in \{17,18,...,37\}$) :

$$\sum_{j \in \{1,2,...,16\} \cup \{38,39,40,41\}} x_{i,j,t,1} = 0, \forall i \in \{51,52,53,54\}, \forall t, \forall s \tag{26}$$

For smart greenhouses ($i \in \{51,52,53,54\}$), only vegetable crops can be grown ($j \in \{17,18,...,37\}$) :

$$\sum_{j \in \{1,2,...,16\} \cup \{38,39,40,41\}} x_{i,j,t,s} = 0, \forall i \in \{51,52,53,54\}, \forall t, \forall s \tag{27}$$

(6) Special crop constraints

Celery cabbage($j = 35$), mooli ($j = 36$) and carrot ($j = 37$) can only be irrigated land ($i \in \{27,28, ..., 34\}$) (s=2) and in the second season of irrigated land can grow any of these three crops:

$$x_{i,j,t,2} = 0, \forall i \notin \{27,28, ..., 34\}, \forall j \in \{35,36,37\}, \forall t \quad (28)$$

$$x_{i,j,t,1} = 0, \forall i \in \{27,28, ..., 34\}, \forall j \in \{35,36,37\}, \forall t \quad (29)$$

$$x_{i,j,t,2} \geq 0, \forall i \in \{27,28, ..., 34\}, \forall j \in \{35,36,37\}, \forall t \quad (30)$$

$$\sum_{j \in \{17,18,...,34\} \cup \{35,36,37\}} x_{i,j,t,2} = 0, \forall i \in \{27,28, ..., 34\}, \forall t \quad (31)$$

For ordinary greenhouses ($i \in \{35,36, ..., 50\}$), in the second season (s=2) can only grow edible fungi ($j \in \{38,39,40,41\}$):

$$x_{i,j,t,2} = 0, \forall i \in \{35,36, ..., 50\}, \forall j \notin \{38,39,40,41\}, \forall t \quad (32)$$

$$x_{i,j,t,2} \geq 0, \forall i \in \{35,36, ..., 50\}, \forall j \in \{38,39,40,41\}, \forall t \quad (33)$$

Edible fungi can only be grown in the second season of ordinary greenhouses:

$$x_{i,j,t,2} = 0, \forall i \notin \{35,36, ..., 50\}, \forall j \in \{38,39,40,41\}, \forall t \quad (34)$$

(7) Planting area constraints

The planting area of each crop should not be less than 30%A_i:

$$x_{i,j,t,s} \geq 0.3A_i, \forall i, \forall j, \forall t, \forall s \quad (35)$$

2.3 Introduction Of Wave Factor

2.3.1 Model analysis

In order to comprehensively consider the uncertainty of the expected sales volume, per mu yield, planting cost and selling price of various crops, as well as the potential planting risk, this study will introduce a fluctuation factor into the model. These fluctuation factors are intended to reflect the inevitable uncertainties in actual agricultural production. Specifically, this study will introduce fluctuation factors to the expected sales volume, per mu yield, planting cost and selling price of various crops to reflect the uncertainty of these variables in actual production. This not only improves the realism of the model, but also provides a more reliable basis for decision making. The set range of the Wave factor is as follows: Figure 5 Wave factor.

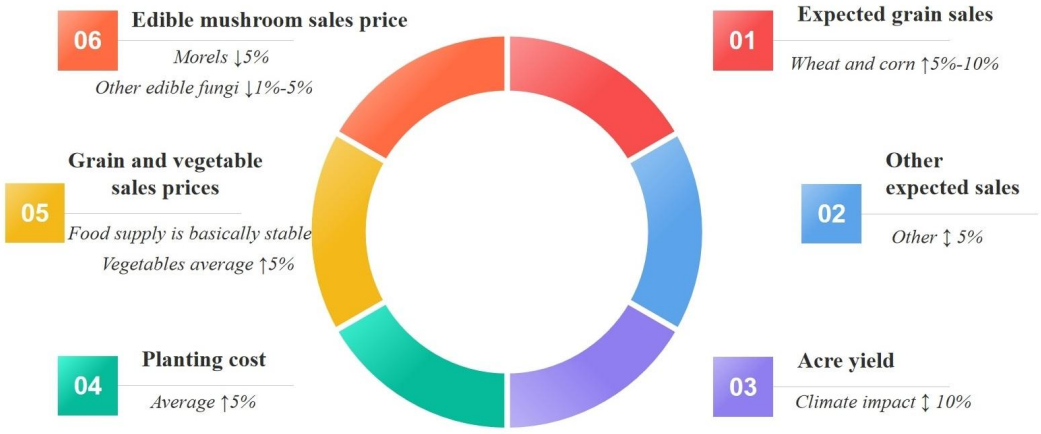

Figure 5 Wave Factor

2.3.2 Model building process

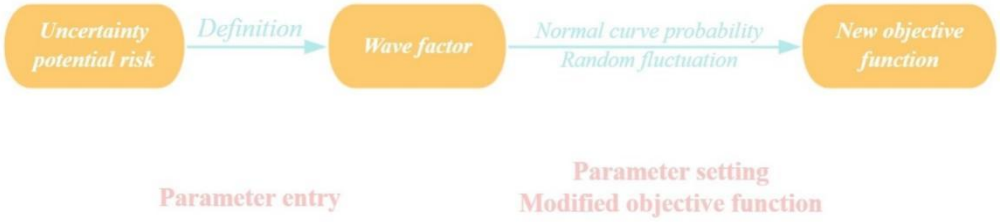

Figure 6 The Introduction Process of Wave Factor

As shown in The introduction process of wave factor in Figure 6, due to the need to comprehensively consider the expected sales volume, acre yield, uncertainty of planting cost and selling price of various crops as well as potential planting risks, the volatility factor is first defined. The constructed expression is used as the coefficient of expected sales volume, per mu yield, planting cost and selling price, and is solved by modifying the input value of the objective function through the random fluctuation of normal curve probability, and then the optimal planting scheme.

2.3.3 Definition of wave factor

(1) Uncertainty of expected sales volume

Assume that the expected sales volume fluctuation coefficient is $\theta_{j,t}^{\text{sales}}$:

$$d_{j,t} = d_{j,t-1} \times \left(1 + \theta_{j,t}^{\text{sales}}\right) \tag{36}$$

Among them, the expected sales volume fluctuation coefficient $\theta_{j,t}^{\text{sales}}$ of corn and wheat is 5% ~ 10%, and the expected sales volume fluctuation coefficient $\theta_{j,t}^{\text{sales}}$ of other crops is 5% on average.

(2) Uncertainty of acre yield

Assume that the yield fluctuation coefficient per mu is $\theta_{j,t}^{\text{yield}}$ and introduce the risk factor $\phi_{j,t}^{\text{risk}}$:

$$y_{j,t} = y_{j,t-1} \times (1 + \theta_{j,t}^{\text{yield}}) \times \left(1 - \phi_{j,t}^{\text{risk}}\right) \tag{37}$$

The area yield fluctuation coefficient of theta $\theta_{j,t}^{\text{yield}}$ of 10% ~ 10%, the risk factor $\phi_{j,t}^{\text{risk}}$ of 5% ~ 5%.

(3) Uncertainty of planting cost

Suppose the growth coefficient of planting cost is $\theta_{j,t}^{\text{cost}}$:

$$c_{j,t} = c_{j,t,s} \times (1 + \theta_{j,t}^{\text{cost}}) \tag{38}$$

The growth coefficient of planting cost $\theta_{j,t}^{\text{cost}}$ is 5% on average.

(4) Uncertainty of sales price

Suppose the selling price volatility coefficient is $\theta_{j,t}^{\text{price}}$:

$$P_{j,t} = P_{j,t} \times (1 + \theta_{j,t}^{\text{price}}) \tag{39}$$

Including grain sales price fluctuation coefficient theta $\theta_{j,t}^{\text{price}}$ for an average of 0%, grain sales price fluctuation coefficient theta $\theta_{j,t}^{\text{price}}$ for an average of 5%, morchella sales price fluctuation coefficient theta $\theta_{j,t}^{\text{price}}$ for the average -5%, The fluctuation coefficient of other edible fungi sales price $\theta_{j,t}^{\text{price}}$ is -5% ~ -1%.

2.3.4 Normal curve probability random fluctuation

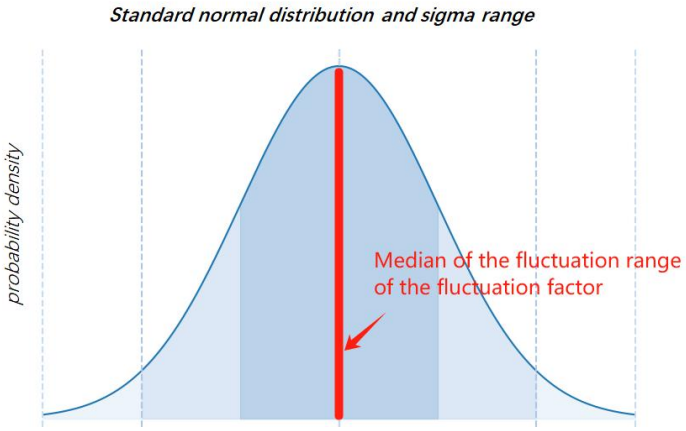

Figure 7 Normal Distribution Probability Distribution Curve

The central limit theorem states that for any sequence of independent uniformly distributed random variables with a distribution form, when the sample size is large enough, the distribution of the sample mean will tend to be normal. This theory provides the basis for crop fluctuation factor probability to be biased to normal distribution. In this study, it is more scientific to replace the normal curve probability random fluctuation factor with the main function[10]. As shown in Figure 7 normal curve probability random fluctuation, the probability of obtaining different sizes of the fluctuation factors within the range is not the same. For example, the fluctuation coefficient of mu yield $\theta_{j,t}^{\text{sales}}$ is -10% ~ 10%, then the probability of obtaining the random factor $\theta_{j,t}^{\text{sales}}$ is greater the closer it is to 0, and decreases to both sides.

2.2.5 Solution method for model

The expected sales volume, acre yield, planting cost and selling price of fluctuation factors were introduced into the objective function of Linear Programming Model for solving.

$$\text{Max} \sum_{t=2024}^{2030} \sum_{i=1}^{54} \sum_{s=1}^{2} \sum_{j=1}^{41} \left[\min\left(q_{i,j,t,s}, d_{j,t}\right) \cdot p_{i,j,t,s} - x_{i,j,t,s} \cdot c_{i,j,t,s}\right] \tag{40}$$

2.4 Introduction Of Spearman Correlation Coefficient

2.4.1 Model analysis

In real life, there may be substitutability and complementarity among various crops, and there is also correlation between expected sales and selling price and planting cost. In order to explore the relationship between them, this study needs to use the correlation analysis model to explore the possible relationship between them. Therefore, this study defines the substitution and complementation coefficient, the correlation coefficient between sales volume and price, and the correlation coefficient between planting cost and price, and introduces them into the linear programming model based on fluctuation factor by establishing constraint conditions.

2.4.2 Model building process

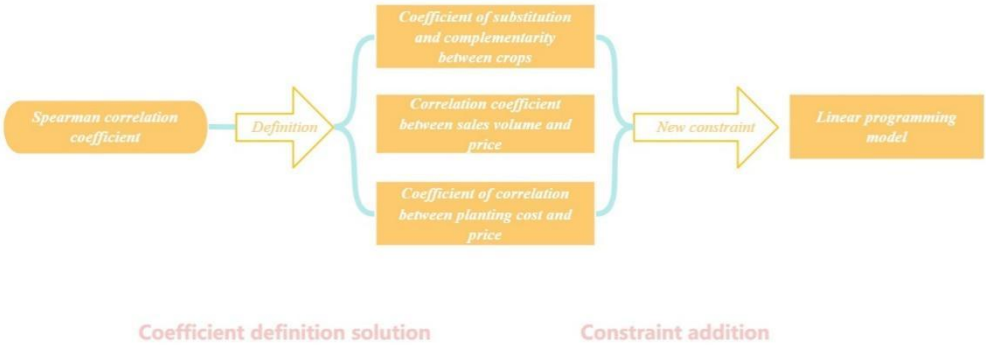

Figure 8 Spearman Correlation Coefficient Introduction Process

As shown in Figure 8 Spearman Correlation Coefficient introduction process, firstly, this study defined the substitution and complementarity coefficient between crops by Spearman. The correlation coefficient between sales volume and price and the correlation coefficient between planting cost and price. Then, the substitutability and complementarity constraints between crops, the correlation constraints between sales volume and price, and the correlation constraints between planting cost and price are added to the linear programming model based on fluctuation factors to solve.

2.4.3 Substitution and complementarity between crops

In this study, the following definitions are given for substitution and complementarity:

Substitution relationship: If two crops are substitutable, an increase in acreage for one crop may reduce the need for the other.

Complementary relationship: If two crops are complementary, an increase in acreage planted with one crop may increase demand for the other.

Based on the linear programming model based on fluctuation factors, the annual planting area variables of each crop are divided into grain, vegetable and edible fungi, and then the correlation analysis is carried out. Since the annual planting area variables of each crop did not conform to the normal distribution, Spearman correlation analysis model was used for analysis, and the results were shown as follows figure 9-11[11]:

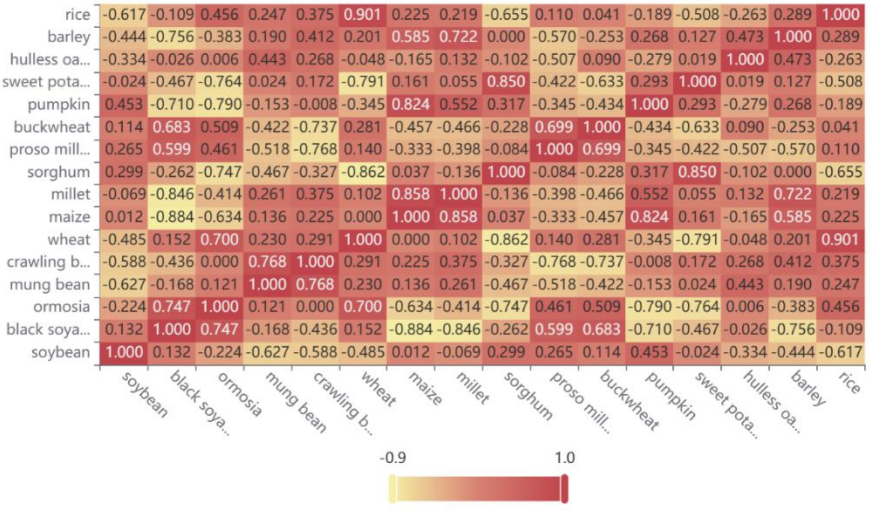

Figure 9 Thermal Matrix of Annual Planting Area Correlation of Food Crops

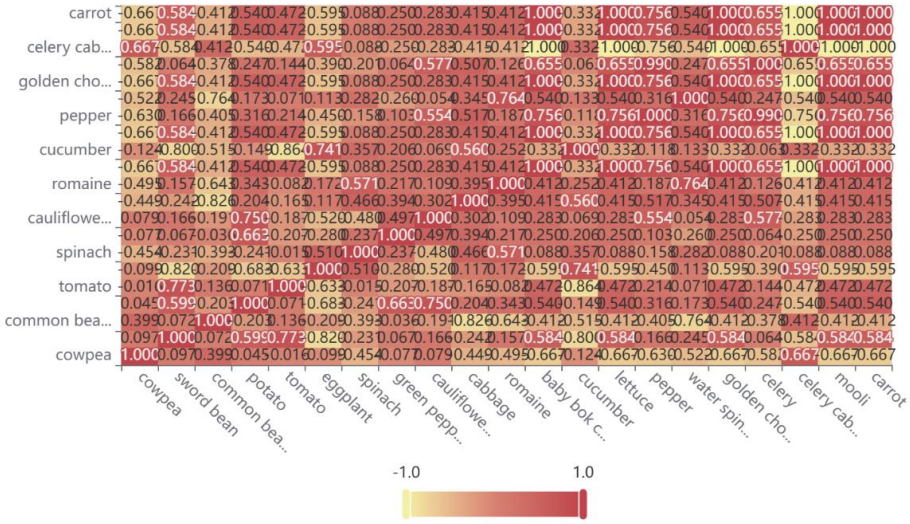

Figure 10 Thermal Matrix of Annual Planting Area Correlation of Vegetable Crops

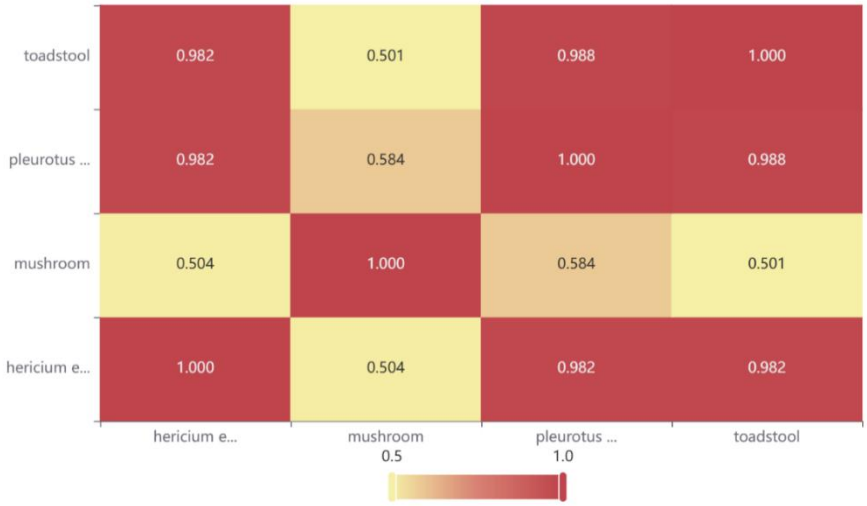

Figure 11 Thermal Matrix of Annual Planting Area of Edible Fungi

From the above three correlation thermodynamic matrices, it can be seen that when crops are negatively correlated with each other, this study believes that there is a substitution relationship between them. On the contrary, there is a complementary relationship. Therefore, the correlation coefficient λ_{y_1,y_2} between crops was defined as the substitution and complementarity coefficient, representing the substitution and complementarity relationship between y_1 and y_2. λ_{y_1,y_2} is negative, and the greater the absolute value of the coefficient, the stronger the substitution. Vice versa.
Therefore, this study optimized the expected sales volume of a certain crop in the current year as follows:

$$d_{y_2,t} = d_{y_2,t-1} + \sum_{j=1}^{41} \lambda_{j,y_2} \cdot x_{i,j,t,s} \tag{41}$$

This study uses the above formula as the first constraint added.

2.4.4 The correlation between expected sales volume, selling price and planting cost

Correlation between sales volume and price: There may be a positive or negative correlation between sales volume and price for some crops. For example, a rise in sales leads to a rise in prices, and vice versa.

$$p_{j,t} = p_{j,t-1} \cdot \left(1 + \gamma_{j,d,p} \cdot \left(d_{j,t} - d_{j,t-1}\right)\right) \tag{42}$$

where $\gamma_{j,d,p}$ is the correlation coefficient representing the expected sales volume of j crop and the selling price.
Use the above formula as the new second constraint.
Correlation between planting cost and price: There may be a positive or negative correlation between planting cost and price of some crops. Rising planting costs lead to rising prices, and vice versa.

$$p_{j,t} = p_{j,t-1} \cdot \left(1 + \gamma_{j,c,p} \cdot \left(c_{j,t} - c_{j,t-1}\right)\right) \tag{43}$$

Where $\gamma_{j,c,p}$ is the correlation coefficient representing the expected sales volume and selling price of j crop.
Use the above formula as the new third constraint.
In this study, Spearman correlation analysis model was used to analyze the expected sales volume and selling price of crops in this year and the planting cost and selling price, and the correlation coefficients were defined as $\gamma_{j,d,p}$ and $\gamma_{j,c,p}$, respectively. Figure 12 below shows the thermal matrix visualization of the correlation coefficients of $\gamma_{j,d,p}$ and $\gamma_{j,c,p}$ of tomatoes.

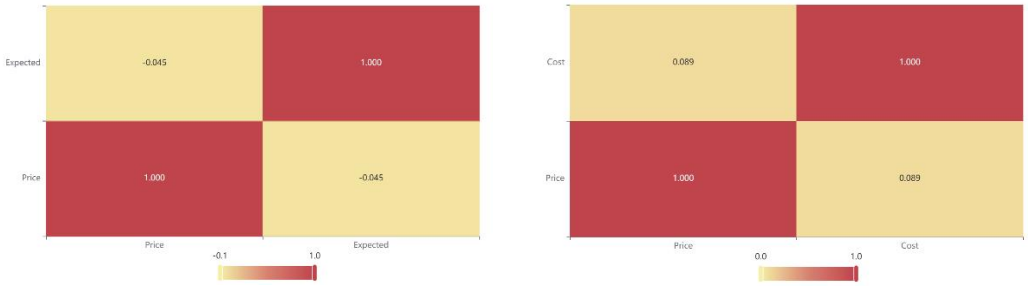

Figure 12 Tomato $\gamma_{j,d,p}$ And $\gamma_{j,c,p}$ Coefficients

Due to space constraints, $\gamma_{j,d,p}$ and $\gamma_{j,c,p}$ coefficients of other crops are shown as follows in Table 1 $\gamma_{j,d,p}$ and $\gamma_{j,c,p}$ coefficients of various crops.

Table 1 $\gamma_{j,d,p}$ And $\gamma_{j,c,p}$ Coefficients of Various Crops

crop	γ_(j,d,p)	γ_(j,c,p)	crop	γ_(j,d,p)	γ_(j,c,p)	crop	γ_(j,d,p)	γ_(j,c,p)
soybean	0.2	0.5	barley	0.12	0.121	cucumber	0.4	0.47
black soya bean	0.52	0.7	rice	0.14	0.214	lettuce	-0.5	0.687
ormosia	-0.5	0.456	cowpea	-0.42	0.75	pepper	-0.643	0.78
mung bean	-0.12	0.72	sword bean	-0.32	0.69	water spinach	-0.964	0.69
crawling bean	-0.1	0.46	common bean	-0.857	0.745	golden choy sum	0.5	0.77
wheat	-0.2	0.345	potato	-0.92	0.698	celery	0.143	0.685
maize	0.54	0.14	tomato	-0.046	0.089	celery cabbage	0.786	0.75
millet	0.11	0.93	eggplant	-1	0.87	mooli	0.036	0.97
sorghum	0.19	0.75	spinach	-0.464	0.61	carrot	-0.929	0.69
proso millet	-0.17	0.27	green pepper	-0.643	0.763	hericium erinaceus	0.786	-0.46
buckwheat	-0.4	-0.17	cauliflower	-0.714	0.473	mushroom	-0.286	-0.69
pumpkin	0.22	-0.12	cabbage	-0.107	0.479	pleurotus nebrodensis	0.75	-0.76
sweet potato	0.14	0.24	romaine	0.286	0.48	toadstool	-0.5	-0.7
hulless oat	-0.14	0.11	baby bok choy	0.857	0.147			

2.4.5 Solution method for model

Objective function:

$$\text{Max} \sum_{t=2024}^{2030} \sum_{i=1}^{54} \sum_{s=1}^{2} \sum_{j=1}^{41} \left[\min\left(q_{i,j,t,s}, d_j\right) \cdot p_{i,j,t,s} + \max\left(0, q_{i,j,t,s} - d_j\right) \cdot K \cdot p_{i,j,t,s} - e_{i,j,t,s}\right] \tag{44}$$

Constraints:
In comprehensive consideration of the expected sales of various crops, the uncertainty of planting cost and selling price, as well as the potential planting risks and the following constraints: Season number constraint, total area constraint, legume planting constraint, repeat crop constraint, crop type constraint, special crop type constraint, planting area constraint, substitution and complementarity constraint between newly introduced crops, correlation constraint between sales volume and price and correlation constraint between planting cost and price. The newly introduced constraint mathematical expressions are shown as follows:

$$d_{y_2,t} = d_{y_2,t-1} + \sum_{j=1}^{41} \lambda_{j,y_2} \cdot x_{i,j,t,s} \tag{45}$$

$$p_{j,t} = p_{j,t-1} \cdot \left(1 + \gamma_{j,d,p} \cdot \left(d_{j,t} - d_{j,t-1}\right)\right) \tag{46}$$

$$p_{j,t} = p_{j,t-1} \cdot \left(1 + \gamma_{j,c,p} \cdot \left(c_{j,t} - c_{j,t-1}\right)\right) \tag{47}$$

3 CONCLUSION

To sum up, the Spearman-Normal stochastic linear programming model is used in this study to obtain the optimal strategy for crop planting and marketing. It can be seen that under the circumstances of considering multiple dynamic factors and constraints, The significance of effectively optimizing the planting scheme of crops is to provide scientific decision support for agricultural production, so as to improve the economic benefits and sustainability of crops. However, due to the high computational complexity of the model and the risk of local optimal solutions, future research directions can consider introducing more intelligent optimization algorithms, such as simulated annealing, particle swarm optimization, etc., to further improve the global search ability and adaptability of the model.

COMPETING INTERESTS

The authors have no relevant financial or non-financial interests to disclose.

REFERENCES

[1] Lee C C, Zeng M, Luo K. How does climate change affect food security? Evidence from China. Environmental Impact Assessment Review, 2024, 104: 107324.
[2] Guo X X, Li K L, Liu Y Z, et al. Toward the economic-environmental sustainability of smallholder farming systems through judicious management strategies and optimized planting structures. Renewable and Sustainable Energy Reviews, 2022, 165: 112619.
[3] Yang L, Wang L, Chu J, et al. Improving soil quality and wheat yield through diversified crop rotations in the North China Plain. Soil and Tillage Research, 2024, 244: 106231.
[4] Filippi C, Mansini R, Stevanato E. Mixed integer linear programming models for optimal crop selection. Computers & Operations Research, 2017, 81: 26-39.
[5] Maa H. Optimization of Crop Planting Strategies Based on Linear Programming and Monte Carlo Simulation. 2024.
[6] Annetts J E, Audsley E. Multiple objective linear programming for environmental farm planning. Journal of the operational research society, 2002, 53(9): 933-943.
[7] Alotaibi A, Nadeem F. A review of applications of linear programming to optimize agricultural solutions. International Journal of Information Engineering and Electronic Business, 2021, 15(2): 11.
[8] Liang K, Lei J, Wu F, et al. Analysis of optimal planting scheme based on the North China region//Journal of Physics: Conference Series. IOP Publishing, 2024, 2898(1): 012004.
[9] Soleimani-Damaneh M. Modified big-M method to recognize the infeasibility of linear programming models. Knowledge-Based Systems, 2008, 21(5): 377-382.
[10] Fradi A, Feunteun Y, Samir C, et al. Bayesian regression and classification using Gaussian process priors indexed by probability density functions. Information Sciences, 2021, 548: 56-68.
[11] Ali Abd Al-Hameed K. Spearman's correlation coefficient in statistical analysis. International Journal of Nonlinear Analysis and Applications, 2022, 13(1): 3249-3255.

Eurasia Journal of Science and Technology
ISSN: 2663-1016
DOI: https://doi.org/10.61784/ejst3067

ELECTRONIC PRODUCT ASSEMBLY DECIS-ION BASED ON THE DUAL PERSPECTIVES OF QUALITY AND COST

HongLei Ye*, SiYi Jiang, Li Zhang, DanYao Yan
School of Mathematics and Statistics, Huaibei Normal University, Huaibei 235065, Anhui, China.
Corresponding Author: HongLei Ye, Email: 18656187306@139.com

Abstract: This paper aims to solve the problem of quality and cost control in the process of electronic product assembly. Through the cost-benefit analysis of each link in the assembly process, the mathematical model is constructed and the optimal decision-making scheme is proposed. The model comprehensively considers the defective rate of parts and finished products, detection cost, assembly cost, market price and other factors, aiming to achieve the best balance between product quality assurance and cost saving. Firstly, two sampling schemes are designed and compared, and a more economic binomial distribution scheme is recommended. Then according to the actual situation encountered in production, the cost and benefit of detecting spare parts, finished products and disassembling unqualified finished products are analyzed, and the optimal decision scheme is obtained after comparing the experimental data. In addition, taking two processes and eight spare parts as examples, three decision-making schemes are proposed to meet different needs. The experimental results can provide decision support for product assembly, help reduce costs, improve product quality and enhance market competitiveness.
Keywords: Simple random sampling; Cost-benefit theory; Decision tree algorithm; Central limit theorem; Product assembly decisions

1 INTRODUCTION

With the rapid development of science and technology, electronic products have become an indispensable part of people's lives, from smart phones to smart homes, the demand and market size of electronic products are continuing to grow. The assembly industry of electronic products is in a critical period of transformation and upgrading, and has huge market potential. For the problems related to product assembly, Zhu Haihua et al. studied the time prediction method based on the complete set of product assembly materials [1], Zhang Jin et al. proposed a risk early warning method for product assembly technical problems [2], and Shen Jitong et al. studied the planning and decision-making problem of material supply mode [3].

In this paper, we study the decision-making problems in the production process of an electronic product in a certain enterprise. The company purchases different kinds of spare parts (spare parts 1 to spare parts 8), and the finished products assembled into different types of spare parts are different. In the assembled finished product, as long as one of the spare parts is unqualified, the finished product must be unqualified; If the spare parts are qualified, the assembled finished product may not be qualified. For unqualified finished products, you can choose to scrap them, or disassemble them, the dismantling process will not cause damage to the spare parts, but the dismantling cost is required (data source: 2024 Higher Education Society Cup National College Students Mathematical Contest in Modeling[4]).

In view of the above process, the relevant mathematical model is established, and the following problems are solved: under the condition that the defective rate of a batch of spare parts does not exceed a certain nominal value, the sampling detection method is used to decide whether to accept this batch of spare parts. According to the two different reliability requirements, a sampling detection scheme with as few detection times as possible was designed, and specific detection results and decision-making schemes were given. Knowing the defective rate of two kinds of spare parts and finished products, we make decisions at all stages of the production process of the enterprise, including whether to test the spare parts, whether to test each finished product that has been assembled, and whether to disassemble the unqualified finished products that have been detected. According to the cost-effectiveness theory, the cost and profit under different decision-making schemes are analyzed, and the specific decision-making schemes and index results are also given for the situation of processes and spare parts. This paper analyzes the impact of sampling detection method on the decision-making scheme, weighs the potential risk loss caused by cost detection and non-detection, considers the market selling price, testing cost and the loss of replacing unqualified finished products, analyzes the dismantling cost and defective rate, and decides the dismantling or direct scrapping, and determines the optimal decision-making scheme according to the cost-benefit theory.

2 DESIGN A DETECTION PLAN BASED ON COST

2.1 Simple Random Sampling Testing

Based on the actual situation, this article makes the following assumptions:

(1) Assuming the sample size is large enough and the failure rate is not an extreme value;

(2) Assuming that the defect rates of spare part 1 and spare part 2 are independent of each other and do not affect each other's quality;
(3) Assuming that during each sampling test, the sample is randomly selected and the probability of each sample being selected is the same, ensuring that the sample is representative.
This article adopts a simple random sampling detection method where the samples follow a beta distribution and a binomial distribution respectively. When the nominal value is 10%, consider whether to accept this batch of spare parts in the following two situations:
(1) Case 1: Does the defect rate of spare parts exceed the nominal value with a 95% confidence level (significance level of α_1 is 0.05);
(2) Case 2: Does the defect rate of spare parts exceed the nominal value with a 90% confidence level (significance level of α_2 is 0.1)

2.1.1 Design samples that follow a beta distribution

In simple random sampling, the probability of all samples being selected is equal. Firstly, establish the hypothesis:
Null hypothesis H_0:The defect rate of spare parts P shall not exceed the nominal value P_0, that is:

$$H_0: \ P \le P_0 \tag{1}$$

Alternative hypothesis H_1:The defect rate of spare parts P exceeds the nominal value P_0, that is:

$$H_1: \ P > P_0 \tag{2}$$

Next, assuming that the overall defect rate is the nominal value, both parts 1 and 2 are defective and labeled as 1, while non defective parts are labeled as 0. Considering the actual situation, that is, the probability of the defect rate being lower than the nominal value is high, and the probability of the defect rate being higher than the nominal value is low, it is considered that this situation conforms to the beta distribution. Generate a random sample based on the beta distribution within the [0,1] interval[5], calculate the number of defective products in the sample, and then calculate the cumulative probability that the number of defective products is equal to or greater than the observed value. If the calculated value p is less than the significance level α_1, the null hypothesis is rejected, that is, if the defect rate of the spare parts exceeds the nominal value, the batch of spare parts will be rejected; if the calculated value p is greater than the significance level α_2, the null hypothesis is accepted, that is, the defect rate of the spare parts does not exceed the nominal value, and this batch of spare parts is accepted.
This article uses MATLAB to generate a random sample multiple times, which contains different numbers of defective products. To avoid accidental results caused by fewer runs, the number of generated samples is increased for different total numbers of spare parts, and the distribution between the defect rate and the value of the sample p is calculated. Taking the total number of spare parts as an example, when the number of runs is 100, the probability of the calculated value p being less than the significance level is α_1 0.13; when the number of runs is 1000, the probability that the calculated value p is less than the significance level α_2 is 0.067. As the generation frequency continues to increase, the probability of the calculated value p being less than the significance level α_1 decreases. According to the principle of low probability, events with very low probability are unlikely to occur in a single experiment. If the value p is considered to be greater than the significance level α_1, the null hypothesis cannot be rejected, and the defect rate does not exceed the nominal value. Through multiple experimental verifications, as shown in the p-value distribution at 100 runs in Figure 1, it is believed that at two levels of significance, when the number of defective products exceeds 13, the spare parts should be rejected.

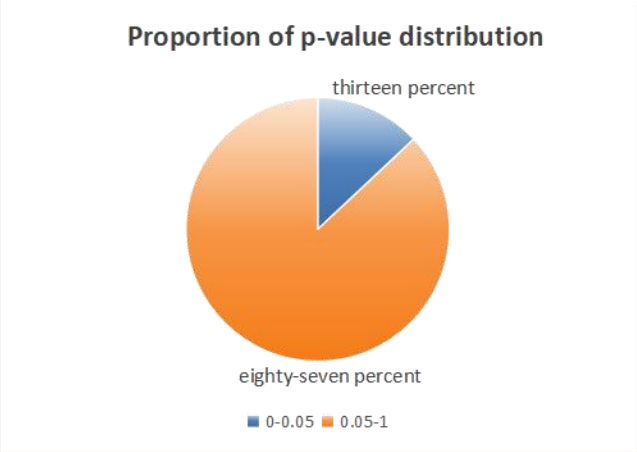

Figure 1 P-value Distribution at 100 Runs

2.1.2 The design sample follows a binomial distribution

For case one, at a significance level of 0.05, if the test results meet the following conditions, the spare parts will be rejected:

$$H_0: \ P \le P_0 \quad \text{VS} \quad H_1: \ P > P_0 \tag{3}$$

If the pass rate $\hat{p} \le P_0$, accept; otherwise, reject. For the rejection criteria in this situation, this is:

$$P(\hat{p} > P_0 \mid H_0) \le 0.05 \tag{4}$$

For case two, at a significance level of 0.1, if the test results meet the following conditions, the spare parts will be accepted:

$$H_0: \ P \ge P_0 \quad \text{VS} \quad H_1: \ P < P_0 \tag{5}$$

If the pass rate $\hat{p} < P_0$,accept; otherwise, reject. For the accepttion criteria in this situation, this is:

$$P(\hat{p} < P_0 \mid H_1) \le 0.1 \tag{6}$$

Calculated from a nominal value P_0 of 0.1, with a 95% confidence level $n \ge \left(\frac{1.96\sqrt{0.1(1-0.1)}}{0.1} \right)^2 \approx 34$,is 34 sampling tests should be conducted. Let n be the threshold for rejection. Based on the binomial distribution $X \sim B(n,0.1)$ has $P(X > k) < 0.05$,use normal approximation to derive the relationship between the number of non-conforming parts k in the sample and the total number of parts n ($Z \approx 1.645$):

$k = 0.1n + 1.645\sqrt{0.09n}$,when n is taken as 100, if there are more than 14 defective products in the sample, they should be rejected.

At a 90% confidence level $n \ge \left(\frac{1.645\sqrt{0.1(1-0.1)}}{0.1} \right)^2 \approx 27$,is 27 sampling tests should be conducted. Similarly, according to the binomial distribution $P(X \le k) \ge 0.9$, the relationship between n and n is derived as follows($Z \approx 1.28$): $k = 0.1n + 1.28\sqrt{0.09n}$

When n is taken as 100, if there are more than 13 defective products in the sample, they should be rejected

The conclusion drawn from the comparison is that option two with fewer detection times should be chosen as the decision-making method to reduce detection costs.

3 MAKING DECISIONS BASED ON QUALITY

3.1 Model Establishment

Initialize whether to detect spare parts, semi-finished products, finished products, and whether to disassemble non-conforming products as 0-1 decision variables, and use a decision tree model to compare costs to obtain the optimal decision[6].

In the spare parts testing stage, each spare part has two options: testing and not testing. Choosing to test may increase costs, but it can ensure quality. Choosing not to test may result in unqualified spare parts entering the assembly process; During the assembly of finished products, only qualified spare parts can enter the assembly process to ensure the basic quality of the finished products; During the finished product testing phase, failure to conduct testing may result in unqualified products entering the market and affecting the reputation of the company;In the stage of handling non-conforming products purchased by users, the enterprise has the responsibility to handle the non-conforming products. Providing replacement services can improve customer satisfaction, but if replacement is not possible, the non-conforming products need to be reprocessed, which increases costs.

According to the production process, without testing spare parts 1 and 2, and without disassembling unqualified finished products, the quantity of finished products is m , and the total cost W_1 is:

$$W_1 = m * (x + y + z_1) \tag{7}$$

The defect rate P_1 is：

$$P_1 = (a + b - a * b + (1 - a) * (1 - b) * c) \tag{8}$$

If: (1) Consider whether to test spare part 1, the total cost W_2 is:

$$W_2 = \begin{cases} W_1 + m * z_2, & \text{Detect spare parts 1} \\ W_1, & \text{Do not detect spare parts 1} \end{cases} \tag{9}$$

The defect rate P_2 is:

$$P_2 = P_1 * (b + c) / (a + b - a * b - (1 - a) * (1 - b) * c) \tag{10}$$

(2)Consider whether to test spare part 2, with a total cost of W_3 is:

$$W_3 = \begin{cases} W_1 + m * z_3, & \text{Detect spare parts 2} \\ W_1, & \text{Do not detect spare parts 2} \end{cases} \tag{11}$$

The defect rate P_3 is:

$$P_3 = P_1 * (a + c) / (b + c) \tag{12}$$

(3) Consider whether to test the finished product, with a total cost of W_4 is:

$$W_4 = \begin{cases} W_1 + m * z_4, & \text{Test finished products} \\ W_1, & \text{Do not test finished products} \end{cases} \tag{13}$$

The defect rate P_4 is:

$$P_4 = P_1 * (a + b - a * b) / (a + c) \tag{14}$$

(4) For non-conforming finished products, consider whether to disassemble them, with a total cost of W_5 is:

$$W_5 = \begin{cases} W_1 + q_2 + q_3 - 2 * m * (a * x + b * y + c * x + c * y), & \text{Disassemble} \\ W_1 + q_2, & \text{Do not disassemble} \end{cases} \tag{15}$$

The net profit margin P_5 is:

$$P_5 = m * (1 - P_4) * q_1 - W_4 \tag{16}$$

(Among them, a, b and c respectively represent the damage rates of parts 1, 2, and 3, x represents the unit price of part 1, y represents the unit price of part 2, z_1 represents the assembly cost, z_2 and z_3 respectively represent the inspection cost of parts 1 and 2, z_4 represents the cost inspection cost, q_1 represents the market price, q_2 represents the exchange loss, and q_3 represents the dismantling cost).

3.2 Model Solving

Taking a defect rate of 10%, a purchase price of 12 yuan/piece, and a testing cost of 2 yuan/piece as an example.
(1)Root node (starting point), decision: whether to detect spare part 1; Option: Yes/No.
(2)The first level decision node
If you choose "Yes" to test spare part 1, the testing cost is 2 yuan per piece. Assuming that the defect rate after testing is 0, that is, all defective products are detected. Authentic product revenue is $90\% \times 12 = 10.8$ yuan, total cost is $12 + 2 = 14$ yuan, each spare part incurs a loss of $10.8 - 14 = -3.2$ yuan. Due to the zero defect rate after testing, the finished product is also genuine and does not require additional testing costs. The final profit is $10.8 - 3.2 = 7.6$ yuan.
If you choose 'No' to test spare part 1, there will be no testing cost, and the defect rate will remain unchanged at 10%.
(3)The second level decision node[7], decision: whether to detect spare part 2; Option: Yes/No.
If you choose "Yes" to test spare part 2, the testing cost is 2 yuan/piece, and the genuine product income is $90\% \times 12 = 10.8$ yuan The total cost is $12 + 2 = 14$ yuan. Each spare part incurs a loss of $10.8 - 14 = -3.2$ yuan.
If you choose "No" to test spare parts 2, there will be no testing cost, and the genuine product revenue will be $12 + 2 = 14$ yuan. The total cost is 12 yuan Each spare part has a profit of $10.8 - 14 = -3.2$ yuan.
(4)The third level decision node, decision: whether to detect the finished product; Option: Yes/No.
If you choose "Yes" to test the finished product: the testing cost is 2 yuan/piece, and the genuine product revenue is $90\% \times 12 = 10.8$ yuan The total cost is $12 + 2 = 14$ yuan Each finished product incurs a loss of $10.8 - 14 = -3.2$ yuan.
If you choose "No" to test the finished product: no testing cost, genuine product revenue of $90\% \times 12 = 10.8$ yuan, total cost of 12 yuan Each finished product incurs a loss of $10.8 - 14 = -3.2$ yuan. Due to not dismantling unqualified products, there are no additional costs or benefits.
Final decision

Inspect spare parts 1, do not inspect spare parts 2 and finished products, and do not disassemble non-conforming products The maximum profit obtained is 10.40 yuan.

For the case of m processes and n spare parts, use probability addition and multiplication rules to calculate the probability of each situation, and add them together to obtain the expression for the damage rate of d . Repeat the process of nesting the decision tree model mentioned above[8].

This decision tree model demonstrates[9] the calculation of expected profits at different decision points and how to maximize profits by selecting different detection strategies This includes whether to inspect spare parts, dismantle semi-finished or finished products, and whether to dismantle non-conforming products. It comprehensively analyzes the costs and profits under different decisions, making the decisions more systematic and scientific.

4 PROVIDE THREE DECISION OPTIONS SUITABLE FOR DIFFERENT TYPES OF MANUFACTURERS BASED ON COST-BENEFIT THEORY

4.1 Risk Management

According to the cost-benefit theory[10], mark spare parts 1, 2, and 3 as A , B , and C respectively, semi finished product 1 is denoted as D and construct the following six decision-making schemes to explore different combinations of whether to inspect spare parts 1, spare parts 2, and finished products, as well as whether to disassemble unqualified finished products:

Plan 1: Do not detect A and B , do not dismantle non-conforming products; plan 2: detect A , do not detect B , do not dismantle non-conforming products; plan 3: do not detect A , detect B , do not dismantle non-conforming products; plan 4: detect A and B , do not disassemble non-conforming products; plan 5: detect A and B , disassemble non-conforming products; plan 6: do not test A and B , disassemble non-conforming finished products.

According to the strategy of minimizing costs and maximizing profits[11], that is, achieving cost minimization and profit maximization while ensuring product quality meets established standards. Cost identification includes inspection costs for spare parts, semi-finished products, and finished products, procurement costs for spare parts, assembly costs for semi-finished and finished products, dismantling costs for non-conforming products, and exchange losses for non-conforming products. Revenue recognition includes the revenue generated from the sale of finished products, as well as the recycling value of spare parts after dismantling of non-conforming finished products.

Fully consider risk factors in the decision-making process to avoid potential losses caused by decision-making errors. Identify eight possible combinations of situations for the damage of semi-finished product 1, as shown in Table 1, and use probability addition and multiplication rules to calculate the probability of each situation. The following is the expression for the damage rate of semi-finished product 1:

$$e = a + b + c - ab - ac - bc + abc + (1-a)(1-b)(1-c)d \tag{17}$$

Table 1 Damage Situation Combination

——	*A*	*B*	*C*	*D*
case1	damage	intact	intact	——
case2	intact	damage	intact	——
case3	intact	intact	damage	——
case4	damage	damage	intact	——
case5	damage	intact	damage	——
case6	intact	damage	damage	——
case7	damage	damage	damage	——
case8	intact	intact	intact	damage

Furthermore, by using the central limit theorem, the defect rate of the sample is approximated as the overall defect rate, thereby improving the confidence level of estimating the defect rate of spare parts and semi-finished products and effectively reducing decision risk[12].

4.2 Provide A Decision-Making Plan

Table 2 Possible Situations Encountered during Product Assembly Process

Spare parts	Defective rate	Purchase price	Testing cost	Partially Prepared Products	Defective rate	Assembly cost	Testing cost	Dismantling cost
1	10%	2	1	1	10%	8	4	6
2	10%	8	1	2	10%	8	4	6
3	10%	12	2	3	10%	8	4	6
4	10%	2	1	——	——	——	——	——
5	10%	8	1	finished product	10%	8	4	6

6	10%	12	2	——	——	——	——	——
7	10%	8	1	——	Market selling price		Exchange losses	
8	10%	12	2	finished product	200		40	

As shown in Table 2, the defect rate, purchase price, testing cost, assembly cost, testing cost, and disassembly cost of semi-finished parts, semi-finished products, and finished products are known. Among them, semi-finished product 1, semi-finished product 2, and semi-finished product 3 are respectively composed of spare parts 1, spare parts 2, spare parts 3 and 4, spare parts 5, spare parts 6 and 7, and spare parts 8. The finished product consists of semi-finished product 1, semi-finished product 2, and semi-finished product 3. Firstly, for semi-finished products, a decision tree model is used to determine the minimum cost of semi-finished products Secondly, for the finished product, provide a decision-making plan for the production process, as well as the basis and corresponding indicators for the decision[13].

4.2.1 Minimize the production cost of the enterprise

Under this decision-making plan, the plan with the lowest production cost for the enterprise is taken as the optimal decision-making plan[14]. At this point, if the finished product is not inspected or damaged, it needs to be disassembled, and the final cost per unit of finished product is calculated to be 133.4 yuan. If enterprises use this decision-making scheme, although they can obtain high profits, they also bear high risks, which is more suitable for enterprises with advanced production equipment and relatively controllable finished product damage rates. The specific decision variable records are shown in Table 3 (where "0" represents "no" and "1" represents "yes").

Table 3 Optimal Decision Plan with Minimum Cost

——	Partially Prepared Products 1	——	Partially Prepared Products 2	——	Partially Prepared Products 3
Whether to detect spare parts 1	0	Whether to detect spare parts 4	0	Whether to detect spare parts 7	0
Whether to detect spare parts 2	0	Whether to detect spare parts 5	0	Whether to detect spare parts 8	0
Whether to detect spare parts 3	0	Whether to detect spare parts 6	0	——	——
Whether to detect semi-finished products 1	0	Whether to detect semi-finished products 2	0	Whether to detect semi-finished products 3	0
Damage rate	0.1	Damage rate	0.1	Damage rate	0.1
Whether to disassemble or not	0	Whether to disassemble or not	0	Whether to disassemble or not	1
cost(yuan)	26	cost(yuan)	26	cost(yuan)	26

4.2.2 Maximize the production cost of the enterprise

Under this decision scheme, the optimal decision scheme is the one that maximizes the production cost of the enterprise. At this time, the cost is not tested and needs to be dismantled after damage. The final calculated cost per unit of finished product is 173 yuan. If the enterprise uses this decision-making scheme, although it requires the least risk, the profit is the least. This scheme is more suitable for enterprises with fixed sales channels and stable production all year round[15]. The decision variable records are shown in Table 4 (where "0" represents "no" and "1" represents "yes").

Table 4 Optimal decision plan under maximum cost

——	Partially Prepared Products 1	Partially Prepared Products 2	Partially Prepared Products 3
Spare parts 1	1	1	1
Spare parts 2	1	1	1
Spare parts 3	1	1	1
Whether to test or not	1	1	1
Whether to disassemble or not	1	1	0
cost(yuan)	40	40	35

4.2.3 Take the median of enterprise production costs

Under this decision-making scheme, the optimal solution is to take the median of the production cost of the enterprise. At this time, if the finished product is not inspected or damaged, it needs to be disassembled. The final cost per unit of finished product is calculated to be 157.5 yuan. Compared to the above two decision-making schemes, this scheme has higher stability and is more suitable for the production of most enterprises. The decision variable records are shown in Table 5 (where "0" represents "no" and "1" represents "yes").

Table 5 Optimal Decision Plan for Taking the Median Cost

——	semi-finished product 1		——	semi-finished product 2		——	semi-finished product 3		
Whether to detect spare parts1	0	1	Whether to detect spare parts4	0	1	Whether to detect spare parts7	0	1	1
Whether to detect spare parts2	1	0	Whether to detect spare parts5	1	0	Whether to detect spare parts8	0	0	0
Whether to detect spare parts3	1	1	Whether to detect spare parts6	1	1	——	—	—	—
Whether to detect or not	1	1	Whether to detect or not	1	1	Whether to detect or not	1	1	1
Whether to disassemble or not	0	0	Whether to disassemble or not	0	0	Whether to disassemble or not	1	0	0
cost(yuan)	33		cost(yuan)	33		cost(yuan)	30.5		

5 CONCLUSION

In this paper, the decision-making problem of electronic product assembly from the dual perspectives of quality and cost is studied. Factors such as whether to detect and whether to disassemble are initialized as 0-1 decision variables, and flexibly adjusted and optimized according to the actual needs and conditions of different manufacturers. In view of the defective rate of spare parts, this paper designs a sampling detection scheme with samples obeying beta distribution and binomial distribution, and reduces the cost for enterprises by calculating and comparing the detection times and rejection standards of the two schemes. According to the assembly situation of each process and spare parts, the decision tree algorithm is used to analyze a variety of decision combinations, and three decision-making schemes suitable for different types of manufacturers are proposed. The model and solution established in this paper can provide decision support for product assembly, help reduce costs, improve product quality, and enhance market competitiveness, which has certain reference significance for the actual production and assembly of electronic products.Although the current research has made significant progress, we recognize that there is still much work to be done. Through continuous efforts and improvement, we hope to provide a more advanced, practical and reliable decision support system for electronic product assembly in future practice, and help the transformation, upgrading and sustainable development of the industry.

COMPETING INTERESTS

The authors have no relevant financial or non-financial interests to disclose.

REFERENCES

[1] Zhu Haihua, Fu Tairan, Li Fei, et al. Prediction of complete set time of complex product assembly material process based on digital twin. Journal of Mechanical Engineering, 2024: 1-15.
[2] Zhang Jin, Liu Jianhua, Zhao Wenhao, et al. Risk early warning method for complex product assembly technology problems based on pre-trained model and similarity algorithm. Journal of Mechanical Engineering, 2024(24): 317-329.
[3] Shen Jitong, Wang Chuangjian, Xu Xianhao. Industrial Engineering and Management, 2023, 28(01):110-119.
[4] 2024 National College Student Mathematical Contest in Modeling. 2024-09-05.
[5] Lin Yaohua, Liang Zhong, Hu Huaping. Cuckoo search algorithm based on beta distribution. Journal of Nanjing University(Natural Science), 2016, 52(04): 638-646.
[6] Wang Jieting, Li Feijiang, Li Jue, et al. Gini index and decision tree method for mitigating stochastic consistency.Science China:Information Science, 2024, 54(01): 159-190.
[7] Wen Hufeng, Shang Tianshuai, Li Jian, et al. Ground state spin prediction of odd A nuclei based on decision tree method. Acta Physica Sinica, 2023, 72(15): 33-41.
[8] Wu Bei. Research and application of performance prediction model based on decision tree algorithm. Xi'an: Xi'an University of Technology, 2019.
[9] Chen Jiajun, Miao Duoqian. An adaptive decision tree algorithm based on the fusion of decision risk cost and attribute preference. Journal of Chinese Computer Systems, 2018, 39(06): 1208-1212.
[10] Li Xinjie. Cost-benefit analysis of enterprises from the perspective of budget, business and financial integration. Modern Business Research, 2024(08): 104-106.
[11] Jin Guomin. Enterprise cost management strategy based on cost-effectiveness. Investment and Cooperation, 2021(10): 38-39.
[12] Jianxiang W, Lu C, Pu H, et al. Decision Tree-Based Data Stratification Method for the Minimization of the Masking Effect in Adverse Drug Reaction Signal Detection. Applied Sciences, 2021, 11(23): 11380-11380.
[13] Lv Xinrong. Reflections on the cost-effectiveness of enterprise internal control. Finance and Economics, 2021(19): 125-126.

[14] Hu Weixiang. On the internal control strategy of start-up SMEs based on the principle of cost-effectiveness. Finance and Economics, 2020(20): 100-101.
[15] Ding Ying Cost benefit balance point analysis of enterprise risk management. Contemporary Accounting, 2018(09): 32-33.